Evaluating the Urban Heat Island for cities of Emilia-Romagna region through numerical simulations

Relatore:

Prof.ssa Silvana Di Sabatino

Presentata da:

Correlatore:

Andrea Zonato

Dott. Alberto Martilli

Sessione I

Anno Accademico 2015/2016

Abstract

Lo scopo di questo studio è la comprensione della dinamica dello strato limite urbano per città dell'Emilia Romagna tramite simulazioni numeriche. In particolare, l'attenzione è posta sull' effetto isola di calore, ovvero sulla differenza di temperatura dell'aria in prossimità del suolo fra zone rurali e urbane dovuta all'urbanizzazione. Le simulazioni sono state effettuate con il modello alla mesoscala "Weather Research and Forecasting" (WRF), accoppiato con le parametrizzazioni urbane "Building Effect Parametrization" (BEP) e "Building Energy Model" (BEM), che agiscono a vari livelli verticali urbani. Il periodo di studio riguarda sei giorni caldi e senza copertura nuvolosa durante un periodo di heat wave dell'anno 2015. La copertura urbana è stata definita con il "World Urban Databes and Access Portal Tools" (WUDAPT), un metodo che permette di classificare le aree urbane in dieci "urban climate zones" (UCZ), attraverso l'uso combinato di immagini satellitari e "training areas" manualmente definite con il software Google Earth. Sono state svolte diverse simulazioni a domini innestati, con risoluzione per il dominio più piccolo di 500 m, centrato sulla città di Bologna. Le differenze fra le simulazioni riguardano la presenza o l'assenza delle strutture urbane, il metodo di innesto e tipo di vegetazione rurale. Inoltre, è stato valutato l'effetto dovuto alla presenza di pannelli fotovoltaici sopra i tetti di ogni edificio e le variazioni che i pannelli esercitano sullo strato limite urbano. Per verificare la bontà del modello, i dati provenienti dalle simulazioni sono stati confrontati con misure provenienti da 41 stazioni all'interno dell'area di studio. Le variabili confrontate sono: temperatura, umidità relativa, velocità e direzione del vento. Le simulazioni sono in accordo con i dati osservativi e riescono a riprodurre l'effetto isola di calore: la differenza di temperatura fra città e zone rurali circostanti è nulla durante il giorno; al contrario, durante la notte l'isola di calore è presente, e in media raggiunge il massimo valore di $4\,°C$ alle 1:00. La presenza dei pannelli fotovoltaici abbassa la temperatura a 2 metri dell'aria al massimo di $0.8\,°C$ durante la notte, e l'altezza dello strato limite urbano dell'ordine $200\,m$ rispetto al caso senza pannelli. I risultati mostrano come l'uso di pannelli fotovoltaici all'interno del contesto urbano ha molteplici benefici: infatti, i pannelli fotovoltaici riescono a ridurre la temperatura durante un periodo di heat wave, e allo stesso tempo possono parzialmente sopperire all'alto consumo energetico, con una conseguente riduzione del consumo di combustibili fossili.

Abstract

The aim of this work is the comprehension of the Urban Boundary Layer (UBL) dynamics for cities of Emilia-Romagna, focusing on the Urban Heat Island (UHI) effect through numerical simulations. The Weather Research and Forecasting (WRF) mesoscale model has been used, coupled with the Building Effect Parametrization (BEP) and the Building Energy Model (BEM) multilayer urban schemes. The period of simulation consists of six hot and cloudless days during a heat wave period of the summer of 2015. Urban land cover has been defined through the World Urban Database and Access Portal Tools (WUDAPT), a method to classify the urban morphology into ten urban climate zones (UCZ) through the combined use of Satellite Imaging and Google Earth software. Several numerical nested domains simulations with a spatial resolution of 500 m have been performed, to evaluate the skills and the weaknesses of each one. Differences in simulations consist is the nesting method, the rural vegetation coverage, and the replacement of urban coverage with rural areas. Moreover, the effect of Rooftop Photovoltaic Panels (RPVP) deployment within the urban context has been tested, to detect the modifications induced by RPVP on the UBL. Model's outputs have been compared with observational data coming from meteorological stations located within the finest domain of the simulation. Results accurately represents the UHI effect, according with observational data: the 2-m air temperature difference between urban and rural areas is not present during daytime, but it takes place during the last hours of the afternoon and reaches its maximum ($\simeq 4\,°C$) around 1:00 local hour. The presence of RPVP decreases both 2-m air temperature and PBL height, with a maximum difference for 2-m air temperature of $0.8\,°C$ during nighttime and for PBL height of $200\,m$ for the total coverage of RPVP. The results demonstrate that the use of RPVP have different benefits: it mitigates warming in urban context during a heat wave period and it can also partially supplies the energy demand with a consequent reduction of fossil fuel consumption.

Contents

List of Figures

8

List of Tables

List of Abbreviations

PBL	Planetary Boundary Layer
UBL	Urban Boundary Layer
UHI	Urban Heat Island
RSL	Roughness Sublayer
ISL	Inertial Sublayer
UCL	Urban Canopy Layer
NWP	Numerical Weather Prediction
WUDAPT	World Urban Database Access Portal Tool
USEB	Urban Surface Energy Balance
LCZ	Local Climate Zone
BEP	Building Effect Parametrization
BEM	Building Energy Model
RPVP	Rooftop PhotoVoltaic Panels
WRF	Weather research and Forecasting (model)
WPS	WRF Preprocessing System
2WN	two-way nesting (method)
1WN	one-way nesting (method)
RH	Relative Humidity
PT	Potential Temperature
TKE	Turbulent Kinetic Energy
ACS	Air Conditioning Systems

Chapter 1

Introduction

The Urban Heat Island (UHI) effect is a well-known phenomenon defined as the difference of temperature between an urban area and the rural one.
The impact of urban structures have been studied for decades, and it is still subject of interest, since the urban world's population keeps increasing.
Cities have deep impacts on climate on different spatial scales: from microscale (building and urban canyon) to mesoscale (city and surrounding areas) to macroscale (regional and global). These impacts include the UHI, air quality, air pollution and CO_2 emissions. At the same time, the urban environment may affect health, energy consumption and water supply.

Numerical Weather Prediction (NWP) modeling is considered an efficient tool for studying the effect of urban structures in a given environment; a wide range of successful applications is well-documented in scientific literature. Numerical modeling deals with different spatial scales: from microscale models (such as Computational Fluid-Dynamics (CFD) models), to single-building models (i.e the study of energy budget for a single structure), to mesoscale models (dealing with atmospheric structures of the order of 10-100 km). A common task for all models is to reproduce accurately the features of urban morphology, with respect to the scale involved. Microscale models require a detailed resolution of urban structures. On the other hand, models with coarser resolution need a parametrization of averaged urban morphology features for the spatial scales involved.
In particular, mesoscale atmospheric models have been widely used in the last years to study urban heat islands, using schemes representing the impact of urban environment within NWP models. The use of properly designed modeling systems provides helpful information to civil protection and urban planning, in order to find mitigation strategies able to contrast the harmful effects of urbanization.

Defining the urban coverage at suitable scales as input for the models is not a trivial task. Moreover, information of urban morphology has been identified as crucial to improving modeling capacity.

The aim of this work is to evaluate the capability of a high-resolution digitized urban landmask in reproducing the UHI effect during a strong heat wave in Emilia-Romagna region.

The urban landuse has been created through the World Urban Database Access Portal Tool (WUDAPT), which provided an urban classes categorization through satellite imaginery. The landmask created with WUDAPT has been thereafter incorporated in the Weather Research and Forecasting (WRF) Model (a next-generation mesoscale numerical weather prediction system), originally developed by the National Center of Atmospheric Research (US) in the last decade. The Building Effect Parametrization [Martilli et al., 2002] and the Building Energy Model [Salamanca et al., 2010] have been coupled with WRF to take into account the created landmask. Once validated the model capacity, the deployment of Rooftop Photovoltaic Panels (RPVP) in contrasting the potentially harmful effect of UHI have been evaluated (i.e. depending on the latitude of the city considered).

Despite the physics describing the urban micro-climate is universal, the lack of a general method for the definition of the urban texture (morphology) is an obstacle for the realization of a robust climatic model. The problem is relevant especially for the study area, where cities are small and spread, and need to be adequately resolved with high resolution landmasks. At the same time, despite building databases are available for the study area considered in this thesis, they are unsuited for the task and their coverage is focused just on largest cities. For these reasons, WUDAPT is the most appropriate tool for the aim of this study: its versatility allows to describe universally the urban morphology. Its resolution can resolve the urban structures at suitable scales for the model used.

An appropriate description of the urban morphology is also a strong skill for the evaluation of mitigation strategies which can be applied in order to contrast the harmful effects of the UHI.

The current introduction chapter is followed by a general review of physical patterns commonly adopted to describe the Urban Bondary Layer (Chapter 2). The focus will be set on the phenomenon which lead to the formation of UHI. The subsequent

(Chapter 3) deals with the urban landmask adopted in this work and the parametrizations used to take into account of urban structures within the model. Then the features of the region and the period object of this study and the setup used for the numerical simulations will be presented (Chapter 4). Finally, the comparison with observational data (Chapter 5) and the evaluation of the simulation resuls (Chater 6) will be discussed.

Chapter 2

State of art: studying the urban climate

In this chapter, the most relevant features of the atmospheric Urban Boundary Layer and its features are described, with particular emphasis on the Urban Heat Island (UHI) effect. Furthermore, the possible mitigation strategies that could be adopted to improve the urban climate are illustrated as well as the state-of-art models employed to numerically analyze this phenomena.

2.1   The influence of the cities on the near surface atmosphere

In a review of United Nations in 2014, it was estimated that 54 % of the world' s population resided in urban areas in 2014. In 1950, 30 % of the world' s population was urban, and by 2050, 66 % of the world' s population is projected to be urban [Nations, 2014]. In particular, the percentage of urban population in Italy is currently of 69% *[data.worldbank.org]*. This means that the urban environment has become the most common ecosystem for humankind, and this phenomena keeps growing. Moreover, urbanization is one of the main anthropogenic processes responsible for big changes in atmospheric and land surface heat exchange process. Studying and modeling the processes which occurs in this contest is become a crucial point in order to improve the standard of living in urban areas, due to the strong impacts of cities on climate on a wide range of spatial scales. Cities environment has significant implications on local climate: temperature, precipitation, humidity, wind and radiation balances show noticeably differences between a city and its surrounding rural areas [Stewart, 2011]. Urbanization has also several implications on human heat release and energy consumption: due to the city influence of on the local climate air pollution, anthropogenic heat increased release and negative influences on human

health are problems commonly found in this context.

2.2 The urban boundary layer

The planetary boundary layer (PBL) is the lowest part of the troposphere, influenced by the processes which take place in the planetary surface. It usually responds to the surface radiative forcing in a time scale of one hour, and it is generally turbulent and with a strong vertical mixing. Above the PBL lies the part of atmosphere not influenced by the surface. Here the wind is geostrophic, i.e. it follows approximately the isobars, and it is usually nonturbolent. The Urban Boundary Layer (UBL) is the part of the atmosphere in which most of the humankind lives, and is one of the most complex microclimate due to its heterogeneity. We now report on the typical characteristic of the UBL, following the review of [Barlow, 2014].

Scales Involved: It is possible to characterize the UBL based on the scales of the urban morphology. Therefore, the smaller one is the street scale ($\simeq 10 - 100$m) where flows are influenced by each individual building. At the neighborhood scale ($\simeq 100 - 1000$m) the atmosphere is influenced by average buildings with height, shape, and density. Finally, the city scale ($\simeq 10 - 20$km) which corresponds to the dimension of city.

Energy Balance: The energy balance within the city is generally different from the balance which takes place on the rural areas, because of the following reasons:

- Sensible heat flux is higher because of buildings materials and increased occupied area;

- The lower fraction of vegetative coverage reduces the latent heat flux;

- High thermal inertia due to the high heat capacity of the building materials, with a great storage within walls, roofs and ground;

- Shadowing and radiation trapping effect within the urban canyons. It affects the global albedo and the net long-wave radiation flux;

- Contribution of the anthropogenic heat release to the solar-driven energy balance, which globally increases the sensible heat flux.

The increased sensible heat flux released strongly affects the vertical structure and then the height of the UBL.
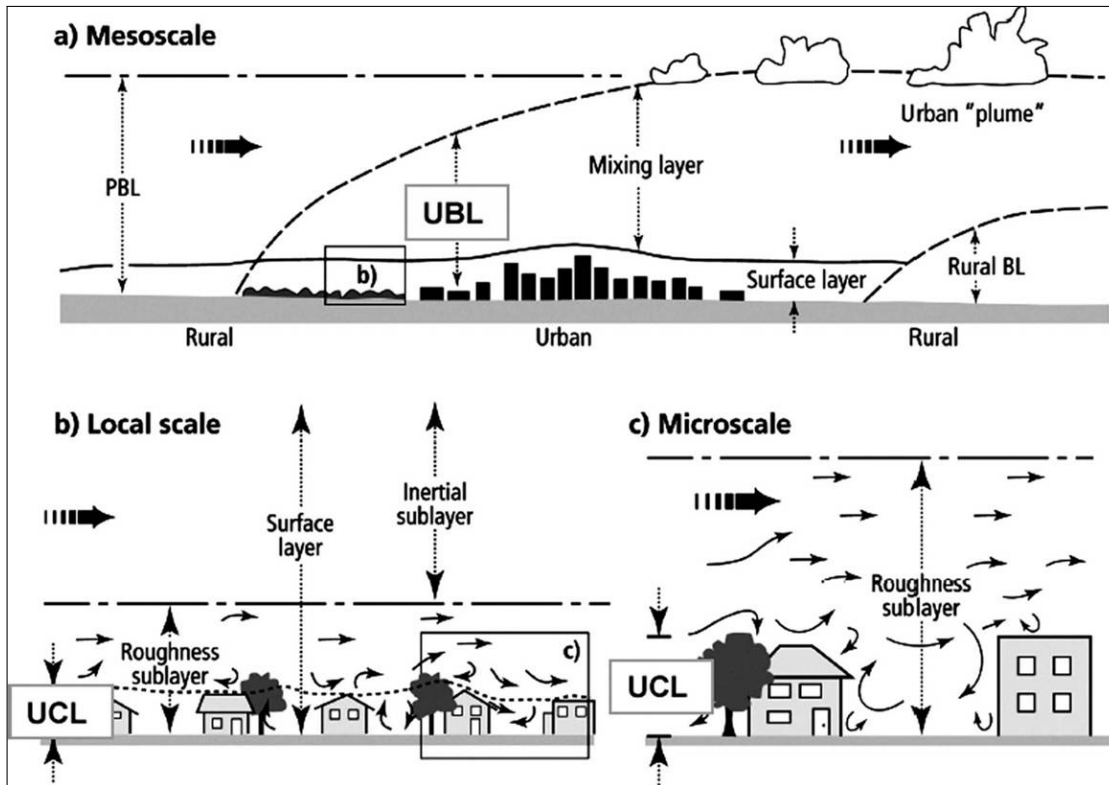
Figure 2.1: Buildings effect on airflow over different spatial scales. From *http://uhiprecip.yolasite.com/*.

The different types of UBL The PBL flow is strongly influenced by surface heterogeneities. In fact, heterogeneities enhance the transfer of kinetic energy from the mean flow into turbulent flow, diminishing the velocity of the mean flow. The roughness of the ground is a relevant variable which affect the turbulent kinetic energy (TKE) production. In the urban context, roughness elements are significantly large, and exert a relevant drag on the flow. It is possible to classify two different roughness layers:

- The urban roughness sublayer (RSL), which has a depth of $2-5H$, where H is the mean building height. Here the flow is high spatially dependent and dominated by turbulence;

- The inertial sub-layer (ISL), above the RSL, where turbulence is homogeneous and not dependent on the height.

  Over the ISL, it is assumed that the UBL has the features of a classical PBL. In particular, during night-time, the positive sensible heat flux drives a nocturnal mixed layer which can be convective or near-neutral. Fig.2.1 represent these different layers.

Larger Scales features: As said before, the UBL structure is driven by the urban surface features, but this is not the only factor. At larger scales ($10 - 100\,\mathrm{km}$) thermal circulations can affect the UBL behavior. For example, coastal cities are subject to sea/land breezes due to land-sea temperature gradients. Therefore, the katabatic/anabatic wind can interact with the thermal circulation of the cities at the feet of the mountains.

2.2.1 The urban surface energy balance

Here the components of the urban surface energy balance (USEB) from [Arnfield, 2003] are reported. For a given volume within the urban canopy, the balance is:

$$Q^* + Q_F = Q_H + Q_E + \Delta Q_S + \Delta Q_A$$

Where:

- Q^* is the net radiation;

- Q_F is the anthropogenic heat flux;

- Q_H is the sensible heat flux;

- Q_E is the latent heat flux;

- ΔQ_S is the storage heat flux;

- ΔQ_A is the advective heat flux;

The storage flux The storage flux is due to the heat stored within the buildings material. In order to correctly simulate the USEB, understanding the storage heat flux is of fundamental importance. It is subject to a large uncertainty, due to the variety of materials with different thermal properties present in a city. Moreover, it is not possible to measure it directly, but only through heat flux differences. It is strongly dependent on solar variation and on the buildings material features.

The anthropogenic flux Of fundamental importance is to be able to simulate the interaction between anthropogenic flux and urban canopy air temperature, e.g. if the temperature is higher, the increase of the air conditioning to maintain constant the temperature inside the building leads to a greater anthropogenic flux. Numerical simulations shows that the impact of the anthropogenic heat flux on the UBL leads to a temperature increase of $O(1\,^\circ\mathrm{C})$ and a consequent increase of the TKE, strongly
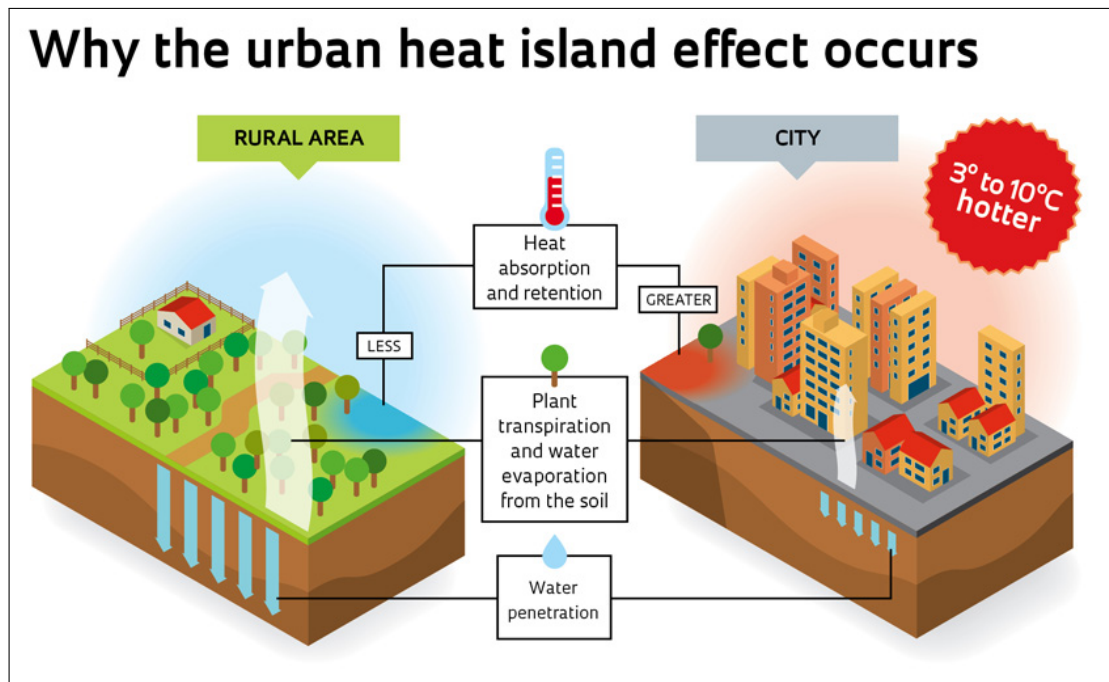
Figure 2.2: Comparison of land-surface heat exchanges between urban and rural areas. From *http://uhiprecip.yolasite.com/*.

dependent on the density of buildings. [De Munck et al., 2013] shows that larger increases were seen during nighttime, despite larger anthropogenic release during the day. This is due to the lower UBL height during night: the mixing of heat takes place in a shallower layer, leading to a temperature increase.

2.2.2 The nocturnal UBL

The nocturnal UBL differs from the day-time UBL, due basically to the absence of the solar radiation forcing; it is possible to outlining the following relevant features:

- In absence of a synoptical wind forcing, a positive heat flux can be maintained after the inversion of the net radiation; the urban surface cools less rapidly than the air above, leading to a convective turbulent layer within the UCL, principally due to the heat stored inside the buildings materials. This convection decays gradually with the surface cooling i.e. with the heat dispersion through the upper and lateral layers.

- In a synoptical forcing condition, cooler rural air could advects over the warmer urban surface, leading to a positive surface heat flux from the surface to the incoming air. This phenomena can form a near neutral layer close to the surface,

with a strong inversion on the upper ones, due to the mixing of warmer air. This thermal layer is identified as "thermal plume".

- In cities close or in the mountains, orography can trigger downslope cool flows, leading to stable layers over the city.

- Coastal cities strongly influence the sea breeze: the breezes could be maintained during the night due to the increased land-sea temperature horizontal gradient, leading to weak convection caused by the cold air advection.

2.3   The urban heat island

The most relevant variable which could better distinguish rural and urban climates is the air temperature: on average cities are warmer than their rural surroundings, and this is the so called Urban Heat Island (UHI) effect, identified as the air temperature difference between the city the close rural areas. The principal causes that lead to this phenomena are related to the urban thermal, moisture, aerodynamic and radiation features, different from the rural ones. These differences are mainly linked to the presence of buildings, which are built with materials of low permeability and high heat capacity. In addition to the urban structures (and then radiation trapping within urban canyons), pollutant emissions and anthropogenic heat release contribute to warm the urban environment.
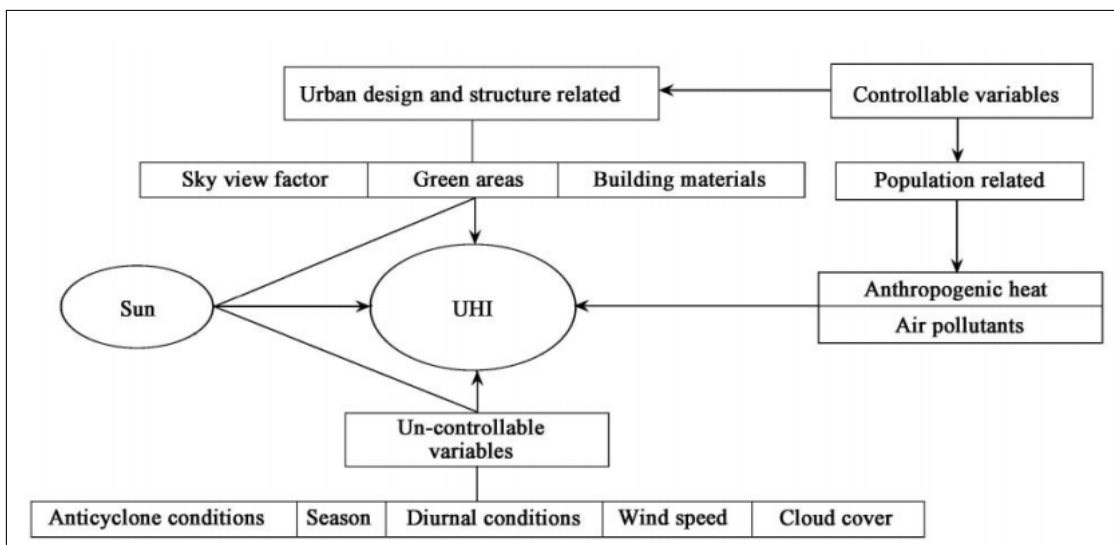
Figure 2.3: Schematic resume of the most relevant factors which contribute to the generation of the UHI [Rizwan et al., 2008].

The air temperature difference caused by the UHI effect has a diurnal and seasonal variability: several studies stated that this phenomena is greater during summer due to the higher incoming solar radiation with respect to winter, and stronger during night-time, because of the heat storage within the urban structures [Charabi and Bakhit, 2011]. For the largest cities, it is also possible to identify temperature variabilities within the same city: the greatest differences have been noticed between high residential and vegetated zones. Green areas within urban environment highly contribute in decreasing UHI effect [Arnfield, 2003]. The intensity of the effect is also related to the synoptical conditions: [Rizwan et al., 2008] reported that anticyclone conditions increase the effect, while increasing wind speed and cloud coverage can diminish the harmful effects due to the urban land use. [Tran et al., 2006] showed the positive correlation between UHI and city population. The population and its density could have both direct and indirect effect on the UHI: increasing the number of people, anthropogenic release grows, and on the other hand a wider building coverage is requested in order to host all the people living in cities. UHI may have harmful effects on urban population especially those located at lower latitudes. The thermal discomfort causes cardiovascular and respiratory problems to the citizens, in particular heat-related illness and fatalities, such as heatstrokes, heat exhaustion, heat syncope especially in the elderly and children. In the same way, respiratory problems are related to the high ozone percentage within the city induced by heat wave events and traffic emissions. A study conducted by [Heaviside et al., 2015] in the West Midlands (UK), suggests that UHI effect contributed around 50% of the total heat-related mortality during the 2003 heatwave. This phenomena will be 3 times stronger in 2080, due to the change in population, population weighting, weather conditions and assuming no change in anthropogenic heat release.

2.3.1 Mitigation strategies to reduce the UHI

It is important to outline the effects and causes of the UHI, in order to find contrasting methods able to reduce the dangerous effect of this phenomena. [Gago et al., 2013] resumes the features of the urban micro-climate into four relevant points:

- A temperature increase with respect to the rural areas;

- A reduction in the daily temperature range;

- A modified wind distribution within the city due to the friction with buildings;

- A water budget that differs from the rural one.

Principal Causes of the UHI effect

Urban Geometry	• Proprieties of urban materials • Radiation Trapping within urban canyons • Building-induced turbulence • Reduced green areas, i.e reduced evapotranspiration
Anthropogenic Heat Release	• Air conditioning systems • Vehicular circulation
Synoptic Conditions	• Heat wave periods • Clear sky and calm wind • Proximity to large water bodies and mountainous terrain

Since modification of urban features cannot take place on large scales (often the city are old or big, then a radical modification of the geometry is too difficult to act), it is necessary to identify the most important elements which affect urban temperature on local scale. Mitigation strategies need to be focused on the following features [Wong et al., 2011]: buildings, green spaces and pavements. Therefore, it is possible to set some parameters in order to evaluate the influence of the previous three elements on the urban environment:

- green areas ratio;

- sky view faction;

- building density;

- wall surface area;

- pavement area;

- albedo.

Mitigation strategies concentrate on the modification of the previous parameters, in order to change the heat surface balance and consequently reduce the UHI effect. Green roofs, cold pavements and green spaces in urban areas are all measures that are helpful to reduce the surface temperature, heat absorption and energy consumption. In fact, evapotranspiration plays a key role in cooling urban surfaces: the process consists in the release of vapor by vegetation forced by solar radiation, that

spread on the surrounding areas [Bowler et al., 2010]. Due to this phenomena, the heat stored within urban materials can diminish. Finally, the research on the mitigation strategies could be lead looking at the effect produced by the following elements:

- green areas and roofs;

- trees and vegetation;

- pavement;

- albedo.

Green areas and roofs: The combined effect of evapotranspiration and shading significantly decreases air temperature, and leads to the formation of cool island in the city, and could reflect their beneficial effects on the surrounding areas. Furthermore, it was found that green spaces reduce the temperature changes produced by building materials. The same effect is caused by green roof; the displacement of vegetation over the buildings can improve building energy performance as well as the environmental conditions of the surroundings. The second effect of green areas within the city is the deposition: pollutant are retained by vegetation.

Trees and vegetation: [Robitu et al., 2006] showed that 10% of the energy consumed in cooling building can be saved through the temperature reduction caused by vegetation. On the other hand, vegetation displacement in the urban context can negative affect the local microclimate in cold climates: in this case vegetation shading and radiation absorption increase heating costs up to 21%.

Pavement: The most relevant aspect of urban pavement which affect the local climate are the horizontal surface exposed to solar radiation, albedo and the thermal capacity. For that reason, in order to reduce the solar radiation absorbed by pavement, the use of smooth, light-colored and flat surfaces tend to be more efficient in reducing the heating effect.

Albedo: Albedo play a key role on the urban radiation budget: the incident solar radiation in absorbed and transformed into sensible heat (stored in building material and released in the atmosphere), which contribute in heating the urban environment. [Salamanca et al., 2016] analyzed the impact of the displacement of high-albedo roofs and rooftop photovoltaic panels (RPVP). This study demonstrates that the deployment of cool roofs and RPVP reduce both near-surface air temperature and cooling energy demand across all the diurnal cycle.

2.4   Models used to investigate the UHI

The study of this phenomenon could involve different spatial scales, with respect to the aim of study [Mirzaei, 2015]. Therefore, different resolutions are required to investigate the most relevant aspects. In the following paragraph a description of the models used to investigate the UHI effect is shown.

Microscale models: The basis of the development of microclimate models is the interaction between a building and its surrounding environment. These models include solar radiation and surface convection induced by buildings' surfaces. Generally the airflow features are resolved using computational fluid dynamics (CFD) models, with a grid resolution of the order of 1 meter. These models can take into account the effect of different parameters such as building features and vegetation on the surface induced convection, human health and urban ventilation. Moreover, microscale models can deal with the effect of pollutant and its diffusion within urban morphology's heterogeneities.

Building-scale models: These models deal with the energy balance for an isolated building, not taking into account the effect of the surrounding ones. The effect of the building and its energy balances (such as urban environment, ventilation, heat exchange through the walls) on the outdoor parameters could be computed. Often these kinds of model are integrated within larger scale models (such as in this current work).

Mesoscale models: These kinds of model deal with the large-scale variation of the UHI effect. Urban-scale features, urban ventilation, pollution dispersion, anthropogenic release balance and mitigation strategies could be investigated through the use of mesoscale models. They can capture the synoptic features of the region of interest and at the same time provide informations about local-scale phenomenon. Often a coupling with coarser or finer scale model is used, in order to better describe variabilities and the balances which take place within the urban environment.

Summary

In this chapter, the most relevant general features of the topic investigated in this work are presented.
Starting from explaining why it is important to study the harmful features of the UHI effect, we have the characteristics of the Urban Boundary Layer (UBL), which is the

part of the Planetary Boundary Layer influenced by urban morphology. UBL has been described focusing on:

- The different spatial scales involved (from street scale to the city scale), and the different types of UBL;

- The energy balance: it is substantially different from the energy balance taking place on rural areas, since buildings heat storage plays a key role in the heat balances;

- The nocturnal UBL: during nighttime, the UBL shows the highest differences with respect to rural areas, since a positive heat flux can be maintained.

Furthermore, the processes which lead to the UHI effect have been discussed: the UHI is principally caused by geometry and composition of urban structures, anthropogenic heat release and absence of synoptic forcing.

Several mitigation strategies can be adopted in order to contrast the harmful consequences induced by the UHI. They concern the increase of urban vegetation and the modification of the value of albedo for urban surfaces.

Finally, in order to introduce further development addressed in this thesis, the most used models commonly adopted to study the UHI have been discussed. Basically, they differ one from another for the spatial scale of interest: microscale models are used to investigate the building and street scale, building-scale models to study the interaction between a building and its surrounding area while mesoscale models to evaluate large-scale variation.

Chapter 3

Outlining the urban morphology

In the first part of this chapter, the method used to define the urban coverage within the region of interest is presented. Several methods can be used: in this work, satellite data have been combined with built digitized data in order to provide an efficient landmask. Moreover, the second part deals with the parametrizations which have been coupled with WRF to take into account the effect of buildings within the UCL: the Building Effect Parametrization [Martilli et al., 2002] and the Building Energy Model [Salamanca et al., 2010].

3.1 Parametrization of the urban morphology

One of the crucial points of the UHI modeling, is the definition of the urban features within the domain of the simulation: information on urban morphology has been identified as critical to improve modeling capacity [Masson, 2006], [Stewart et al., 2014], [Chen et al., 2011].

Moreover, since the mesoscale model has a finest resolution of 500 m, it is necessary to identify for each grid cell averaged values describing coherently the features of the buildings. Therefore, parametrizing the urban morphology is not a trivial task. In addition, another problem is linked to the lack of real data to be used within the model. The urban landscape can be created assembling from several sources, such as land-use/cover maps, building databases and satellite/lidar data [Brousse et al., 2016]. In this work, the use of satellite data has been chosen, and the urban morphology has been parametrized through the recently developed World Urban Database Access Portal Tool (WUDAPT) software (with a spatial resolution of 100 m), and later interpolated into the mesoscale model grid (with a spatial resolution of 500 m).

3.2 The WUDAPT software

3.2.1 Creating the urban landmask with WUDAPT

In order to identify a correct parametrization for the urban morphology, the World Urban Database Access Portal Tool (WUDAPT) has been used [Bechtel and Daneke, 2012], [Stewart and Oke, 2012], [Bechtel et al., 2015]. WUDAPT allows to classify urban structures into 17 different classes (Local Climate Zones,LCZ), ten of which are urban, and other seven rural (not considered in WRF landuse classification). The prototype of each class ais reported in Fig. 3.1.

At each urban climate zone (UCZ) are associated several variables (thermal coefficients, building length scales, height distribution and vegetative covering ratio) that can be chosen within a range of values established empirically. In order to capture the correct urban coverage to be implemented in the model, the following process has to be followed, as reported in WUDAPT's guide (*www.wudapt.org*):

- **Creation of the LCZ training areas:** Through the use of Google Earth Pro, LCZ polygons have been manually built for each class within the study area. This process is necessary in order to make a comparison between training areas and satellite data. Several zones are requested to represent truly the diversity of urban landscape. This process is characterizing correct landscape using photographs describing the typical land cover and building prototype associated with each LCZ. The training areas used in this work are shown is Fig. 3.2;

- **Comparison with satellite data:** Training areas need to be compared with satellite data.In order to distinguish between the different urban classes, three clear-sky and cloudless days Landstat8 satellite images (with a spatial resolution of $100\,m$) have been used in SAGA GIS software [Conrad et al., 2015]. Nine images per day have been chosen, each one representing a different wave length of the radiation reflected by the surface .
  In particular the days chosen for this work are the 18/03/213, the 16/07/2013 and the 10/06/2014: it is important to use data for several days, in order to avoid systematic errors due to a single-day analysis. SAGA GIS automatically classify the pixels in the region of interest into LCZ types, superimposing the training area scenes to the satellite data. In other words, SAGA GIS is able to detect the different features within the study area (from the satellite data), and assign to the pixels not covered with the training polygons the correct LCZ type;

- **Iteration process:** Once created the first raw classification, the LCZ map has been compared with the underlying Google Earth landscape; this is useful to

Built types	Definition	Land cover types	Definition
1. Compact high-rise	Dense mix of tall buildings to tens of stories. Few or no trees. Land cover mostly paved. Concrete, steel, stone, and glass construction materials.	A. Dense trees	Heavily wooded landscape of deciduous and/or evergreen trees. Land cover mostly pervious (low plants). Zone function is natural forest, tree cultivation, or urban park.
2. Compact midrise	Dense mix of midrise buildings (3–9 stories). Few or no trees. Land cover mostly paved. Stone, brick, tile, and concrete construction materials.	B. Scattered trees	Lightly wooded landscape of deciduous and/or evergreen trees. Land cover mostly pervious (low plants). Zone function is natural forest, tree cultivation, or urban park.
3. Compact low-rise	Dense mix of low-rise buildings (1–3 stories). Few or no trees. Land cover mostly paved. Stone, brick, tile, and concrete construction materials.	C. Bush, scrub	Open arrangement of bushes, shrubs, and short, woody trees. Land cover mostly pervious (bare soil or sand). Zone function is natural scrubland or agriculture.
4. Open high-rise	Open arrangement of tall buildings to tens of stories. Abundance of pervious land cover (low plants, scattered trees). Concrete, steel, stone, and glass construction materials.	D. Low plants	Featureless landscape of grass or herbaceous plants/crops. Few or no trees. Zone function is natural grassland, agriculture, or urban park.
5. Open midrise	Open arrangement of midrise buildings (3–9 stories). Abundance of pervious land cover (low plants, scattered trees). Concrete, steel, stone, and glass construction materials.	E. Bare rock or paved	Featureless landscape of rock or paved cover. Few or no trees or plants. Zone function is natural desert (rock) or urban transportation.
6. Open low-rise	Open arrangement of low-rise buildings (1–3 stories). Abundance of pervious land cover (low plants, scattered trees). Wood, brick, stone, tile, and concrete construction materials.	F. Bare soil or sand	Featureless landscape of soil or sand cover. Few or no trees or plants. Zone function is natural desert or agriculture.
7. Lightweight low-rise	Dense mix of single-story buildings. Few or no trees. Land cover mostly hard-packed. Lightweight construction materials (e.g., wood, thatch, corrugated metal).	G. Water	Large, open water bodies such as seas and lakes, or small bodies such as rivers, reservoirs, and lagoons.
8. Large low-rise	Open arrangement of large low-rise buildings (1–3 stories). Few or no trees. Land cover mostly paved. Steel, concrete, metal, and stone construction materials.		
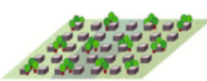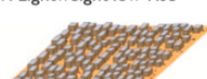
VARIABLE LAND COVER PROPERTIES

Variable or ephemeral land cover properties that change significantly with synoptic weather patterns, agricultural practices, and/or seasonal cycles.

Built types	Definition	Land cover types	Definition
9. Sparsely built	Sparse arrangement of small or medium-sized buildings in a natural setting. Abundance of pervious land cover (low plants, scattered trees).	b. bare trees	Leafless deciduous trees (e.g., winter). Increased sky view factor. Reduced albedo.
		s. snow cover	Snow cover >10 cm in depth. Low admittance. High albedo.
10. Heavy industry	Low-rise and midrise industrial structures (towers, tanks, stacks). Few or no trees. Land cover mostly paved or hard-packed. Metal, steel, and concrete construction materials.	d. dry ground	Parched soil. Low admittance. Large Bowen ratio. Increased albedo.
		w. wet ground	Waterlogged soil. High admittance. Small Bowen ratio. Reduced albedo.

Figure 3.1: The local climate zone (LCZ) classification scheme and its 17 standard classes. From [Stewart and Oke, 2012].
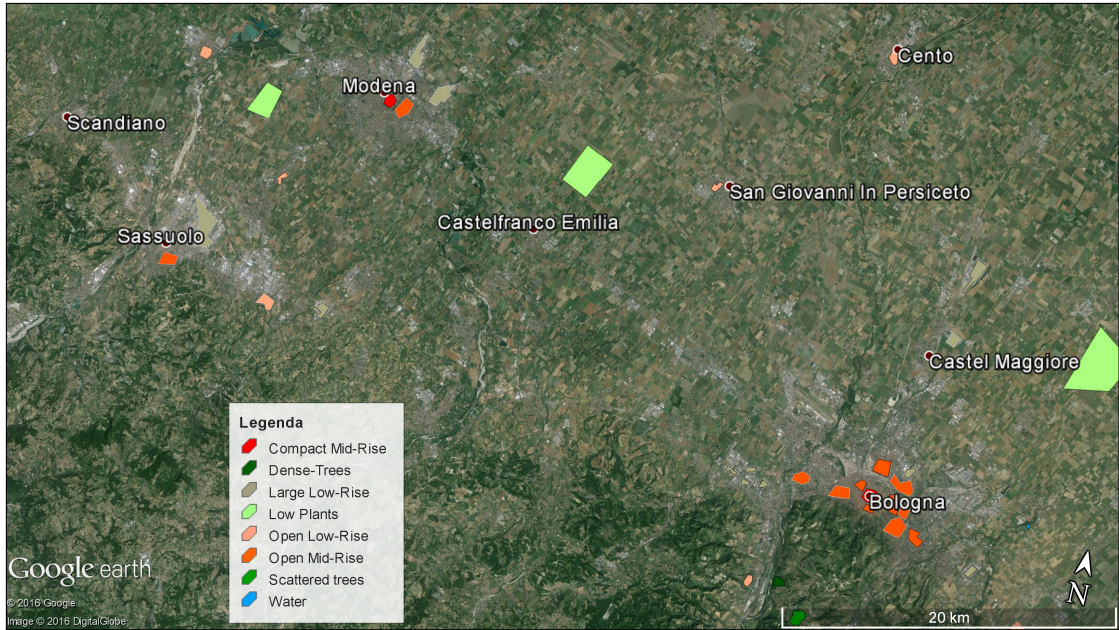
Figure 3.2: Digitized training areas for the study area considered.

refine the LCZ classification, until the comparison with the real data map will result satisfactory.

The resulting map for the study area considered (including the urban zones of Bologna, Modena, Ferrara, Reggio Emilia, Sassuolo and Imola) is shown in Fig. 3.3. The urban coverage built with WUDAPT shows that the urban coverage is 684.73 km^2; 0.93% is Compact Mid-rise (LCZ 2), 26.00% Open Mid-Rise (LCZ 5), 35.32% Open Low-Rise (LCZ 6) and 37.09% Large Low-Rise (LCZ 8). This means that there are not areas classified as Compact High-Rise (LCZ 1), Compact Low-rise (LCZ 3), Open High-rise (LCZ 4), Lightweight Low-Rise (LCZ 7) and Heavy Industry (LCZ 10).

3.2.2 Including the LCZ map into WRF

The next step, is to include the resulting urban coverage within the finest domain of the model: since the grid resolution of the WUDAPT grid is 100 m, and that one of the WRF is 500 m, an interpolation method is requested. In fact, within the same model grid cell, there are several LCZ classes, and an averaged value for the grid cell need to be identified. Therefore, has been decided to choose the most present LCZ value within each cell (following the guide provided by [Martilli et al., 2016]). This means that, for the calculation of the atmospheric parameters, the mesoscale model will consider the values belonging to the LCZ with the high coverage rate in the grid cell considered. Fig.3.4 shows the resulting LCZ classification superimposed on the
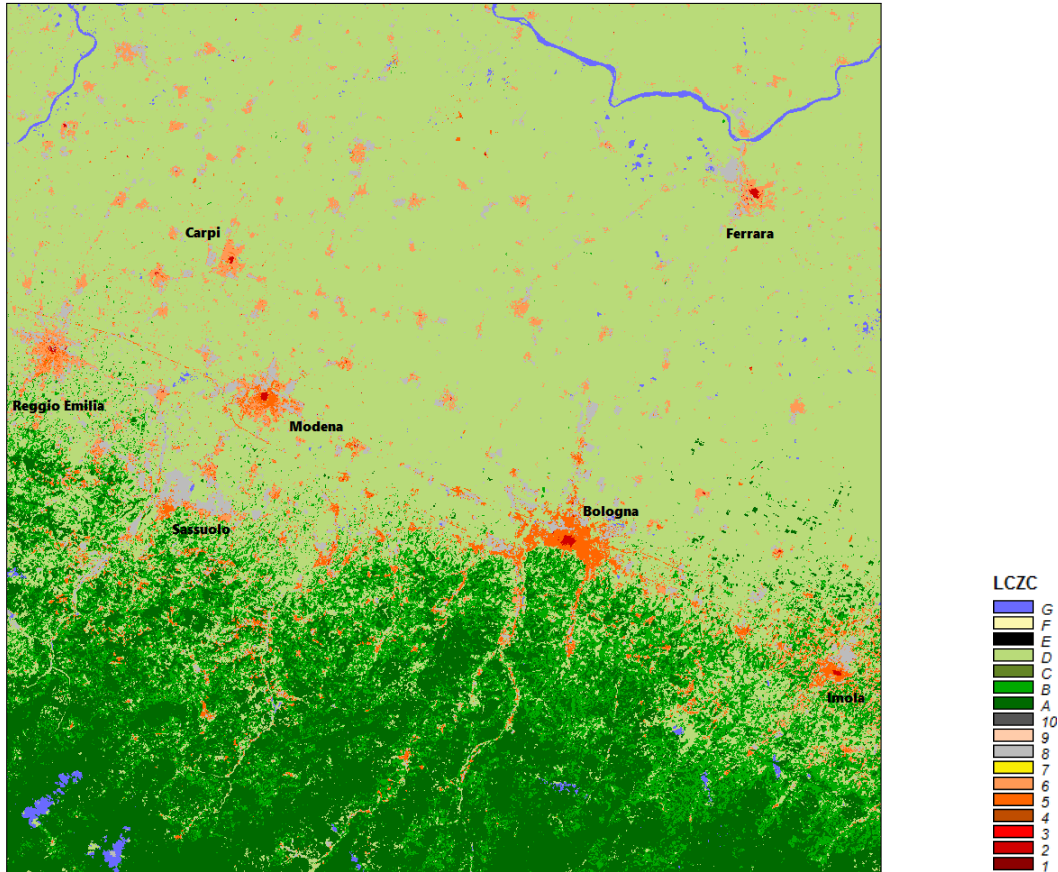
Figure 3.3: Urban morphology defined through WUDAPT; classes from 1 to 10 are urban type, while the others from A to G are rural/water types.

Google Earth map of the study area.

The final result, shows that the urban coverage is 400.25 km^2; 1.2% is Compact Mid-rise (LCZ 2), 23.05% Open Mid-Rise (LCZ 5), 33.35% Open Low-Rise (LCZ 6) and 42.35 % Large Low-Rise (LCZ 8).

3.3 Comparison between WUDAPT and WRF urban landmasks

The interpolation into the finest grid on the mesoscale 500 m leads to a loss of information. In this section, a comparison between the two landuse is performed.
In Tab. 3.1 the percentages of coverage of the different LCZ areas are shown. The value at the bottom of the table refers to the fraction of urban coverage with respect to the total surface of the domain. Results show an higher rate of coverage for the WUDAPT urban landscape (7.31% vs 4.78%): this a reasonable result, because inter-
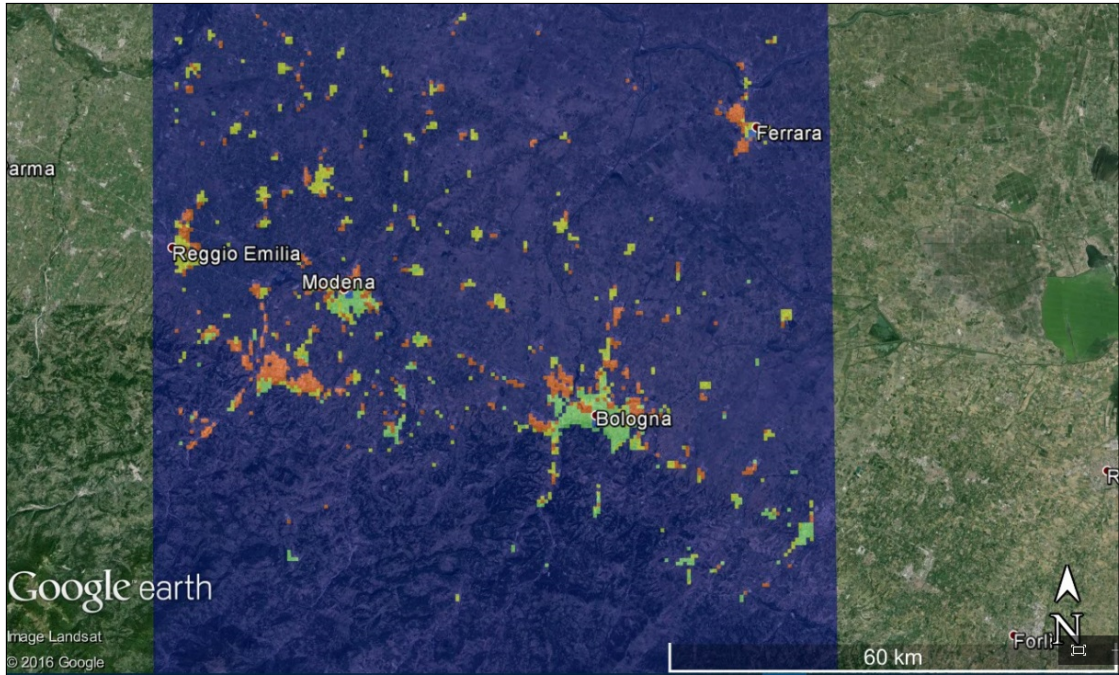
Figure 3.4: Urban morphology for the mesoscale model projected into Google Earth map. Each pixel has a resolution of 500 m. Cyan pixels identify LCZ 3, green pixels LCZ 5, yellow pixels LCZ 6 and orange pixels LCZ 8.

polating the WUDAPT grid into the coarse grid, small towns cannot be detected during interpolation. When the urban pixels are less dense, the interpolation through the most present value for each grid cell "chooses" a rural cell even though an urban one.

Checking class per class, LCZ 2 and LCZ 8 results most present in the mesoscale grid with respect to the finest one. Since in the domain considered city centers and industrial areas are the most clustered in defined zones, they are easier to be detected by the interpolation, then their percentage of covering is higher in the coarser grid. On the other hand, LCZ 5 and LCZ 6 are more scattered and surrounded by rural areas than the first two, so the most present value within the mesoscale pixels is rural.

Focusing on the city of Bologna, the resulting urban landuse for the coarser grid often covers rural surround areas, better distinguished by the WUDAPT grid. As shown in Fig. 3.5, rural areas within the urban environment are not detected: since the most present value within each pixel of 500 m of resolution is always urban, all WRF cells for (and close) the city of Bologna have been detected as urban.

Urban Coverage Percentage		
	WUDAPT (%)	**WRF (%)**
LCZ 2	0.93	1.2492
LCZ 5	26.66	23.05
LCZ 6	35.32	33.35
LCZ 8	37.09	42.35
Urban Coverage	7.31	4.78

Table 3.1: Comparison between the urban coverage percentage between WUDAPT grid (100 m of resolution) and WRF grid (500 m of resolution).
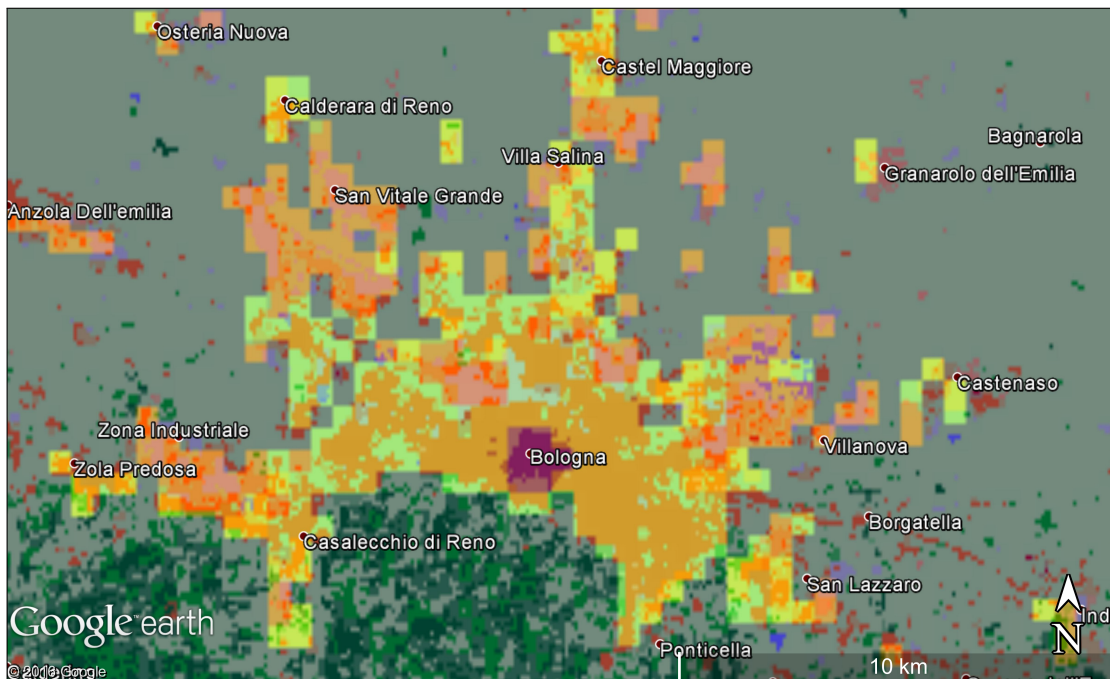
Figure 3.5: Comparison between WUDAPT grid (opaque) and WRF grid (transparent) for the city of Bologna. The larger spread of the coarser one even in rural areas is evident.

33

3.4 Definition of the urban parameters

After the classification of the urban coverage into LCZ, it is necessary to assign to each class its own parameters. The variables requested, different for each class are: fraction of urban landscapes which does not have vegetation, heat capacity, thermal conductivity, emissivity, roughness length and albedo for roof, ground and building wall, height distribution for the buildings (values are computed by steps of 5 meters), street and buildings width. Values used in this work are shown in Tab. 3.2. Since most of the parameters are not available for the study area, input data for the simulations have been leaved as default. Variations with respect to default values concerns the thermal coefficients for the LCZ 2 and LCZ 5: the most employed material for roofs and walls is solid brick [Oke, 1987]. At the same time, given that most of ground is made of asphalt, also the characteristic values of this material has been set as input for the simulations. Finally, the last values which have been changed from the default setting are the height of the buildings: through the analysis of the height of building belonging to the city center (free data available on the website *www.dati.comune.bologna.it*), and given that LCZ 2 and LCZ 5 assume on average the same height, the mean percentage of buildings in the same range of height for each 5 meter level has been computed.

Table 3.2: Thermal coefficients and length scales for the buildings for each UCZ.

	UCZ 2	UCZ 5	UCZ 6	UCZ 8
Urban Fraction	1	0.7	0.65	0.85
Roof Heat Capacity $[\frac{J}{m^3K}]$	1.37×10^6	1.37×10^6	1.44×10^6	1.80×10^6
Roof Thermal Conductivity $[\frac{J}{msK}]$	0.83	0.83	1.00	1.25
Roof Albedo	0.20	0.20	0.20	0.20
Roof Emissivity	0.90	0.90	0.90	0.90
Roof Roughness Length $[m]$	0.01	0.01	0.01	0.01
Ground Heat Capacity $[\frac{J}{m^3K}]$	1.94×10^6	1.94×10^6	1.47×10^6	1.80×10^6
Ground Thermal Conductivity $[\frac{J}{msK}]$	0.75	0.75	0.60	0.80
Ground Albedo	0.10	0.10	0.10	0.10
Ground Emissivity	0.95	0.95	0.95	0.95
Ground Roughness Length $[m]$	0.01	0.01	0.01	0.01
Wall Heat Capacity $[\frac{J}{m^3K}]$	1.37×10^6	1.37×10^6	2.0×10^6	1.80×10^6
Wall Thermal Conductivity $[\frac{J}{msK}]$	0.83	0.83	1.25	1.25
Wall Albedo	0.20	0.20	0.20	0.20
Wall Emissivity	0.90	0.90	0.90	0.90
Road Width $[m]$	10	33.3	12.4	32.5
Buildings Width $[m]$	10	10	10.5	28.8
Buil. % with h < 5 m	\	\	40	35
Buil. % with 5 <h< 10 m	20	20	40	65
Buil. % with 10 <h< 15 m	30	30	20	\
Buil. % with 15 <h< 20 m	20	20	\	\
Buil. % with 20 <h< 25 m	20	20	\	\
Buil. % with 25 <h< 30 m	10	10	\	\

3.5 Parametrization of the effect of Urban Morphology on near surface atmosphere

After the discussion on the methods used to parametrize the presence of buildings and urban structures within the study area, the main features used to take into account the effect of the urban landmask on the atmospheric dynamics is presented. The two schemes used in this work are the Building Effect Parametrization (BEP) [Martilli et al., 2002] and the Building Energy Mode (BEM) [Salamanca et al., 2010]. While BEP takes into account the influence of buildings and urban heterogeneities on the UCL, BEM computes heat fluxes between the indoor and outdoor sides of each building. It also takes into account the presence of air conditioning systems (ACS),

windows and equipment inside the buildings' rooms.

In the next two sections these two schemes are discussed.

3.5.1 The BEP scheme

This multi-layer parametrization links the urban-scale phenomenon ($10\,\text{m} - 10\,\text{km}$) with the meso-scale features ($10 - 100\,\text{km}$), with the aim to compute the effect of the smaller scale on the mesoscale circulation. Since the horizontal dimensions of the domain are on the order of mesoscale, the horizontal grid resolution cannot be such detailed to resolve completely the urban heterogeneities. This leads to the fact that urban morphology effect on the PBL is not completely resolved, but need to be averaged with respect to the resolution of the model. Moreover, parameterizing such turbulent and complex flows, it is not possible to use the traditional constant-flux layer approximation through the Monin-Obukhov similarity theory within the RSL. Since the meso and the urban scales have different dimensions, but they exchange information each other, an average and interpolation process is necessary.

The mesoscale model

The following conservation equations represent the mesoscale features of the UBL dynamics. Capital letters denote Reynolds averaged variables, while small letters represent the respective turbulent fluctuation (i. e. if $\tilde{A}$ is a variable, it can be seen as $\tilde{A} = A + a$, where A is the Reynolds averaged variable, and a' its respective fluctuation):

- Mass:

$$\frac{\partial \rho U_i}{\partial x_i} = 0$$

  Supposing the anelastic approximation.

- Momentum:

$$\frac{\partial \rho U_i}{\partial t} = \frac{\partial P}{\partial x_i} + F_i$$

  with

$$F_i = \frac{\partial \rho U_i U_j}{\partial x_j} - \frac{\partial \rho \overline{u_i w}}{\partial z} - \rho \frac{\theta'}{\theta_0} g \delta_{i3} - 2\varepsilon_{ijk}\Omega_j \left(U_k - U_k^G\right) + D_{Ui}$$

  where the terms on the right hand side represent respectively the mean transport, the vertical turbulent transport (w refers to the vertical component of turbulent momentum flux), the buoyancy ($\theta' = \theta - \theta_0$, where θ identifies the potential temperature) with the Boussinesq approximation, the Coriolis force (U_k^G

36

is the k-component of the geostrophic wind), and the last term (D_{Ui}) resumes all the forces induced by the interaction with the urban morphology.

- Energy:

$$\frac{\partial \rho \theta}{\partial t} = \frac{\partial \rho \theta U_i}{\partial x_i} + D_\theta - \frac{1}{C_p}\Big(\frac{P_0}{P}\Big)^{\frac{R}{C_p}}\frac{\partial R_{lw}}{\partial z}$$

where C_p is the specific heat at constant pressure, R the gas constant, P_0 the reference pressure and R_{lw} is the longwave radiation flux. D_θ takes into account of the effect of urban surfaces on the potential temperature budget.

- Air Humidity:

$$\frac{\partial \rho H}{\partial t} = \frac{\partial \rho H U_i}{\partial x_i} - \frac{\partial \rho \overline{wh}}{\partial x_i} + D_H$$

where H is the mean absolute humidity and h its turbulent fluctuation. D_h takes into account of the effect of the latent heat from surfaces on the humidity balance.

The K-theory approach to parametrize the vertical fluxes is used. If A is the mean part of a given variable and a its turbulent component, the turbulent vertical transport is computed as:

$$\overline{wa} = -K_z\frac{\partial A}{\partial z}$$

where K_z is the vertical diffusion coefficient. In order to calculate K_z, two equation are requested: one expressing the dependence of the diffusion equation on the kinetic energy (E) and length scale (l_k), and a prognostic equation where the dependence between E and l_k is considered. These two equations are:

$$K_z = C_k l_k E^{1/2}$$

$$\frac{\partial \rho E}{\partial t} = -\frac{\partial \rho U_i E}{\partial x_i} - \frac{\partial \rho \overline{we}}{\partial z} + \rho K_z(l_k, E)\Big[\Big(\frac{\partial U_x}{\partial z}\Big)^2 + \Big(\frac{\partial U_y}{\partial z}\Big)^2\Big] - \frac{g}{\theta_0}\rho K_z\frac{\partial \theta}{\partial z} - \rho C_\varepsilon\frac{E^{3/2}}{l_\varepsilon} + D_E$$

where the third and fourth terms on the right hand side are respectively the shear and buoyant production terms, the fifth is the dissipation term and the last takes into account of the presence of the buildings. The first equation is the $k - l$ closure scheme based on [Bougeault and Lacarrere, 1989]. l_k and l_ε are computed taking into account of the maximum distance that an air parcel can reach due to buoyancy effect up and down.

The Urban Model

As said before, BEP works with two different grids of different scales: the mesoscale and the urban-scale. They interact between each other, with the smaller one giving feedbacks to the coarser grid and vice versa. The urban scale grid used in BEP is able to represent within the mesocale grid the vertical features of the urban morphology, in order to take into account the sink of momentum and the source of heat fluxes due to the presence of buildings. However, this smaller grid is not able to represent exactly the urban morphology, so mean vertical and horizontal parameters for each cell are needed as input. These parameters are: street width (W), building width (B), mean height (h) and height probability distribution ($\gamma(h)$).
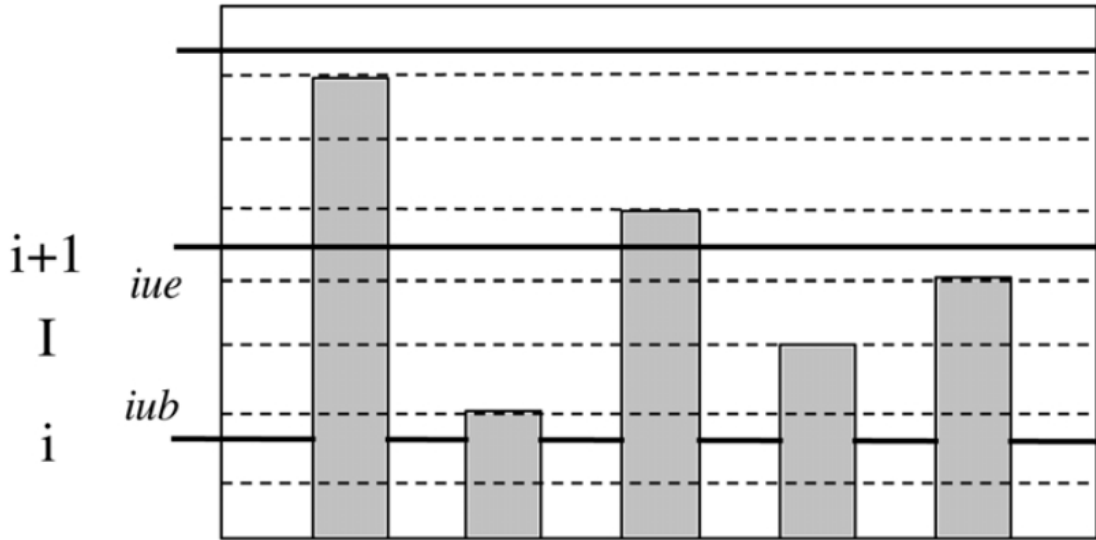
Figure 3.6: Representation of the urban grid (dashed lines) and mesoscale grid (solid lines). iub and iue are the first and the last urban levels within the mesoscale level I (from [Martilli et al., 2002]).

By now, it is important to take into account the interaction between the two grid, then the IU index refers to the urban grid, I to the mesoscale grid (at the same level of the horizontal face of the cell), while iu and i refers to the value in the center of the cell respectively for the urban and mesoscale grid. Now, the area fraction occupied by building for each vertical level z_{iu} (over the ground) is computed, both for horizontal and vertical direction:

$$S^H_{iu=1} = \frac{W}{W+B} S^H_{tot}$$

$$S^H_{iu>1} = \frac{W}{W+B} \gamma(z_{iu}) S^H_{tot}$$

38

$$S_{IU}^{V} = \frac{\Delta z_{IU}}{W+B}\Gamma(z_{iu+1})S_{tot}^{H}$$

where S_{tot}^{H} is the total horizontal surface of the grid cell, Δz_{IU} is the grid spacing (could vary with the height) and $\Gamma(z_{iu+1}) = \sum\limits_{ju=iu}^{nu}\gamma(z_{ju})$ is the probability to have building higher of equal than z_{iu+1}. The computation could be performed for different direction, in order to take into account of the different directions of the incident wind. In our case, just the N-S and W-E directions are considered.

Effect of the Urban Morphology on the Airflow

In the equations for the mesoscale model, a D_A term is added, in order to consider the effect of buildings and urban surface on the airflow. The effects considered in this parametrization are:

- loss of momentum due to the drag induced by buildings;

- transformation of mean kinetic energy into turbulent kinetic energy;

- shadowing and radiation trapping effects within urban canyons.

Turbulent Momentum Flux   The turbulent momentum flux which originates due to the drag of horizontal surfaces for each level iu is:

$$\vec{F}u_{iu}^{H} = -\rho\frac{k^2}{\left[ln\left(\frac{\Delta z_{IU}}{2z_0 iu}\right)\right]^2}f_m(\frac{\Delta z_{IU}}{2z_{0iu}},Ri_B)|U_{IU}^{H}|\vec{U}_{IU}S_{iu}^{H}$$

where U_{IU}^{H} is the horizontal component of the wind, f_m an empirical function dependent from the bulk Richardson number computed at level IU ($Ri_B = \frac{-g}{T_{IU}}\frac{z\Delta\theta_v}{(U_{IU}^{H})^2}$, where θ_v is the virtual potential temperature), k is the Von Karman constant and z_{0iu} is the roughness length at the level iu. The turbulent momentum flux due to the vertical surface is computed as:

$$\vec{F}u_{iu}^{V} = -\rho C_{drag}|U_{IU}^{V}|\vec{U}_{IU}^{V}S_{IU}^{V}$$

where $\vec{U}_{IU}^{V}$ is the wind speed perpendicular to the vertical surfaces and C_{drag} is the drag coefficient equal to 0.4 (computed from measurements in wind tunnel).

Turbulent Temperature Flux   As in the computation of the momentum flux, the sensible heat turbulent flux due to the horizontal surfaces is calculated as:

$$F\theta_{iu}^H = -\rho \frac{k^2}{\left[ln\left(\frac{\Delta z_{IU}}{2z_0iu}\right)\right]^2} f_h\left(\frac{\Delta z_{IU}}{2z_{0iu}}, Ri_B\right)|U_{IU}^H|\Delta\theta S_{iu}^H$$

where $\Delta\theta$ is the temperature difference between the horizontal surface and the air. For the vertical temperature it is not possible to use the previous equation, because this kind of fluxes depends on the temperature differences between air and walls and on the street direction. Taking into account just of the N-S direction of the street the flux of sensible heat from walls is given by:

$$F\theta_{iu}^V = -\frac{\eta}{C_p}\left[\left(\theta_{air} - \theta_{IU}^{WEST}\right) + \left(\theta_{air} - \theta_{IU}^{EAST}\right)\right]S_{IU}^V$$

where η is an empirical variable depending on the horizontal wind speed at the considered level.

Turbulent Kinetic Energy Flux In the equation for the turbulent kinetic energy, a parametrization for the buoyancy and shear therms is required. These terms are not computed as fluxes, because of the TKE is a volumetric variable. Multiplying the shear and buoyancy production terms for the volume of the respective grid cell, the resulting term is:

$$Pr_{iu}^H = \left[-\frac{\left(\frac{Fu_{iu}^H}{\rho S_{iu}^H}\right)^{3/2}}{k\frac{\Delta z_{IU}}{2}} + \frac{g}{\theta_0}\frac{F\theta_{iu}^H}{\rho S_{iu}^H}\right]S_{iu}^H\Delta z_{IU}\rho$$

.

for the horizontal direction, while for the vertical direction:

$$Fe_{IU}^V = C_{drag}|U_{IU}^V|^3 S_{IU}^V$$

Computation of the urban morphology effect terms

Finally, one calculated the turbulent fluxes for momentum, temperature and kinetic energy, the inclusion of these terms into the equation is needed. The term reflecting the urban morphology effect are the D_A terms appearing in the previous mesoscale equations. Then, adding the vertical and horizontal terms and dividing for the volume of the mesoscale grid cell, the resulting term is:

$$D_{A_I} = \frac{Fa_I^H + Fa_I^V}{V_I}$$

where all the variables are calculated for the mesoscale grid, i.e. an averaging process for the urban scale grid cells within the same mesoscale grid cell is necessary.
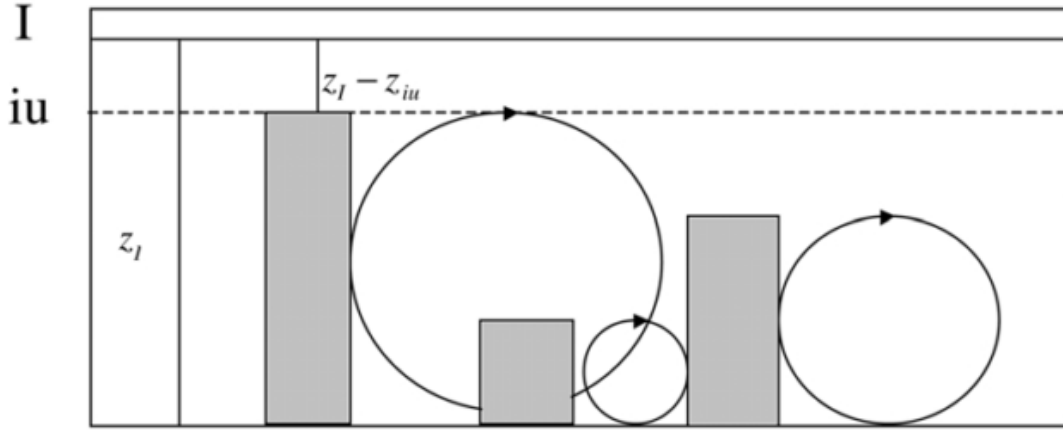
Figure 3.7: Representation of the typical turbulent length scales within the urban canopy from [Martilli et al., 2002].

In order to calculate numerically the vertical variation of the turbulent fluxes, the discretization of the mesoscale grid is used, but only for the cells not occupied by buildings:

$$\frac{\partial \rho \overline{wa}}{\partial z} = \frac{1}{V_I^A}(\rho \overline{wa}_i S_i^A - \rho \overline{wa}_{i+1} S_{i+1}^A)$$

Computation of the turbulent length scales

Within a urban parametrization, it is necessary to take into account of the effect of the buildings on the length scale. The l_k and l_ε length scales are values required to compute the turbulent kinetic energy dissipation term and the diffusion terms through the $k-l$ closure (and the respective prognostic equation). The length scales parametrization presented here is a modification of that one proposed by Bougeault and Lacarrere (1989). In order to evaluate this parameter, as scale dimension of building the height has been chosen. Since the buildings does not have the same height within a grid cell, the following assumption is taken into account: while the lower levels can be influenced by building of all height, at higher levels the predominant vortices are induced by only the higher buildings. Finally, the length scale for a level I is computed as:

$$\frac{1}{l_{b\,I}} = \sum_{iu=ibu}^{nu} \gamma(z_{iu})\frac{1}{z_{iu}}$$

where ibu is the lowest level of the urban cell within the considered mesocale cell, and nu is the highest level of the urban grid. This new length scale is added to

41

the traditional length scale computed in absence of the urban morphology:

$$\frac{1}{l} = \frac{1}{l_{old}} + \frac{1}{l_b}$$

This sum takes place both for the diffusion and dissipation length scales, and since the value is every time positive acts increasing the dissipation term. The second modification is for the height above the ground. While in a flat terrain case this value is simply the distance between the center of the grid cell and the ground, in the urban case it is necessary to compute an average height for the grid cells, weighting over the fraction filled with building and the fraction of canyon floors:

$$l_{ground}|_I = \frac{1}{(\frac{W}{B+W})\frac{1}{z_I} + \frac{B}{B+W}\sum_{iu=1}^{ibu-1} \gamma(z_{iu})\frac{1}{(z_I-z_{iu})}}$$

3.5.2 The BEM scheme

The model [Salamanca et al., 2010], deals with the parametrization of the heat exchange between the inner side of a building and the surrounding atmosphere. The diffusion of heat through walls, floors and roofs, the natural ventilation, the radiation exchanged between the indoor surfaces, the anthropogenic heat release (by occupants and equipment) and the energy consumption due to ACS are taken into account. Moreover, it is coupled with the BEP scheme, explained in the previous chapter: since an averaged value for each mesoscale cell is requested, BEM computes the values of each variable for every building, and based on this provides the requested averaged values for the grid cell. More precisely, BEP provides to BEM the outdoor air temperature, humidity, and incident radiation as boundary conditions for the computation of the balances which take place within the buildings. On the other hand, BEM gives to BEP the buildings materials temperature, and all the heat fluxes linked to all the processes which take place due to the interaction between buildings and the surrounding atmosphere.

Parametrization of the interaction between a building and the surrounding atmosphere

With the aim to compute the effect of a building within the atmospheric context, a building included in its neighborhood is considered as a pile of boxes, with each box representing a singular floor. The meaning and unit of measurement for each variable is reported in Tab. 3.3 at the end of the chapter.

Indoor temperature and humidity The equations describing the temporal variation of room temperature and humidity are:

$$Q_B \frac{dT_r}{dt} = H_{in} - H_{out}$$

$$l\rho V_B \frac{dqv_r}{dt} = E_{in} - Eout$$

where:

- $Q_B = \rho C_P V_B$ is the heat capacity, and V_B the total volume of air within the room;

- l is the total latent heat of evaporation per mass unit.

- $H_{in} = \sum_j A_j^{wind} h_{wind,j}(T_{wind,j} - T_r) + \sum_i A_i^{wall} h_{wall,i}(T_{wall,i} - T_r) +$
  $+ (1 - \beta)C_p\rho V_a(T_a - T_r) + A_f q_E + A_f P\Phi_P q_{hs}$:
  the first term represents the heat exchange between windows and indoor air, and the second between all internal surfaces (walls, ceiling, pavements) and indoor air. The thirdf is the sensible heat exchange through ventilation, while the last two terms correspond to the internal sensible heat generated from equipment and occupants. The heat generated from occupants and equipment is supposed to be distributed isotropically in the interior.

- $E_{in} = (1-\beta)l\rho V_a(q_{Va} - q_{Vr}) + A_f P\Phi_P q_{hl}$. The first right-hand term is the vapor through ventilation, while the second one is the evaporation from occupants.

- H_{out} and E_{out} refer to the sensible and latent heat released by ACS.

The heat diffusion equation describing the temporal variation of temperature between the outdoor and indoor sides of the walls is:

$$\frac{\partial T_{wall}}{\partial t} = \frac{\partial}{\partial x}\left(K_s \frac{\partial T_{wall}}{\partial x}\right)$$

computed numerically for several layers within the wall. Neglecting the latent heat transport through walls, the boundary condition at the indoor and outdoor surfaces in obtained solving an energy budget equation:

$$\frac{\partial T_{wall}|_{surface}}{\partial t} = \frac{1}{\Delta x}\left(C_s^{-1}HF - \frac{\partial}{\partial x}K_s\frac{\partial T_{wall}|_{surface-1}}{\partial x}\right)$$

here Δx is the depth of each layer, $HF = (1-alb)R_s + \varepsilon Rl - \varepsilon\sigma T_{wall}^4|_{surface} + H$. C_s ($JK^{-1}m^{-3}$) is the specific heat of the first layer and $H = h(T_r - T_{wall})$ is the sensible heat flux entering in the wall surface from the outdoor/indoor air.

Window Temperature Since each window is very thin, the temperature difference between the two sides of the window is neglected. Besides, even the heat absorption is supposed to be equal to zero, so in order to compute the window temperature thee following budget equation is computed:

$$\rho_{wind} C_{wind} \Delta_{wind} \frac{dT_{wind}}{dt} = \Phi$$

where ρ_{wind}, C_{wind} ($JK^{-1}m^{-2}$) and Δ_{wind} are respectively the density, the heat capacity and the thickness of the glass and

$$\Phi = \varepsilon_{wind}(Rl_{out} - \sigma T^4_{wind}) + H_{out} + \varepsilon_{wind}(Rl_{in} - \sigma T^4_{wind}) + H_{in}$$

is the flux balance of energy (Wm^{-2}) where the H terms represent the sensible heat fluxes from the outdoor and indoor sides of the window and the Rl terms are the incoming longwave radiation from both sides of the window. The radiation terms appearing in this equation take into account even of the indirect radiation, i.e. the radiation trapped within the urban canyons.

Shortwave radiation It is supposed that the radiation reaching the interior surfaces from the windows is uniformly distributed. At the same time, the reflection of radiation is isotropic in all directions. Since each room has windows, the total solar radiation is the sum of the radiation coming directly from windows and the radiation reflected by the interior surfaces of the same room. Therefore, the radiation reaching the wall i is given by:

$$Rs_i = Rs + \sum_{j \neq i} alb_j Rs_j \Psi_{ji}$$

$$\Psi_{ji} = \frac{A_j f_{ji}}{A_i} = f_{ij}$$

$$alb_j = alb_{wall,j}(1 - \alpha_{wind,j}) + alb_{wind,j}\alpha_{wind,j}$$

This is a set of six equation (each one for a surface inside the room, the four walls, the ceiling and the pavement), where f_{ij} is the view factor of the wall i with respect to the wall j.

Long-wave radiation The long-wave radiation for the wall i belonging to the interior side of the room, is the sum of all the reflection and emission terms from the other walls of the same room. If $\varepsilon^S_j = \varepsilon_{wall,j}(1 - \alpha_{wind,j})$ is the emissivity of the wall i weighted over the surface not cover with windows, $\varepsilon^W_j = \varepsilon_{wind,j}\alpha_{wind,j}$ is the emis-

sivity of the surfaces covered by windows, the incoming long-wave radiation for the wall i is computed as:

$$Rl_i = \sum_{i \neq j} \sigma \Phi_{ji} \left(\varepsilon_j^S T_{wall,j}^4 + \varepsilon_j^W T_{wind,j}^4 \right) + \sum_{i \neq j} \left(1 - \varepsilon_j^S - \varepsilon_j^W \right) Rl_j \Phi_{ji}$$

as for the case of the short-wave radiation, this balance is computed for all the six walls of the same room.

Heat balance for air conditioning systems The following parametrization of the ACS effect on the release of sensible heat can be applied to both the equipment sensible heat release and the air conditioned latent heat release. The computation deals with the term H_{out} appearing on the equation used before for the calculation of the inner room temperature. Is has been assumed that ACS has a target temperature T_{target} and a gap of comfort ΔT where the indoor temperature is forced to lie inside the gap. Assuming that at time n the air conditioning is not used, then $H_{out} = 0$, and the temperature at time $n+1$ (T^P) discretizing the equation for the calculation of the indoor temperature is:

$$T^P = \frac{\Delta t}{Q_B} H_{in}^n + T^n$$

Three different patterns are possible, depending on the value assumed by T^P:

- $|T^P - T_{target}| < \Delta T$. In this case the indoor temperature belong to the gap, then $H_{out}^n = 0$ and $T^{n+1} = T^P$.

- $T^P - T_{target} > \Delta T$. The indoor temperature is bigger than the sum of the target temperature and the comfort gap. The sensible heat released is computed as:

$$H_{out}^n = H_{in}^n - \frac{Q_B}{\Delta t} (T_{target} + \Delta T - T^n)$$

since the air conditioned systems have an upper limit for its efficiency, called δ_{AC}, if $\left| \frac{H_{out}^n - H_{in}^n}{Q_B} \right| > \delta_{AC}$ the value of the released sensible heat is calculated as:

$$H_{out}^n = H_{in}^n + \delta_{AC} Q_B$$

with $H_{out}^n > H_{in}^n$. Finally, the temperature at time $n+1$ is calculated as:

$$T^{n+1} = \frac{\Delta t}{Q_B} (H_{in}^n - H_{out}^n) + T^n$$

- $T^P - T_{target} < \Delta T$. The indoor temperature is lower than the sum of the target temperature and the comfort gap. The sensible heat released is computed as:

$$H_{out}^n = H_{in}^n - \frac{Q_B}{\Delta t}(T_{target} - \Delta T - T^n)$$

even in this case, the heating system has an upper limit for the efficiency, called δ_{HS}. If $\left|\frac{H_{out}^n - H_{in}^n}{Q_B}\right| > \delta_{HS}$ the value of the released sensible heat is calculated as:

$$H_{out}^n = H_{in}^n - \delta_{HS}Q_B$$

with $H_{out}^n < H_{in}^n$. The temperature at time $n+1$ is calculated as:

$$T^{n+1} = \frac{\Delta t}{Q_B}(H_{in}^n - H_{out}^n) + T^n$$

this parametrization force the indoor temperature to stay always in the comfort range. This forcing is reflected in the heat released outdoor.

3.6   Rooftop photovoltaic panels parametrization

In this work, the effect of rooftop photovoltaic panels (RPVP) deployment has been tested. RPVP parametrization is based on the scheme proposed by [Masson et al., 2014] and [Salamanca et al., 2016]; since in BEP-BEM the dependence from the roof's inclination is neglected, the same happens also for RPVP, that in this model are assumed to be parallel and attached to the roofs. Moreover, we assume that RPVP cannot conduct heat, so the Fourier law for the heat conduction is neglected. In addition, in this parametrization the fraction of coverage is taken into account: for the fraction not covered with RPVP, the normal heat exchange balance is computed, while for the covered part the following method is used. Since the model employed is a mesoscale model and the grid resolution cannot resolve exactly the heterogeneity of buildings, an averaged sensible heat exchange balance is computing, weighting the variables involved over the fraction of roof covered and not covered by RPVP. The sensible heat flux balance is parametrized as follows (Fig. 3.8):

$$(1 - \alpha_{PV})SW_{sky}^{\downarrow} + LW_{sky}^{\downarrow} - LW_{PV}^{\uparrow} + LW_{roof}^{\uparrow} - LW_{PV}^{\downarrow} = E_{PV} + H$$

Where, with all the variable expressed in W/m^2:

- $SW_{sky}^{\downarrow}$ is the upcoming solar radiation;
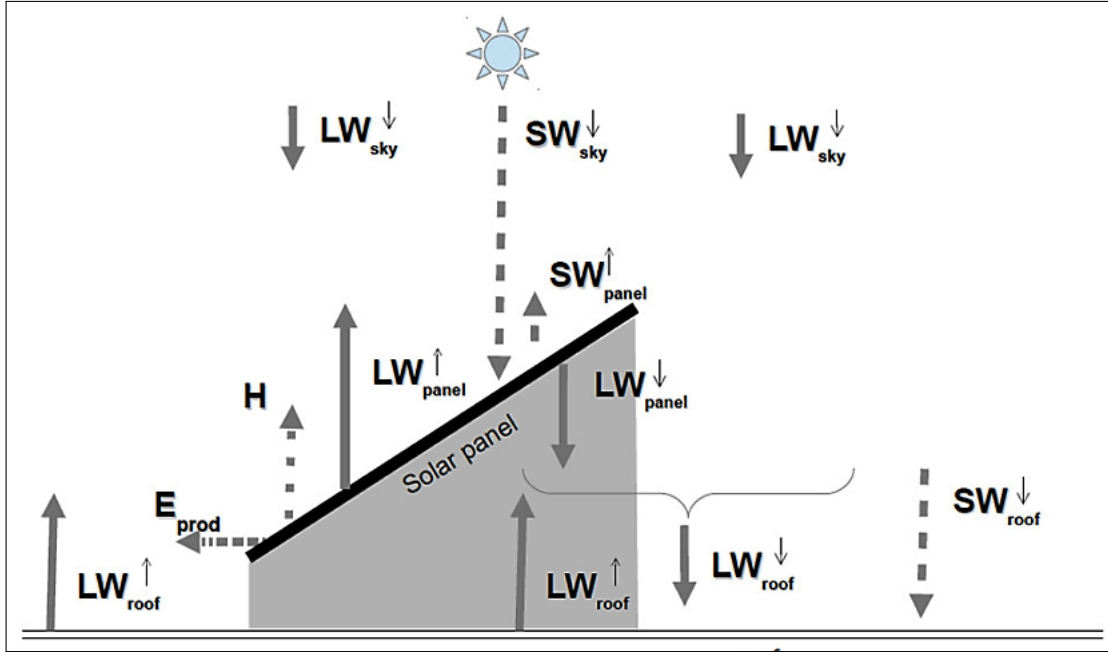
Figure 3.8: Schematic diagram of the energy balance of the solar panel and its impact on radiation received by the roof. From [Masson et al., 2014]

- $\alpha_{PV} SW^{\downarrow}_{sky}$ is the solar radiation reflected by the RPVP. $\alpha_{PV} = 0.11$ is the RPVP albedo;

- $LW^{\downarrow}_{sky}$ is the upcoming long-wave radiation;

- $LW^{\uparrow}_{PV} = \varepsilon_{PV} \sigma T^4_{PV} + (1 - \varepsilon_{PV}) LW^{\downarrow}_{sky}$ is the outgoing longwave radiation emitted by the RPVP. $\varepsilon_{PV} = 0.93$ is the RPVP emissivity;

- $LW^{\uparrow}_{roof}$ is the outgoing long-wave radiation emitted by the roof;

- $LW^{\downarrow}_{PV}$ is the long-wave radiation flux gained by the roof coming from the PV panel. Under the hypothesis that the temperature of the panel is approximately equal to the air temperature of the first layer above the roof, it is parametrized as $LW^{\downarrow}_{PV} = \sigma T^4_{air}$;

- E_{PV} is the total energy captured from the RPVP and converted in electricity. Since the RPVP are more efficient at 25 °C than at higher or lower temperatures, the energy production is computed as:
$E_{PV} = eff_{pv} \times SW^{\downarrow}_{sky} \times \min(1, 1 - 0.005 \times (T_{PV} - 298.15))$,
where the surface temperature of the RPVP is computer as $T_{PV} = T_{air} + 0.05 \times SW^{\downarrow}_{sky}$. $eff_{pv} = 0.15$ is the efficiency of a typical monocrystalline PVP.

- H is the outgoing sensible flux from the RPVP to the atmosphere.

Finally, taking into account the presence of RPVP over the roofs, the radiative contribution to the energy balance on the roofs without RPVP coverage for the longwave and shortwave components is computed as follows:

$$SW_{roof}^{\downarrow} = (1 - f_{PV}) \times SW_{sky}^{\downarrow}$$

$$LW_{roof}^{\downarrow} = (1 - f_{PV}) \times LW_{sky}^{\downarrow} + f_{PV} \times LW_{PV}^{\downarrow}$$

where f_{PV} is the fraction of the roof covered by the solar panels.

Table 3.3: List of symbols used in BEM

	List of symbols for BEM
$alb_{wall,j}$	albedo of the indoor surface of the wall j
A_f	floor area (m^2)
A_i^{wall}	area of the wall i (m^2)
A_j^{wind}	area of windows per wall (m^2)
C_P	specific heat of air ($JK^{-1}kg^{-1}$)
$h_{wall,i}$	convective heat transfer coefficient between indoor air and the wall i ($WK^{-1}m^{-2}$)
$h_{wind,j}$	convective heat transfer coefficient between indoor air and the window in the wall j ($WK^{-1}m^{-2}$)
l	latent heat of evaporation (Jkg^{-1})
T_a	outdoor air temperature (K)
T_r	indoor air temperature (K)
$T_{wall,i}$	indoor surface temperature of the wall i (K)
$T_{wind,j}$	temperature of the window in the wall j (K)
P	peak number of occupant per floor area ($person\ m^{-2}$)
q_E	sensible heat released from equipment per floor area (Wm^{-2})
q_{hl}	latent heat generation form occupants ($W person^{-1}$)
q_{hs}	sensible heat generation form occupants ($W person^{-1}$)
q_{Va}	outdoor specific humidity ($kg\ kg^{-1}$)
q_{Vr}	indoor specific humidity ($kg\ kg^{-1}$)
Rl_j	long-wave radiation received by the wall j (Wm^{-2})
Rs_j	short-wave radiation received by the wall j (Wm^{-2})
Rs	solar radiation passing through windows received directly by the indoor walls (Wm^{-2})
V_a	total ventilation rate ($m^3 s^{-1}$)
$\alpha_{wind,j}$	percentage of window in the wall j
β	thermal efficiency ($0 \leq \beta \leq 1$)
$\varepsilon_{wall,j}$	emissivity of the indoor wall j
ε_{wind}	emissivity of the windows
Φ_P	ratio of hourly occupants P ($0 \leq \Phi_P \leq 1$)
K_s	thermal conductivity ($m^2 s^{-1}$)

Summary

In this chapter, the method adopted to create the urban coverage and parametrize the presence of urban structures has been presented.

In the first part, the creation of urban morphology (through the definiton of typical Urban Climate Zones) using the WUDAPT software has been shown. Landsat8 images have been compared with a digitized land mask, in order to distinguish between 10 urban classes. The urban coverage for the study area has been created, with a spatial resolution of 100 m. Furthermore, how to insert this landuse into the NWP model is explained. This is an important step for the creation of urban morphology, since WUDAPT provides a 100 m resolution mask, while the mesoscale model works with a finest resolution of 500 m. Later, the two urban landuses have been compared, in order to detect the errors committed interpolating the WUDAPT grid into the mesoscale grid.

In order to characterize each Local Climate Zone defined through WUDAPT, it is necessary to assign the typical coefficients and length scales describing the urban morphology. With this aim, the values inserted as input for the simulations are those which better describe the features of the cities of Bologna and Modena, objectives of this study.

In the second part, we have dealt with the schemes coupled with the mesoscale model to take into account the urban morphology. The first one is the Building Energy Parameterization (BEP) [Martilli et al., 2002] (which parametrizes the effect of buildings structures on the airflow), while the second one is the Building Energy Model (BEM) [Salamanca et al., 2010] (which computes heat and temperature fluxes between the indoor and outdoor sides of each building). Finally, the parametrization used to consider the effect of Rooftop Photovoltaic Panels deployed over the roofs (and its effects on radiation and energy production) have been explained.

Chapter 4

Case study and simulations set up

The first part of this chapter deals with the most relevant features of the region that are subject of this study. After a brief explanation of the typical climatic and geographical characteristic of Emilia-Romagna (and in particular the city of Bologna), attention is paid for the period considered in the simulations.

Therefore, the second part regards the characteristics of the NWP model used to run the simulations, its set up (besides the urban morphology, treated in the previous chapter) and the kinds of simulation performed.

4.1   Features of the area of interest

4.1.1   The climate of Po Valley

The Po Valley is situated on the northern part of Italy, between Alps and Apennines.
It extends approximately 650 km in east-west direction, with an area of 46,000 square kilometers including its Venetic extension not actually related to the Po River basin; it runs from the Western Alps to the Adriatic Sea.

Climate is characterized by a wide temperature range: the mean temperature during winter oscillates between $0\,°C$ and $4\,°C$ while during summer the mean maximum temperatures go from $25\,°C$ (in the areas on the north-west side of the valley) to $30\,°C$ (within the biggest cities). During summers, with the presence of sub-tropical anticyclonic conditions, temperature can go beyond $38\,°C$. Precipitation occurs especially during spring and autumn, but stormy phenomenon are frequent during summer.

The presence of mountains on the northern (Alps) and southern (Apennines) sides leads to thermal inversion conditions, due to the drainage flows form the mountain slope. At the same time, the "bora" wind coming from the north-west side can enter

directly in this region.

The Adriatic Sea has a mitigation effect on the coastal areas. However, this Sea is too shallow and narrow to influence the internal areas of the Po Valley. At the same time, all the other warm winds are blocked from the mountains.

During summer, the isolation due to the presence of the mountains all around the valley facilitates the stagnation of warm and humid air, leading to hot and sultry condition especially during hot wave periods. The high value of the humidity during summer is often the source of strong storms and hailstorms.

4.1.2 The cities of Bologna and Modena

Bologna ($44°29'38''$ N, $11°20'34''$ E) is a city of 387.500 inhabitants, capital of Emilia-Romagna region and the seventh most populated city in Italy. It is located at the center of the so called "Città metropolitana di Bologna",where almost one million lives.

Bologna is situated at the feet of Apennines Mountains between the rivers Reno and Savena; its center is situated at 54 meters above the sea level. The historical center, with a quasi-round shape, is one of the most wide and ancient cities of all Europe. The urbanization developed radially from the city center, more in the northern direction than in the southern one, because of the presence of the hills.

Modena ($44°38'41''$ N, $10°55'32''$ E) has 185.000 inhabitants, and its center is situated at 34 meters above the sea level. It is located on the open Po Valley, 15 km North from the Appennines. As Bologna, it developed radially from the city center. Due to low value of wind velocity in the whole Po Valley, fog is often present inboth cities. Moreover, this feature of the wind velocity has a bad influence on the air pollution, which reaches very high values during periods with absence of synoptic wind forcing.

4.1.3 Study period: the heat wave

In order to evaluate the UHI effect for cities of the study area, a period of very high temperature anomaly has been chosen. This kind of phenomenon is called heat wave.

A Heat wave is defined as a period of several days to weeks of abnormally hot weather [Trenberth et al., 2012].

At the same time, numerous studies have documented that the human-induced climate change has increased the frequency of heat waves across the globe [Christidis et al., 2011]. One of the main effects of heat waves is the short-term increase in the

number of death [D'Ippoliti et al., 2010].

The month of July 2015 has been characterized by a subtropical air mass with stable conditions on Italy. This has led to a monthly mean temperature 4°C higher than the monthly mean temperature referring to the period 1961-1990, with peaks of 7°C. Due to these strong stable conditions, precipitations revealed a negative anomaly with respect to the previous years [Centro Operativo per la Meteorologia, 2015].

Focusing on the city of Bologna, a data analysis for mean, minimum and maximum daily temperature for the month of July is shown (Fig. 4.1).
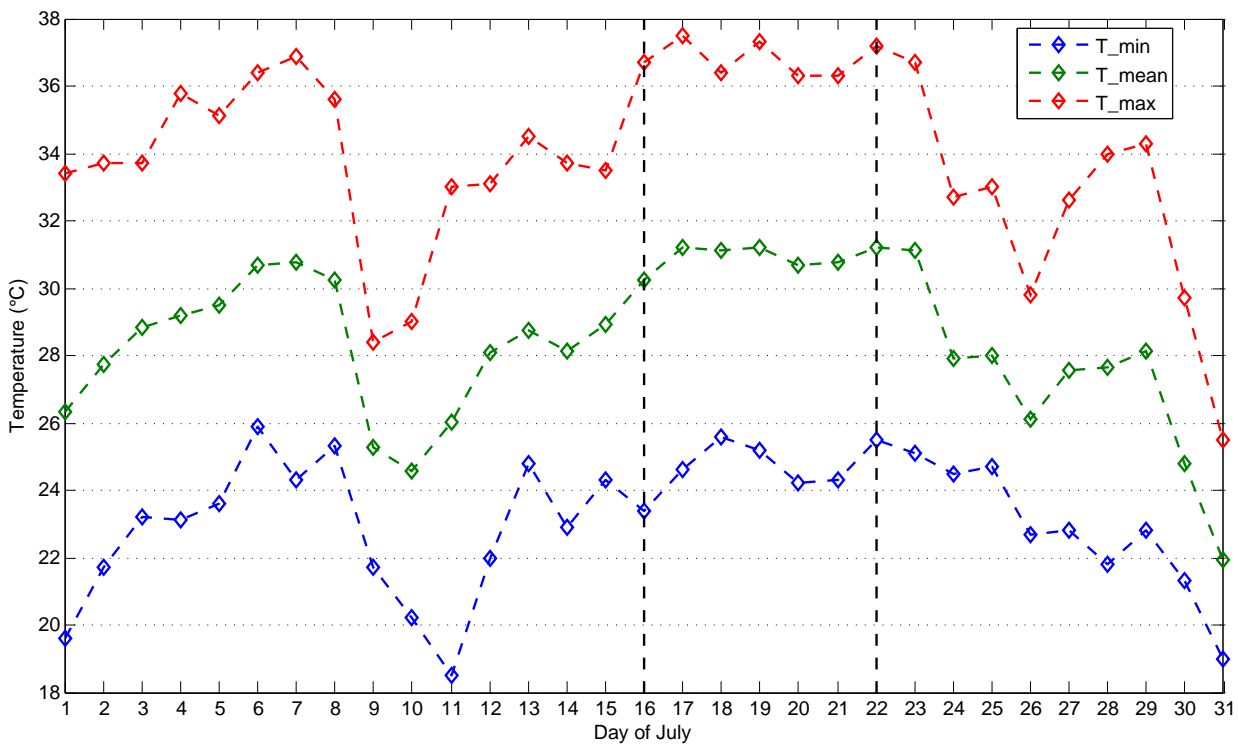
Figure 4.1: Daily minimum, mean and maximum 2-meter temperature for the month of July 2015. Data come from a weather station situated in the urban area of Bologna.

As we can see, the longest and warmest period, characterized by a strong heat wave, is the one that lies between the 16th and the 22nd of the same month. The maximum temperature was twice above 37°C and is always higher than 36°C. At the same time, mean temperature lies always between 30°C and 32°C. Then, the study of the UHI for cities of Emilia-Romagna region is focused on this time period, in order to detect the effects of this heat wave on the urban micro-climate.

In particular the period considered goes from the 20:00 of the 15th of July 2015 until the 18:00 of the 22nd of the same year (time expressed in local hour)

We decided to start the simulation on the day before with respect to the period of

Stations classification			
	Rural	**Hill**	**Urban**
Temperature	18	18	5
Humidity	17	5	3
Wind	2	5	3

Table 4.1: Number of stations which provide the relative variable for each landuse category.

interest: the first 10 hours of simulation (from the 20:00 of the 15th July to the 05:00 of 16th of July) have not be taken into account: a spin-up time is requested in WRF for its initialization.

4.2   Observational data

In order to detect the capability of the model, a comparison with observational data coming from whether stations within the study area is requested. Observational Data have been downloaded from a website belonging to the Agenzia Regionale per la Protezione dell'Ambiente dell' Emilia-Romagna (ARPAER, *www.arpae.it*).
The online database is called *Dexter* [Lazzeri, 2006], and allows to free download several meteorological variables provided every hour. Downloadable data are temperature, wind velocity and direction, relative humidity, atmospheric pressure, precipitation, snow and mean solar radiation. All these data are available for the last ten years. For this work, only observational data coming from stations within the region of interest have been used. In particular, 41 weather stations have been considered and the variable which have been compared with the model are temperature, wind velocity, wind direction and relative humidity. Tab. 4.4, shows the principal features of the weather stations used to make a comparison with simulation outputs.
In addition, not all the stations considered can capture each variable requested for this analysis (temperature, relative humidity, wind direction and velocity). In order to evaluate the consistency of the model used and of the parametrization coupled with it, we distinguished between rural, hill and urban stations, in particular for each variable the number of station for each zone is shown in Tab. 4.1.

The exact position for each station is shown in Fig 4.2, 4.3, 4.4, for the rural, hill and urban areas respectively.
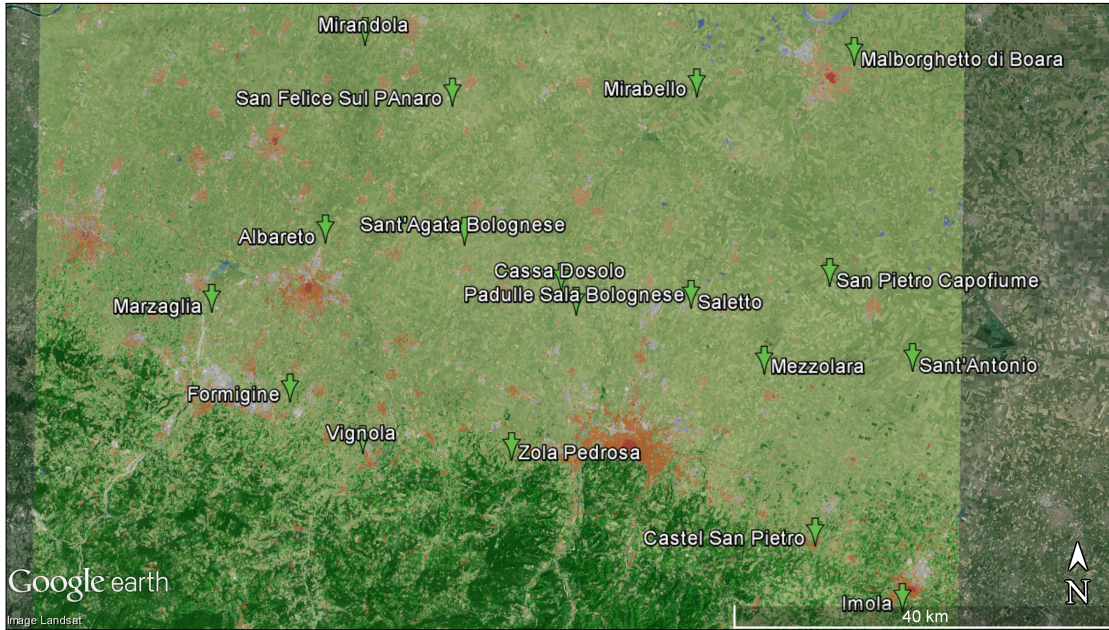
Figure 4.2: Rural stations within the finest grid.WUDAPT landmask has been overlayed

4.3 The WRF model

WRF is a non-hydrostatic mesoscale numerical weather prediction (NWP) model developed by the National Center for Atmospheric Research (NCAR) [Skamarock et al., 2008]. The WRF system contains two dynamical solvers, referred to as the ARW (Advanced Research WRF) core and the NMM (Nonhydrostatic Mesoscale Model) core. In this work, the ARW-WRF core is used, in particular version 3.2. To run real case simulations, it's necessary to prepare initial and boundary conditions for every domain. In the next chapter this process is explained.

4.3.1 WRF Preprocessing System

The WRF Preprocessing System (WPS) is a set of three programs used to create a group of files which contain boundary and initial conditions for simulations.

Geogrid

The first one is called *geogrid*, whose role is to define the domains of the simulations and interpolate satellite geographical and morphological data for each grid. The user can define the number, the dimension and the resolution of each grid, and from what

Weather stations features					
Station Name	X Cell Position	Y Cell Position	Altitude (m)	Station Longitude	Station Latitude
San Pietro Capofiume	164	104	11	11.6226	44.6538
Sant' Agata Bolognese	88	114	18	11.1449	44.6950
Imola	178	36	42	11.7129	44.3453
Saletto	135	100	18	11.4411	44.6323
Mezzolara	150	86	20	11.5338	44.5711
Sant Antonio	181	86	8	11.7327	44.5686
Castel San Pietro	160	50	58	11.5970	44.4111
Padulle Sala Bolognese	111	99	25	11.2906	44.6278
Zola Predosa	97	69	65	11.2001	44.4961
Cassa Dosolo	108	104	22	11.2686	44.6539
Vignola	66	71	100	11.0041	44.5041
Albareto	59	115	28	10.9567	44.7021
Formigine	51	82	90	10.9094	44.5512
Mirandola	68	156	18	11.0163	44.8861
San Felice Sul Panaro	86	143	16	11.1258	44.8261
Mirabello	137	144	10	11.4543	44.8318
Marzaglia	35	101	54	10.8060	44.6371
Malborghetto Di Boara	170	150	4	11.6613	44.8580
Loiano	117	17	741	11.3265	44.2609
Sasso Marconi	104	57	275	11.2413	44.4397
Settefonti	139	49	330	11.4616	44.4026
CaBortolani	79	36	691	11.0845	44.3468
Invaso	100	9	460	11.2226	44.2263
Vergato	83	23	193	11.1131	44.2878
Casoni Di Romagna	133	15	708	11.4254	44.2536
Monghidoro	116	8	825	11.3213	44.2196
Bologna San Luca	113	66	286	11.2984	44.4787
Castel Del Rio	146	7	183	11.5083	44.2142
Sestola	28	11	985	10.7687	44.2321
Pavullo	38	31	678	10.8283	44.3196
Monteombraro	67	43	700	11.0088	44.3763
Montefiorino	5	33	632	10.6227	44.3281
Montese	56	21	920	10.9421	44.2769
Serramazzoni	31	55	826	10.7871	44.4289
Polinago	22	36	754	10.7298	44.3436
Guiglia	64	55	456	10.9924	44.4325

Bologna Urbana	117	70	78	11.3288	44.5008
Bologna Torre Asinelli	120	69	148	11.3468	44.4942
Modena Urbana	52	105	73	10.9170	44.6564
Ferrara Urbana	164	144	26	11.6211	44.8325
Dipartimento Berti Pichat	122	70	45	11.3573	44.5002

Table 4.4: Features of the weather stations within the domain. In the first column is reported the name of the station, in second and third the position within the mesoscale grid, in the fourth the altitude over the sea level and in the last two the real position in coordinates.
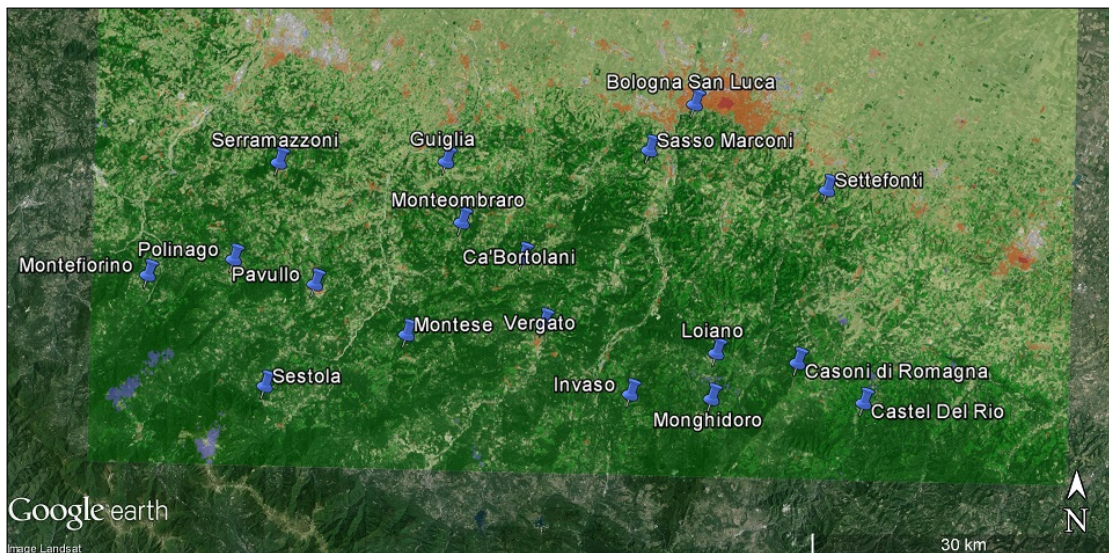
Figure 4.3: Hill stations within the finest grid. WUDAPT landmask has been overlayed.
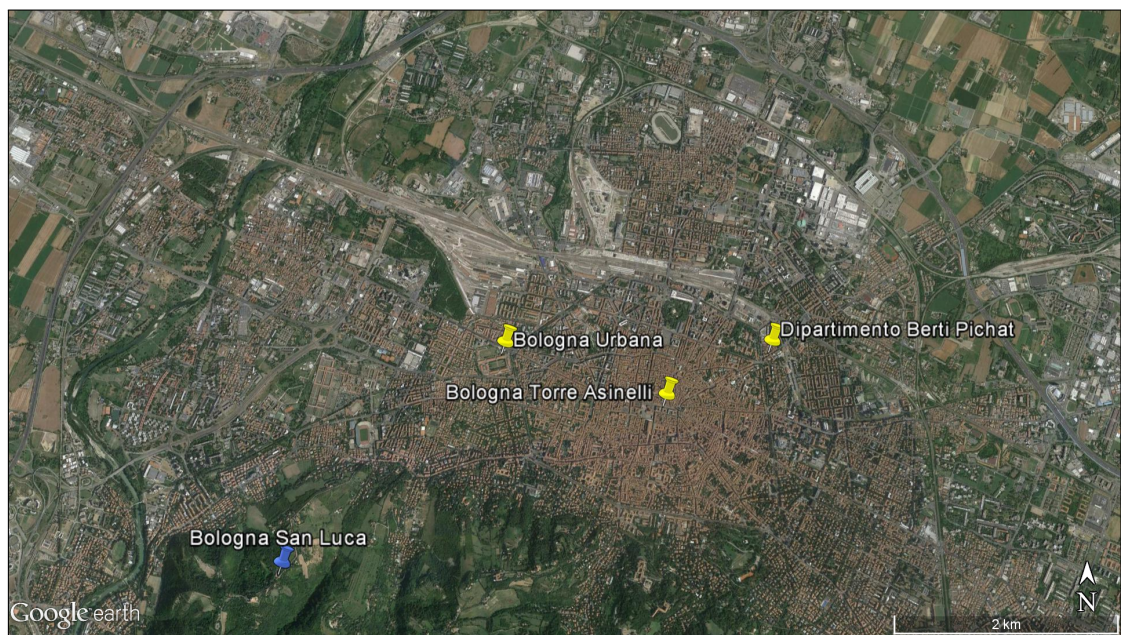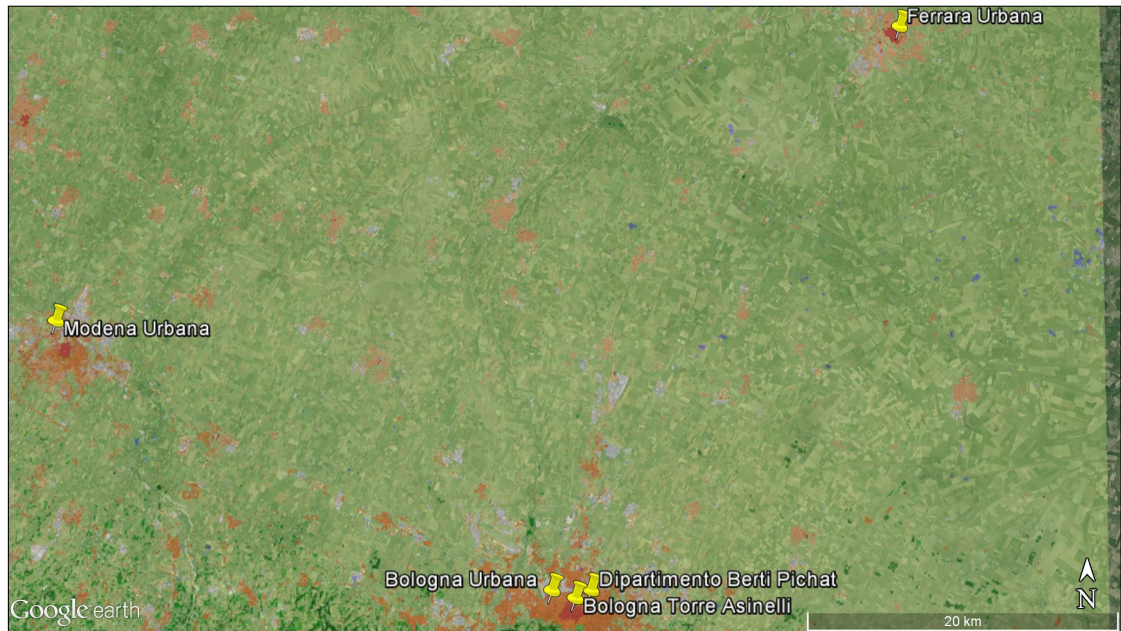
Figure 4.4: Urban stations within the finest grid, for all the city (top) and with a focus on the city of Bologna (bottom). WUDAPT landmask has been overlayed for the upper figure.

Table 4.5: Features of the five domains.

Domain	Resolution (km)	n. points S-N	n. points W-E
1	40.5	101	101
2	13.5	151	151
3	4.5	151	151
4	1.5	199	199
5	0.5	184	184

satellite to get these data (consequently, the categorization of geographical data depends on the kind of classification the user will chosen). Using nested domains is important because large area of high resolution model run is too expensive, then in this way it is possible to avoid to increase uselessly CPU time. In this case, five different nested domains have been created, with the smaller one centered on the city of Bologna. The resolution of the bigger domain is 40.5 km, that one of the following is 13.5, and so on, with a resolution ratio of 1/3, so the smaller domain has a resolution of 500 m. Fig. 4.5 shows the nested domains, in particular it focus on the finest grid, while Tab.4.5 shows grids features. MODIS satellite's data are used here, with a spatial resolution of 30" (around 1 km). Consequently, geogrid will interpolate soil categories, land use category, terrain height, annual mean deep soil temperature, monthly vegetation fraction, monthly albedo, maximum snow albedo, and slope category to the model grids following the MODIS's satellite classification. MODIS landuse classification distinguishes between 20 classes, included water and snow covered areas. The class 13 identifies urban areas: since these areas have been covered with the WUDAPT landmask, the model has been set in order to recognize each urban area as WUDAPT landmask.

Ungrib

The second program, called *ungrib*, is necessary to convert meteorological boundary and initial conditions data into readable files for WRF. These NCEP FNL (Final) Operational Global Analysis data [National Centers for Environmental Prediction, 2016] are on 1-degree by 1-degree grids prepared operationally every six hours. This product is from the Global Data Assimilation System (GDAS), which continuously collects observational data from the Global Telecommunications System (GTS), and other sources, for many analyses. These data are necessary in order to provide boundary

Figure 4.5: WRF 5-nested domains projected into Google Earth.

conditions for the parent domain and initial conditions for all domains. Downloaded meteorological data refers to the period taken into account for the simulations.

Metgrid

Finally, the program *metgrid* links the two kind of data created in *geogrid* and *ungrib*; it horizontally and vertically interpolates meteorological data extracted from ungrib into the simulation domains defined by geogrid.

It creates a group of files called $met\_em\_<domain>\_<date>.nc$. In this case, boundary conditions have been interpolated every six hours. Boundary conditions need to be provided for the parent domain: the interpolation takes place within all grid cells, with 1° resolution which is the resolution of the NCEP FNL data. In addition, initial conditions for all the domains is required, both in horizontal and vertical direction. At the same time, initial data has been interpolated on the vertical direction, within 27 vertical levels for each domain. As said before, the days considered for simulations go from the 16th of July until the 22th of the same month.
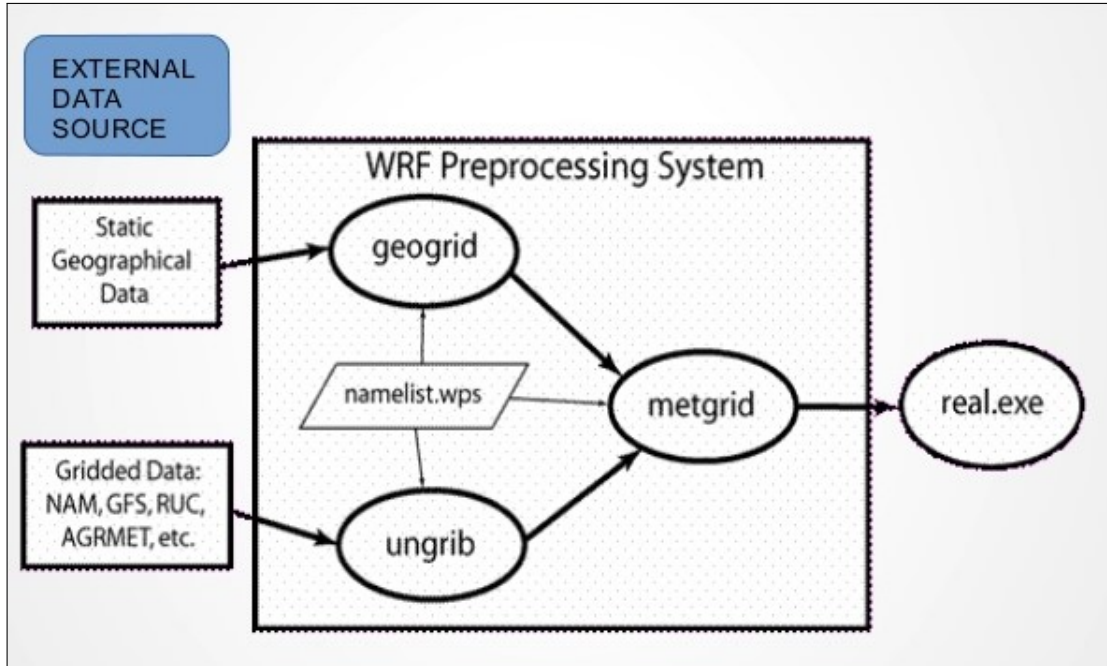
Figure 4.6: Schematic representation of the WRF Preprocessing System

4.4 WRF initialization

4.4.1 Setting boundary and initial conditions

Now, from the $met\_em\_ < domain > \_ < date > .nc$ files, simulations have to be initialized.

In order to perform the initialization, the *real.exe* file allows to interpolate boundary and initial conditions within the cell of the simulations. The grid cell horizontal resolution is the same of the $met\_em\_ < domain > \_ < date > .nc$ files, while the vertical resolution is finer:

51 levels have been chosen within a terrain-following hydrostatic-pressure vertical coordinate system denoted by η and defined as:

$$\eta = \frac{p_H - p_T}{p_S - p_T}$$

p_H is the hydrostatic component of the pressure, while p_S is the pressure at the top of the domain (set at 5000 Pa) and p_T the one at the ground. This coordinate system is superimposed to the topography of the domain. Then, η varies from 1 at the ground to 0 at the top of the domain. The variation is not linear: since the pressure variation with height is exponentially decreasing, at the same time the depth of each vertical level increases with height. In order to provide the scales of vertical levels, in the

first 100 m over the terrain height there are 10 vertical levels, while the last 10 levels occupy 17 km on the vertical.

4.4.2   Providing the parametrizations for the atmospheric dynamics

The executable file called *wrf.exe* contains all the informations about physics in order to compute the spatial and temporal variation of the atmospheric dynamics. It is necessary to provide the parametrizations for each physical phenomena that occurs within each domain. In this section we focus on the most relevant parametrizations adopted in this model, since other schemes (such as clouds, precipitation, snow and radiation schemes) are not important for the topic of this work. Moreover, with the aim to provide simulations with better quality, two techniques have been used in order to prevent numerical waves which propagate within the domain due to the numerical computation: the first one is a dumping scheme [Skamarock et al., 2008] which takes place in the upper levels of atmosphere. It diffuses vertical waves which reflect within the domain. The second one is a 6th order diffusion scheme [Knievel et al., 2007], used to diffuse numerical noise within the PBL at the 6th order derivative. The following parametrizations have been adopted:

- The BEM+BEM scheme [Martilli et al., 2002], [Salamanca et al., 2016] discussed above for the interaction between urban areas and PBL. This parametrizations take place just for the finest domain (500 m of resolution);

- The Bougeault and Lacarrere scheme for the $k-l$ closure of PBL [Bougeault and Lacarrere, 1989];

- The Rooftop Photovoltaic Panels parametrization for urban areas [Salamanca et al., 2016].

- The Smagorinsky scheme for the horizontal diffusion closure [Skamarock et al., 2008]

- The Unified Noah Land-Surface Exchange scheme for the interaction between rural areas and near surface atmosphere [Chen and Dudhia, 2001];

The time-step is grid-resolution dependent: the time step (in seconds) for each simulation need to be lower than six times the grid spatial resolution in kilometers (CFS method). This means that, if the parent domain has a grid resolution of 40.5 km, the maximum time-step allowed for this resolution is of 243 seconds, and so on

62

for the finer grid, with a maximum time step allowed for the finest grid of 3 seconds. However, WRF version 3.2 used in this work presents some problems linked to the clouds parametrization, so the pressure variable can assume the value NaN (Not a Number, i.e. a number divided by zero). In order to resolve this problem, it is necessary to diminish the time-step: in our case a time-step of 105 seconds for the parent domain has been set. In addition, the numerical method used to compute the temporal evolution for each equation is the Runge-Kutta scheme at the 3rd order.

4.4.3 Description of the simulations performed

A total of 15 simulations have been performed in this study, all for the same time period ($16^{th} - 22^{nd}$ July 2015) and within the same nested grids, each for testing working hypotheses. Below, we describe only the most relevant ones.

Outputs of the model are updated with a frequency of one hour. There are two different possibilities to run the simulation: the first method, called *two-way nesting* (2WN), allows the nested domains to run simultaneously. Lateral boundary condition is provided by parent domain at every parent step, and information exchange happens both for course and finer domain, then the variables feedback is bidirectional.

On the other hand the second called *one one-way nesting* (1WN) method, doesn not let a bidirectional feedback, so information exchange occurs only from the course to the finest domain. In this work, the 2WN and an hybrid one have been used.

The hybrid method is the following:

a 2WN simulation with a finest resolution of 1.5 km and a time-step of 105 seconds for the parent domain has been performed (i.e this simulation has not been performed including the finest domain). Thereafter, 500 m grid resolution simulations have been made with the 1WN method, using outputs from the previous simulation as input boundary conditions taken every hour. Basically, the process is this:

- First 2WN simulation with simultaneous running domains 1,2,3 and 4 with output every hour. Boundary conditions updated for the parent domain every 6 hours;

- Interpolation of the output belonging to the 4th domain (with a grid resolution of 1.5 km); in order to obtain boundary conditions for the finest domain (with a grid resolution of 0.5 km);

- Several 1WN simulations for the finest domain, everyone with the same boundary and initial conditions but with different settings, with a time-step of 2 seconds.

FOr the second method it is requested, , that the boundaries of the finest cell need to be at least 5 grid cells far from the coarser grid for all the 4 side of the domain. This is necessary, since in this 5 grid cell region the variables interpolation of the informations coming from the coarser domain takes place.

Now the computational time requested for the two methods is discussed. These are the elapsed times to compute one time step (with respect to the computer cluster used to run the simulations):

- $d_1 (40.5\,\text{km}) \simeq 30\,\text{s}$

- $d_2 (13.5\,\text{km}) \simeq 10\,\text{s}$

- $d_3 (4.5\,\text{km}) \simeq 3\,\text{s}$

- $d_4 (1.5\,\text{km}) \simeq 1\,\text{s}$

- $d_5 (0.5\,\text{km}) \simeq 0.2\,\text{s}$

Since the time-step ratio between two nested domains is of 1/3, for the calculation of one time-step of the parent domain, 3 iterations for the 2nd, 9 iterations for the 3rd, 27 for the 4th and 81 iterations for the 5th domain are requested. The total amount is of 121 iterations, with a total time for a time-step of the parent domain of 112 seconds. Then, using the one-way nesting method, the computational cost is reduced of 40 iterations. More precisely, the computational cost for the finest domain is just the 14% of the total computational cost.

In addition it is possible to increase the time-step of the finest domain so the computational time gain is relevant for the 1WN method: for 2WN the time step of the 5th domain is of 1.3 seconds, while for the 1WN method is set to 2 seconds (it needs to be at most 6 times the spatial resolution in kilometers, i.e. lower than $6 \times 0.5 = 3$ seconds for the finest domain). Moreover, 1WN is very useful if the aim is to investigate the difference between similar patterns, since the boundary conditions for the finest domain are exactly the same (this do not happen for the two-way nesting method, becouse informations are exchanged between all domains).

In Tab.4.6 the features of each simulation performed in this work are shown. The first one (URB) is the "control" simulation: the presence of the city has been taken into account within a one-way nesting simulation. In all the simulations with the air conditioning system (ACS) switched "ON", the system works all the 24 hours of the day, with $T_{target} = 25\,°\text{C}$ and a comfort range of $0.5\,°\text{C}$. Moreover, the heat generated by equipments is multiplied by a factor (lying in the $[0,1]$ range) which take into account of the lesser use during night-time.

Table 4.6: List of simulations performed and its features

Sim. Name	One/two-way nesting	Urban Landuse	RPVP fraction	Cultivated Areas	Air Cond. Systems
URB	One Way	Yes	0.00	Croplands	On
URB_NEST	Two Way	Yes	0.00	Croplands	On
NOURB	One Way	No	0.00	Croplands	/
PV_0.25	One Way	Yes	0.25	Croplands	On
PV_0.50	One way	Yes	0.50	Croplands	On
PV_0.75	One Way	Yes	0.75	Croplands	On
PV_1.00	One Way	Yes	1.00	Croplands	On
URB_BARR	One Way	Yes	0.00	Barren and Sparsely Vegetated	On

The second one (URB_NEST) is equal to URB, but computed with the 2WN method: outputs of this simulation have been used in order to demonstrate the consistency of the 1WN.

The third one, called NOURB, has been made in order to evaluate the effect of the presence of the cities in the area considered, through a comparison with the URB simulation. Urban areas (i.e. all the LCZ coverage) have been substituted with the "croplands" rural class.

The following four simulations (PV_0.25, PV_0.50, PV_0.75, PV_1.00) using the same boundary conditions of the URB simulation, have been performed with several fractions of coverage of rooftop photovoltaic panels (1/4 ,1/2 , 1/2, 3/4 and 1), in order to evaluate the effect of the solar plants on the energy consumption/production and on the atmospheric dynamics.

One other post-processing simulation has been ran, in order to check the effect of a dryer and less vegetated rural area with respect to the croplands coverage of the URB simulation (URB_BARR). Dealing with the outputs, 169 hours have been simulated in total (from the 20:00 of the 15th of July until the 18:00 of the 22nd of the same month) , but in the following analysis the first 11 hours have not been taken into account, since it is the spin-up period of the simulation.

Summary

In the first part of this chapter, we have dealt with the climatic and morphological features of the study area, in order to focus the reader's attention on the context where the simulations are performed. We also outlined the characteristic of the heat wave, focusing on that one of the month of July of 2015, object of this study.

Later, the features of the weather stations used for the comparison with the model

outputs have been presented. Several weather stations are located within the study area: 41 of which provide the temperature, 25 relative humidity and 10 wind velocity and direction. Weather stations have been divided into three different classes, with respect to the kind of area where they are located: we distinguished between rural, hill and urban weather stations.

The second part deals with the working principles of the Weather Research and Forecasting (WRF) mesoscale model. This is the NWP, coupled with the "urban" parametrizations, chosen to run the simulations.

First of all, the preprocessing system has been presented. It allows to define the domain of simulation, the boundary and initial conditions. Five nested domains have been created, with the finest one centered in the city of Bologna with a spatial resolution of 500 m. MODIS satellite provided the features of morphology, while boundary and initial conditions came from the NCEP Operational Global Analysis database.

Physical parametrizations used for simulations have been presented, focusing on the nesting methods adopted for the information exchange between the various domains.

Finally, the pattern of simulations performed in this work have been presented: in total we run eight simulations, each one with different features.

Chapter 5

Results, Part I: comparison with observational data

In this chapter, a model validation in is performed through the comparison with data provided by weather stations. As said in the previous chapter, the observational data (OBS) are provided by 41 weather station within the study area. The discussion of results will take place in the following way: the variables analyzed here are temperature, wind speed and direction and relative humidity, each one evaluated at the altitude of the station. For each variable, we distinguish between rural, hill and urban areas, in order to evaluate the skills of the model in reproducing the features of these areas. The following discussion will regard the skills and the weaknesses of several simulation, with the aim to outline an optimal setting.

5.1 The statistical method

Since a comparison with observational data is needed in order to verify the efficiency of the parametrizations and models used, a consistent statistical method is required. Tthe statistic analysis can be conducted averaging the six days data (both observational data and simulations output) into a diurnal cycle. This is a reasonable method, since all values objects of this study slightly oscillate on daily average over the period of simulation, as shown in Fig. 5.1 for the weather station of Bologna Urbana.

In the period considered, the daily-mean temperature (computed averaging from 6:00 to 5:00 of the next day, local hour) oscillates between 30.7°C and 31.7°C, the wind direction between 263° and 302° , wind speed between 1.35 m/s and 1.7 m/s and relative humidity between 28% and 35%. All this variables oscillates in a very small range during this six-days period, due to the very stable synoptic conditions which favors the heat wave.
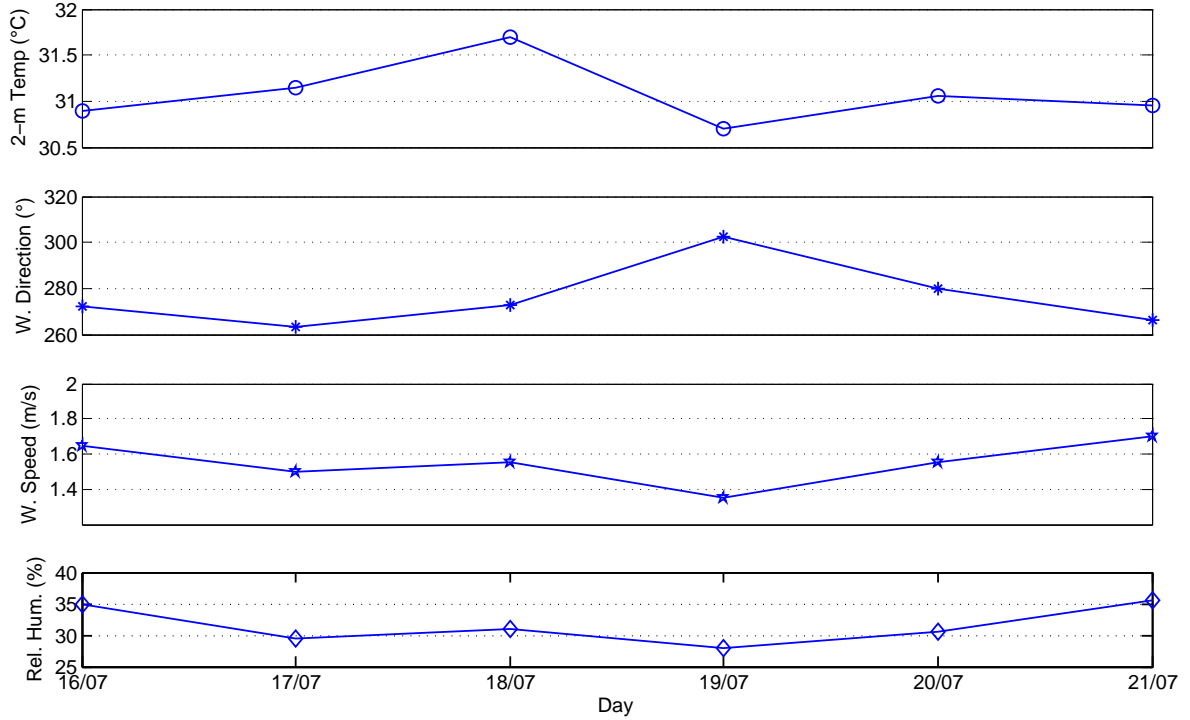
Figure 5.1: 24-hour averaged values of 2-m air temperature,10-m wind direction, wind speed and relative humidity registered by the Bologna Urbana weather station. Average have been computed for all variables from 6:00 to 5:00 of the next day.

Therefore, each 24-hour period can be treated as a observation of the same "population". We will proceed validating the model trough a comparison for all the days of simulation, while the projection into a single diurnal cycle will be used as an useful tool to detect the typical trend of some variables during the heat-wave period.

Another important question is how to identify the correct cell where each weather station stays within the domain of the simulation: first of all, the the distance between the position of the weather station and the center of each grid cell is computed.

Then, the cell used to make the comparison with observational data is that which present the minimum distance from the position of the weather station.

Once identified the correct cells, the correct vertical level of the model domain has been chosen. For the rural areas, each station lies in the first level of the grid cell (10 meter high from the ground), while for the urban areas, the only station situated at higher levels than the second is "Bologna Torre Asinelli", which is located on the seventh vertical level.

As regards the hill areas, it has not been possible to find the correct vertical level of the three dimensional grid which identifies the correct position of the weather sta-

68

tions in this area. The problem is linked to the terrain height of the model: since the hill morphology is highly heterogeneous , i.e. the gradient of altitude is highly variable in the horizontal direction, the model cannot capture the morphological variability, and the altitude of the model can differ from the real terrain height of hundreds of meter. The following comparison between observational data and model outputs in hill areas shows the higher errors.

Now we proceed with explaining the statistical parameters used for the model validation. If A is a variable, A_o is the value observed by a weather station, A_m the value provided by a simulation and N the number of hours of the time period considered (in our case N=169(hours of simulation)-10(spin-up period)=159), the values used in order to evaluate the efficiency of the model with respect to observational data are:

- **Root-Mean-Square Error:**

$$RMSE = \sqrt{\sum_{l=1}^{N} \frac{(A_m^l - A_o^l)^2}{N}}$$

- **Mean Bias:**

$$MB = \sum_{l=1}^{N} \frac{A_m^l - A_o^l}{N}$$

- **Hit rate:**

$$HR = \sum_{l=1}^{N} \frac{n_l}{N}$$

$$n_l = \begin{cases} 1 & if \, |A_l^o - A_l^m| \leq k \\ 0 & if \, |A_l^o - A_l^m| > k \end{cases}$$

RMSE is used to evaluate, on time average, how far is the simulation value from the observed one. On the other hand, MB is useful to detect if the model underestimates of overestimates the real value, since it can assume both negative and positive values. Finally, HR (used only for temperature) computes how many times the model value is closer at least of k from the observed values. In other words, HR is 1 if A_l^m is at every hour in the range $[A_l^o + k, A_l^o - k]$ and 0 if it is never in this range.

In this work, HR have been computed for $k = 1.5\,°C$.

Four different simulations have been compared with observational data: URB_NEST, URB, NOURB, URB_BARR. In particular, we will focus on the efficiency of the 1WN method (comparing URB_NEST with URB), on the effect of the urban coverage (comparing URB with NOURB), and on the different type of rural areas (comparing URB with URB_BARR).

5.2 Temperature

In the following section, the comparison between observed and simulated temperature is shown.

Since the comparison has been performed for several station, here we analyze the result of 4 stations for rural areas, 4 stations for hill areas and 5 stations for urban areas.

5.2.1 Rural Areas

Here the comparison of temperature for rural areas between observational data and simulation output is discussed, for the weather stations of "Mezzolara", "Albareto", "Malborghetto di Boara" and "Mirabello". In Fig. 5.2 the temperature time series for observational data and URB NEST and NOURB simulations for four rural weather stations are shown. In the following figures, the MB (Fig. 5.3), the RMSE (Fig. 5.4) and HR (Fig. 5.5)are displayed. The highest value of temperature reached is $\simeq 37\,°\mathrm{C}$ among all stations, while the lowest $\simeq 19\,°\mathrm{C}$. All simulations considered can capture this range, except for a little underestimation during nighttime for in all the considered areas. In fact, the MB shows on average an underestimation of temperature for all simulations: the greater value is reached by NOURB, while the lowest by URB_BARR (which overestimates temperature for "Mezzolara" station). The values assumed by URB_NEST and URB lay in that range, not showing a relevant difference between each other. The similar trends shown by all stations, despite their distance, demonstrate the stable conditions and the low variability during an heat wave period.

These trends are reflected also in the RMSE: the lowest value is assumed for all stations by URB_BARR, while the greatest by NOURB. The RMSE also provides informations about the efficiency of the model: all the RMSEs of the simulations considered lay in the range $[1.4\,°\mathrm{C}, 1.9\,°\mathrm{C}]$, so it is possible to affirm that model outputs are in good agreement with observational data. On the other hand, looking at the HR, for all stations the simulations assume a temperature difference no more than $1.5\,°\mathrm{C}$ at least the 60% of times, with peaks of 70% for URB_BARR. From this comparison we can deduce some important considerations about the model used:

- URB_NEST and URB simulations shows similar values of errors and HR, with no particular trends. In addiction, the weather stations do not belong to the cells close to the boundary of the domain (where interpolation between the finest and coarser grid takes place). This means that the 1WN method is efficient as the 2WN method in representing rural areas air temperature in the
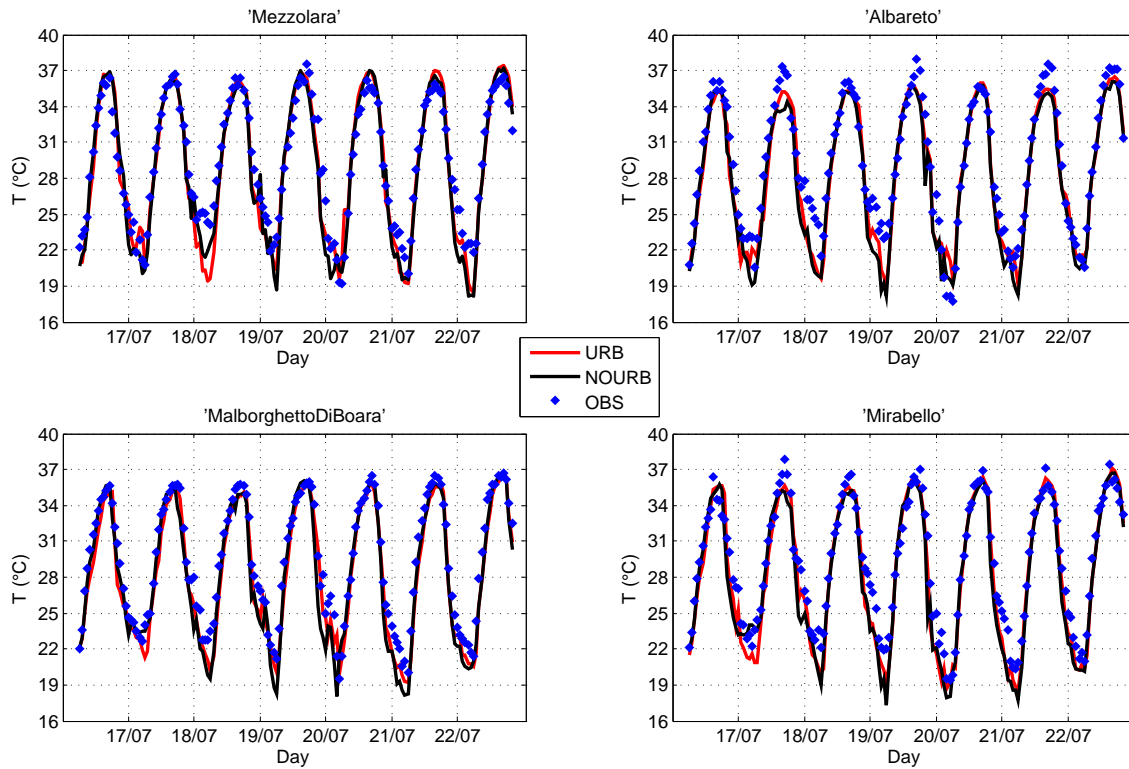
Figure 5.2: Temperature time series of Observational data (blue dot), URB _NEST (red line) and NOURB(black line) for four different rural weather stations. All the period of simulation have been taken into account (neglecting the spin-up period).The value in the x-axis refers to the 00:00 of each day.

inner cells of the domain.

- The NOURB simulation is that one which shows the gratest errors and a conequent lower HR (in particular the temperature is underestimated for all stations). This means that the presence of urban structures affects not only the areas where the city is located, but also the closest rural areas, through horizontal heat advection.

- The best simulation representing the temperature trend for rural areas is URB_BARR: for this setting, the percentage of vegetation coverage in rural areas is smaller then the URB simulations. The vegetation influences the temperature through evapotranspiration: solar radiation is converted into latent heat rather than sensible heat. Since the dominant contribute in increasing the near-surface temperature is due to the sensible heat release, if solar radiation is converted into latent heat, the effect of vegetation is to diminish the temperature through evapotransiration. Therefore, the rural areas that better represents the vegetation behavior during the heat wave period is "Barren and Sparsely Vegetated".

71
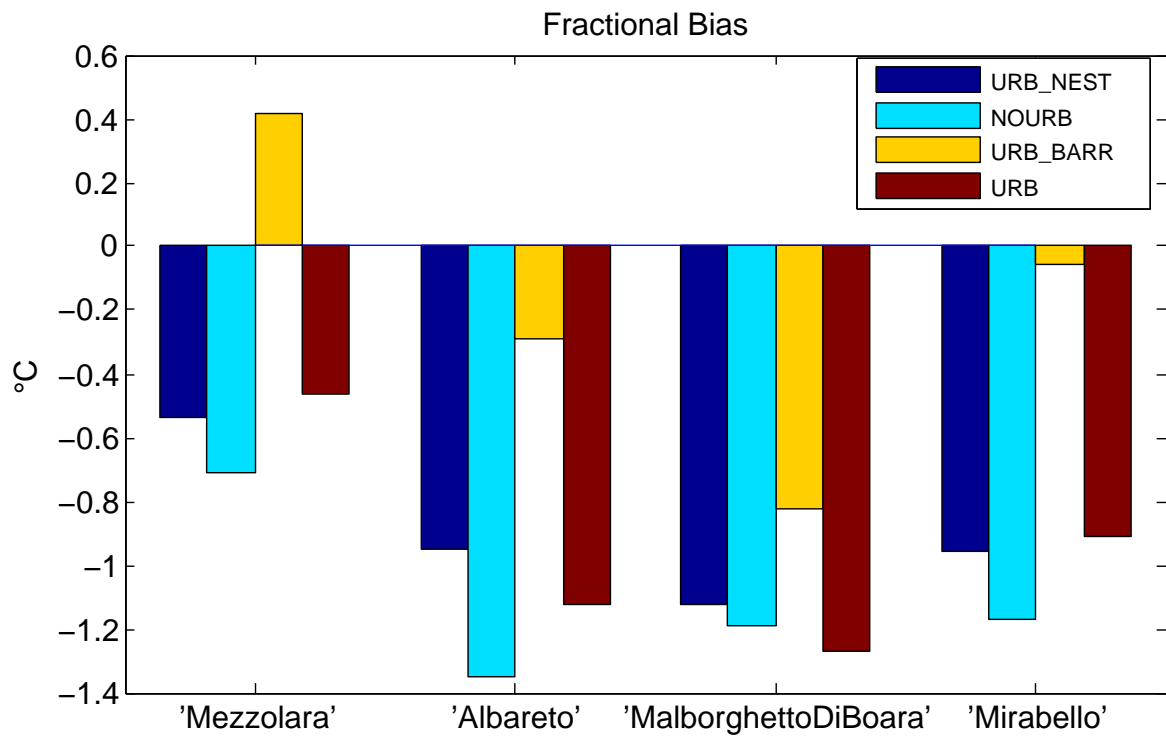
Figure 5.3: Temperature Mean Bias between OBS and URB_NEST (blue bars), NOURB (cyan bars), URB_BARR (yellow bars) and URB (red bars) for the four rural weather stations considered.
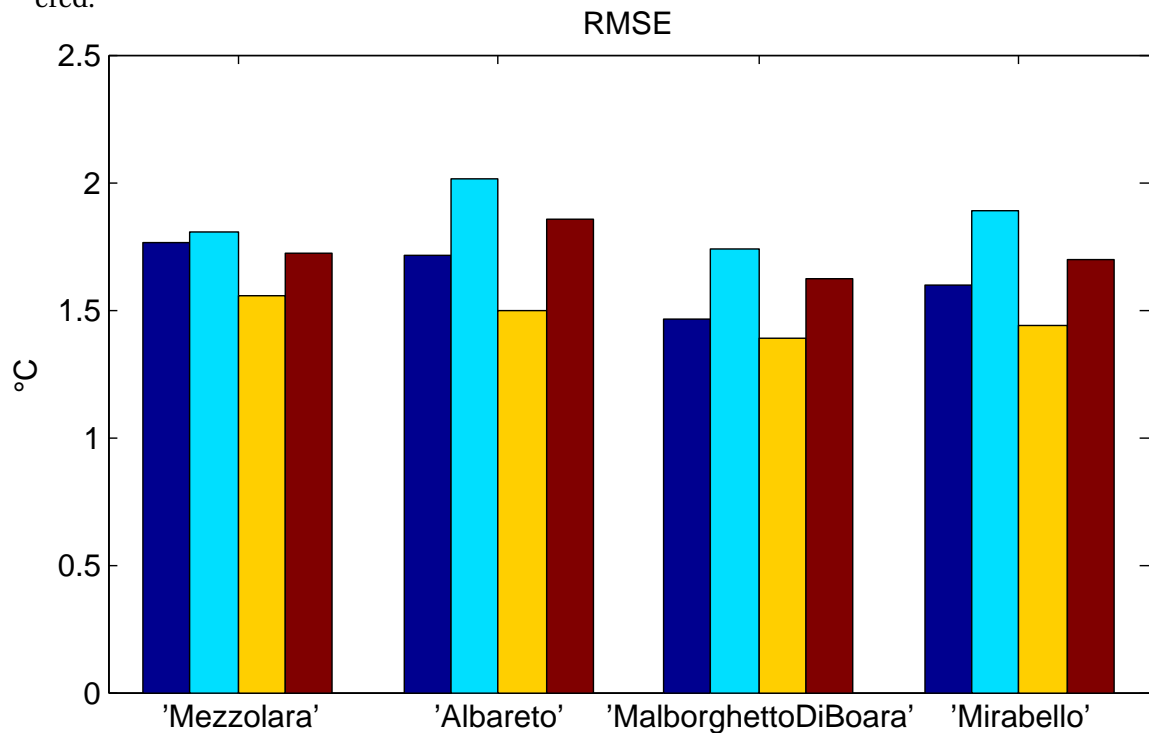
Figure 5.4: Temperature RMSE between OBS and URB_NEST (blue bars), NOURB (cyan bars), URB_BARR (yellow bars) and URB (red bars) for the four rural weather stations considered.
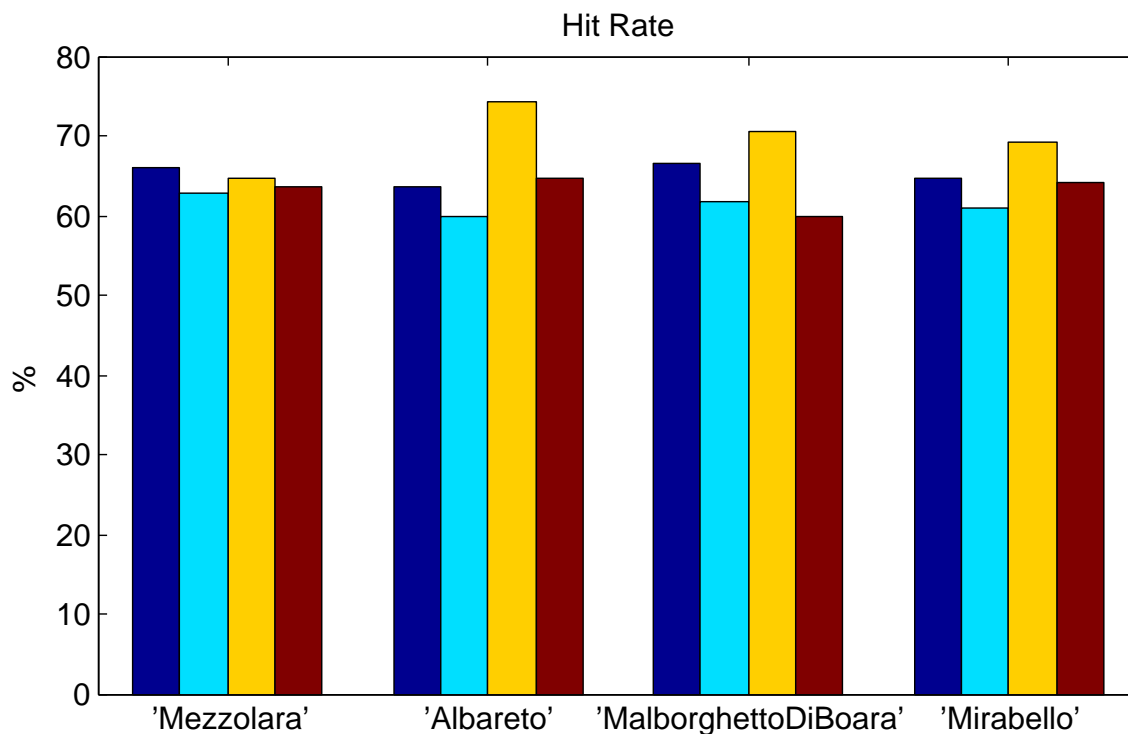
Figure 5.5: Temperature Hit Rate between OBS and URB_NEST (blue bars), NOURB (cyan bars), URB_BARR (yellow bars) and URB (red bars) for the four rural weather stations considered.

5.2.2 Hill Areas

As said before, the hill areas within the finest domain of the simulations present a strong heterogeneity, which affects the efficiency of the model in reproducing the atmospheric dynamics over these areas. In Fig. 5.6 the time series for four hill weather stations is shown. These stations are those that better represent the temperature trend, since they are the less affected by morphological heterogeneity. The other stations show great biases between observational data and simulations output, since the model is not able to represent the heterogeneity of these areas. In fact, the RMSE assumes great values than the RMSE in rural areas, it lies in the range $[1.3\,^{\circ}\text{C}, 2.3\,^{\circ}\text{C}]$ (Fig. 5.8).

For these stations, the temperature range is $[37\,^{\circ}\text{C}, 19\,^{\circ}\text{C}]$, strongly dependent on the station considered, since they are situated at different altitude. Therefore, for this area the higher variability is not between different simulations, rather than different stations. The station which shows the lowest error is "Monteombraro", since the station is located far from mountain slopes, while the worst is "Bologna San Luca", situated not far from the city of Bologna on the hills slope. The MB is shown in Fig. 5.7. Despite the lowest value is assumed by "Serramazzoni" station, in this grid cell we cannot identify a good behavior of temperature trend: while the station is located
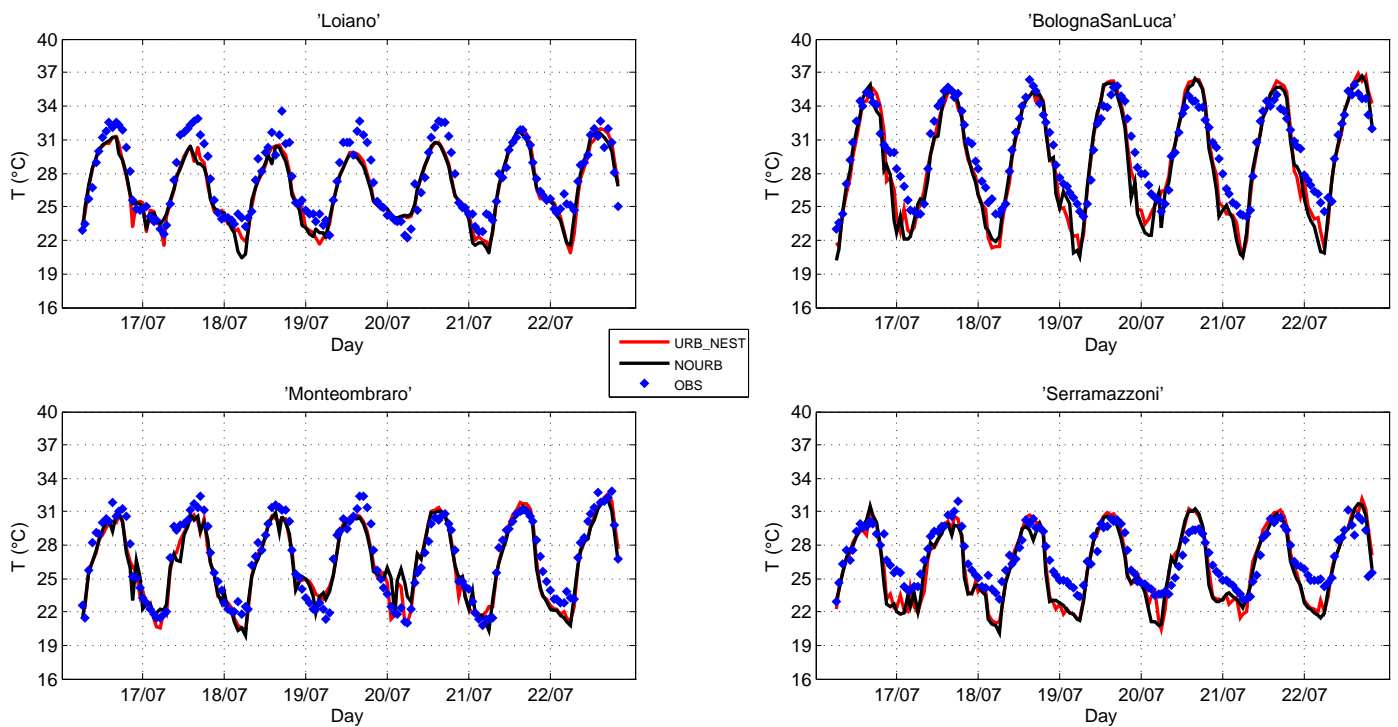
Figure 5.6: Temperature time series of OBS (blue dot), URB _NEST (red line) and NOURB(black line) for four different hill weather stations. All the period of simulation have been taken into account (neglecting the spin-up period).The value in the x-axis refers to the 00:00 of each day.
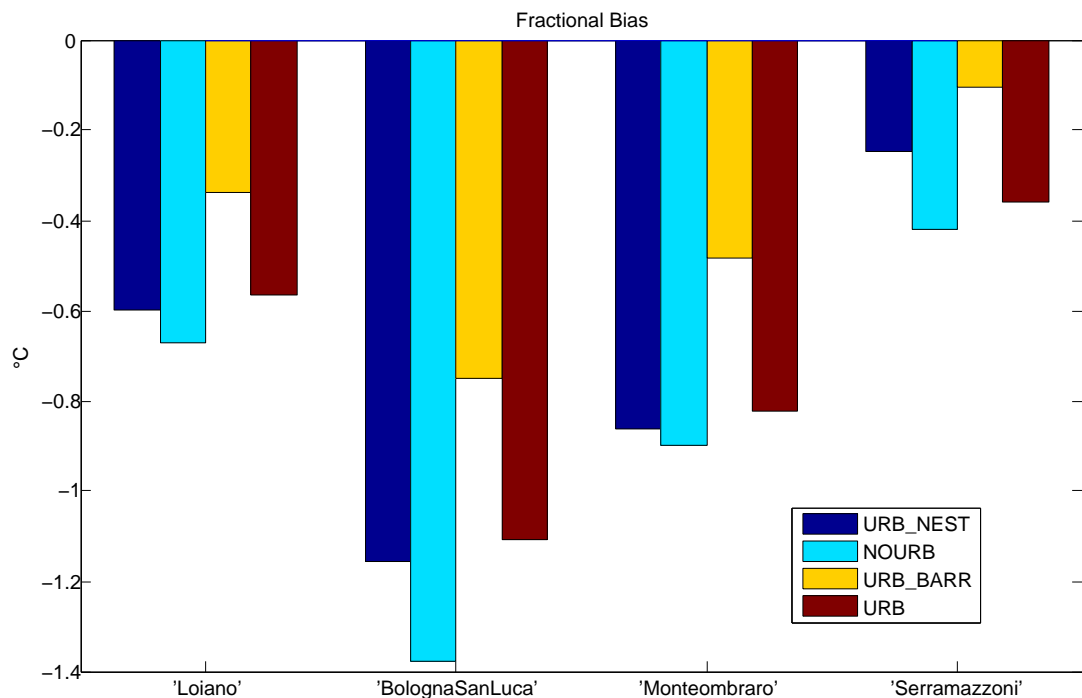
Figure 5.7: Temperature Mean Bias between OBS and URB_NEST (blue bars), NOURB (cyan bars), URB_BARR (yellow bars) and URB (red bars) for the four hill weather stations considered.
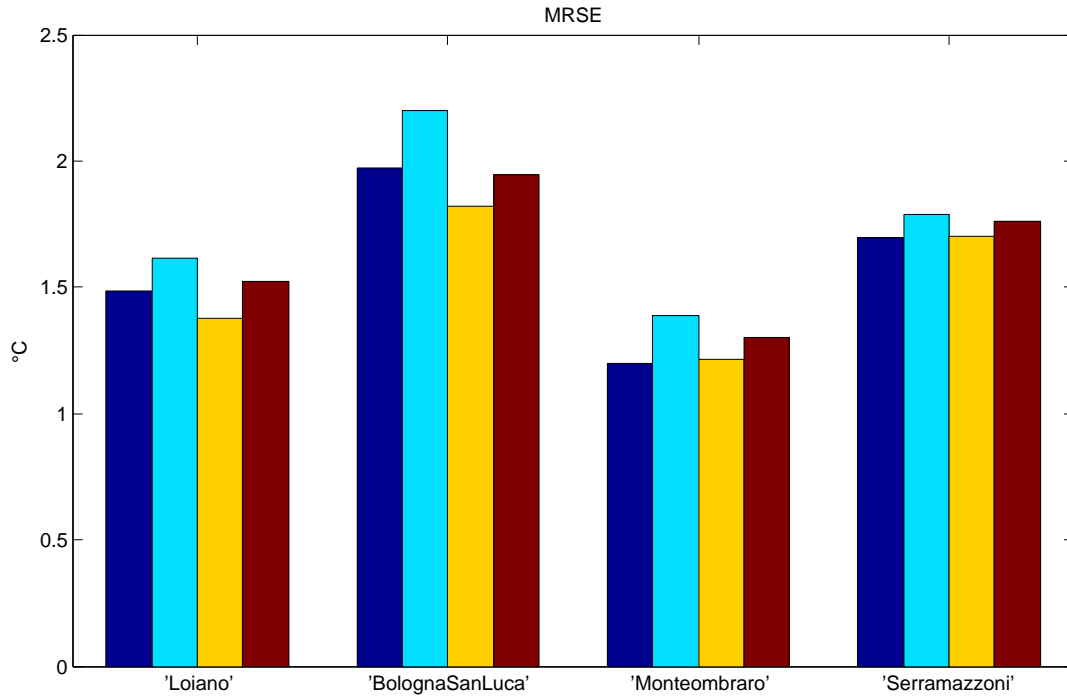
Figure 5.8: Temperature RMSE between OBS and URB_NEST (blue bars), NOURB (cyan bars), URB_BARR (yellow bars) and URB (red bars) for the four hill weather stations considered.
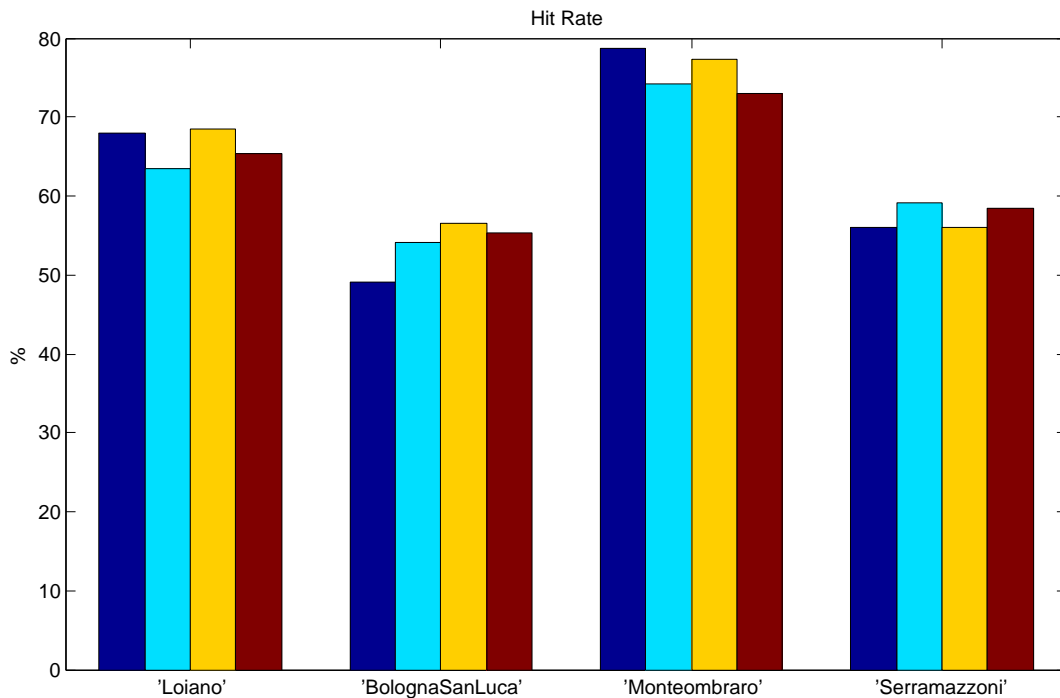
Figure 5.9: Temperature Hit Rate between OBS and URB_NEST (blue bars), NOURB (cyan bars), URB_BARR (yellow bars) and URB (red bars) for the four hill weather stations considered.

at 826 meter of altitude, the grid cell of the model is situated at 656 meter. Therefore, the daily temperature range is higher for the model than the station, and the MB is strongly affected by this difference in altitude (positive temperature differences are balanced by negative temperature differences, with a resulting close-to-zero value of MB). Moreover, for all simulations and for all stations the temperature is underestimated. The HR is for all stations at least of 50% (Fig. 5.9) with the best value assumed by the "Monteombraro" station (70%). Regarding the difference between the various simulations, it is possible to repeat the same considerations for the rural areas: it is not possible to find great differences between URB_NEST and URB, and as in the previous case, the most performant simulation is URB_BARR. At the same time, the difference between URB_BARR and URB is not so relevant such as the rural case, since the rural coverage percentage is lower. In the hill areas, the most present rural classes are "Deciduous Broadleaf Forest" and "Mixed Forests", so the effect of changing the cultivated areas is not so relevant as in the previous section. At the same time, the difference between URB and NOURB is lower than that in the previous case. Looking at the MB, the higher difference is for the "Bologna San Luca" station: while for the others stations the difference is negligible, for this station the difference is greater because of the closeness with the city of Bologna. In fact here the underestimation of temperature is relevant for NOURB, since the heat advection for Bologna affect also the closest rural zones.

5.2.3   Urban Areas

In this section, we evaluate the efficiency of the model in representing the urban temperature, through the comparison with weather stations located within the cities of Bologna, Modena and Ferrara.

First of all, we characterize the temperature trend for the city of Bologna (in Fig. 5.10 the temperature trend for the "Bologna Urbana" station is shown, for URB simulation and Observational data).

The minimum temperature is reached at 6:00 ($\simeq 25\,°C$), while the maximum temperature at 17:00 ($\simeq 36\,°C$). The model can accurately represent the temperature trend shown by the station: however there is a clear underestimation during nighttime, with a maximum of ($\simeq 1\,°C$) at 23:00.

Now we proceed evaluating the modeled temperature for all urban stations:

It is clear, as it is shown in Fig. 5.11, the different behavior of temperature time series between URB_NEST and NOURB for all stations: while the first one follows the observational data trend for the whole time period, the simulation performed substituting urban areas with croplands clearly differs from observation during nighttime. This
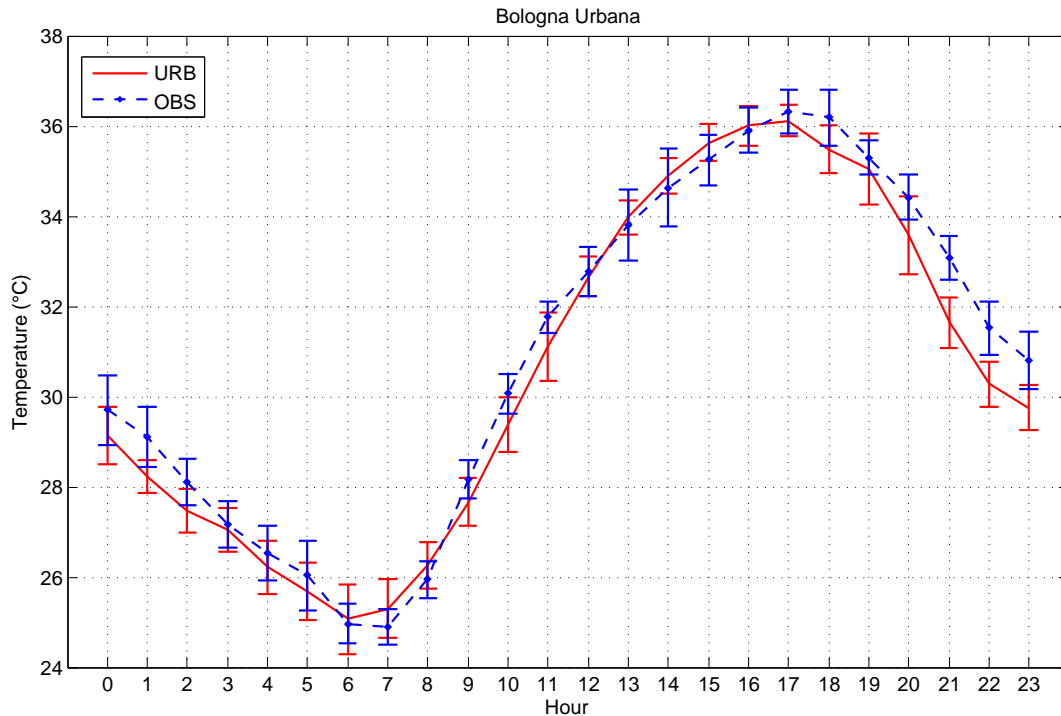
Figure 5.10: Diurnal Cycle of air Temperature for URB simulation and Observational data in corrispondance of the weather station "Bologna Urbana". Errorbars are calculated between mean temperature and temperture of each day.

is the UHI effect, which cannot be detected by NOURB since in this simulation the city is not present. The difference in temperature between URB_NEST and NOURB can be of 6°C. The separation starts during the first hours of the night, and finishes rapidly when the sun rises.

The evaluation of UHI effect will be discussed in detail in the following sections. Obviously, the systematic error committed removing the city from the surface affect all the statistic parameter: the MB (Fig. 5.12) shows a great mean underestimation of temperature for all urban station for NOURB.

The same considerations can be made for the RMSE (Fig. 5.13) and HR (Fig. 5.14): the RMSE reaches a value of 4.4°C for the "Modena Urbana" station, while the HR is always less than 50%. These values significantly differ from the values provided by other simulations, then in the following analysis the NOURB simulation will not be taken into account. Regarding the simulations which take into account of the urban morphology, the best results are provided by "Bologna Urbana", "Modena Urbana" and "Dipartimento di Fisica" stations. For all the simulations (except for NOURB) the RMSE is lower than 1.5°C for the three stations cited above. At the same time, the MB is always slightly negative while the HR always higher than 60%. For these three sta-
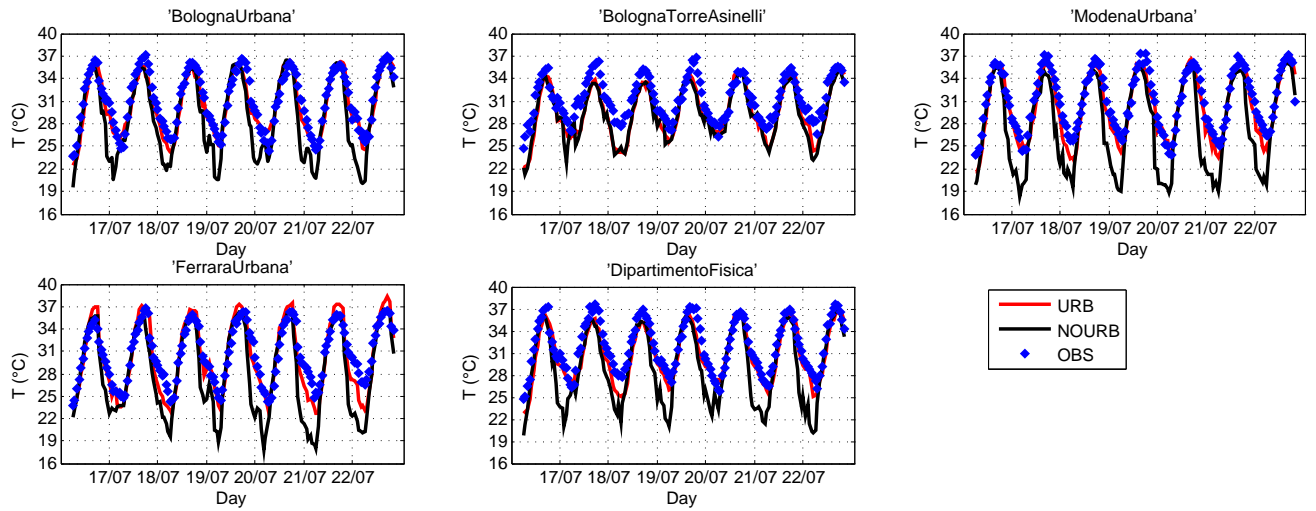
Figure 5.11: Temperature time series of OBS (blue dot), URB _NEST (red line) and NOURB(black line) for five different urban weather stations. All the period of simulation have been taken into account (neglecting the spin-up period).The value in the x-axis refers to the 00:00 of each day.

tions is not possible to notice substantial differences between the simulations, since the use of different rural area classes does not influence the temperature behavior within the city context.

These results confirm the efficiency of the 1WN method: for all the areas considered, the errors are similar to those of the two-way nesting simulation. However, URB_NEST seems to better reproduce the observational data for all stations (as it is possible to notice for the HR), but the differences are too little to determine the mechanism which leads to that difference."Bologna Torre Asinelli" is the station that which shows the greater errors and the lowest HR. The station is situated at the top of Torre degli Asinelli (96 meter from the ground), and in order to compare the simulation outputs with the observational data, the temperature have been evaluated at the 7th terrain-following level (while for the other urban stations we collect temperatures from the first or second level). However, the model cannot identify the tower within the grid cell: the buildings height is represented as a mean distribution within the grid cell, and buildings with the same height of the tower has not been taken into account, since the presence of just one tall building cannot affect the urban atmospheric dynamics.

On the other hand, the observed data are affected by the presence of the tower: the heat exchange between the tower and the free atmosphere strongly affect the near-tower temperature. Therefore, it acts warming up the air close to the building. Finally it is possible to affirm that, while the observed data are affected by the presence

78
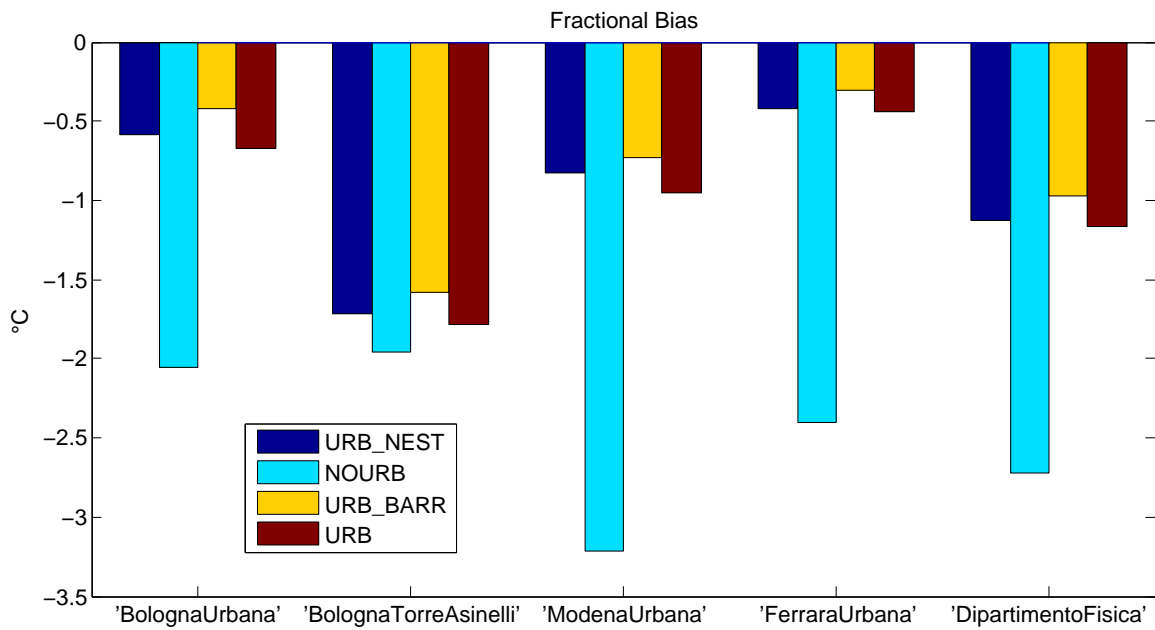
Figure 5.12: Temperature Mean Bias between OBS and URB_NEST (blue bars), NOURB (cyan bars), URB_BARR (yellow bars) and URB (red bars) for the four urban weather stations considered.
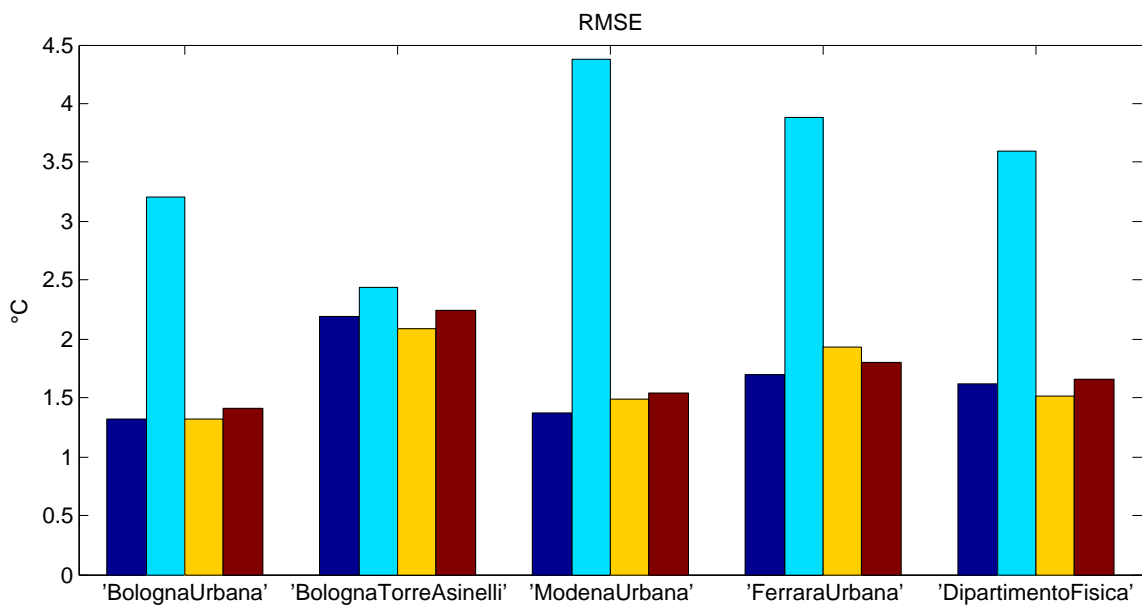
Figure 5.13: Temperature RMSE between OBS and URB_NEST (blue bars), NOURB (cyan bars), URB_BARR (yellow bars) and URB (red bars) for the four urban weather stations considered.
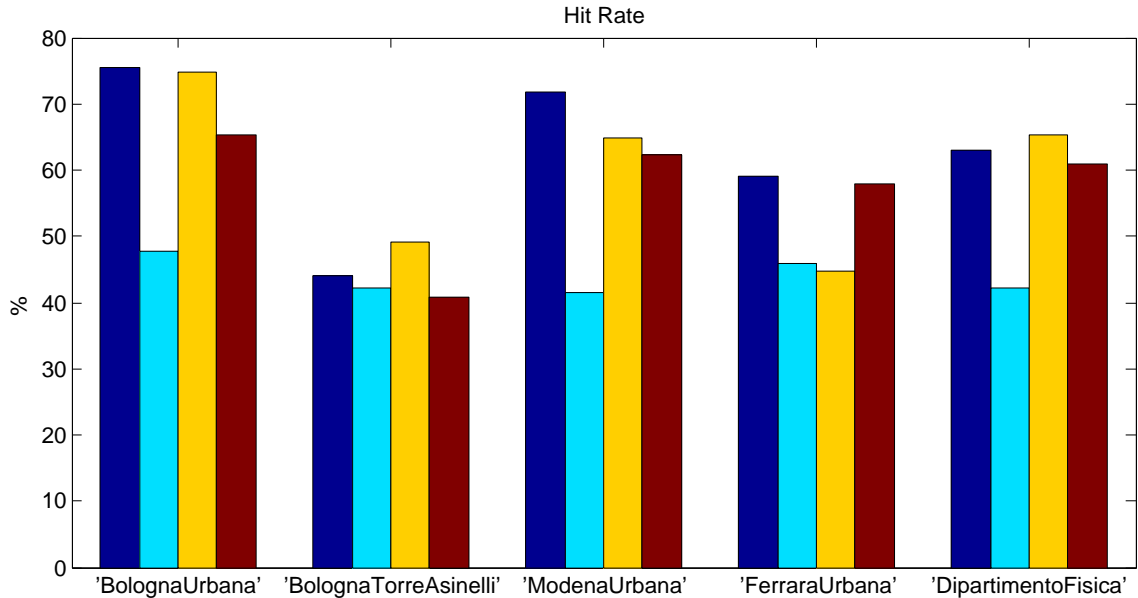
Figure 5.14: Temperature Hit Rate between OBS and URB_NEST (blue bars), NOURB (cyan bars), URB_BARR (yellow bars) and URB (red bars) for the four urban weather stations considered.

of the tower, the model grid cell chosen for the comparison is not directly affected by the presence of the building, leading to a greater error and in particular a greater underestimation of temperature for all simulations. Regarding the "Ferrara Urbana" station, it presents highest RMSE and MB (and lower HR) than the other urban stations close to the ground, for all simulations considered. This worst reproduction of UBL dynamics can lies in the definition of urban morphology:

the creation of urban landuse has been conducted manually digitizing the urban areas. Since this digitization has been made focusing on the city of Bologna and Modena, probably the definition of the urban morphology for the city of Ferrara is less coherent than that of the other cities, especially for the definition of thermal coefficients of buildings materials.

5.3 Relative Humidity

In the following section, the comparison between observed and simulated relative humidity (RH) is shown. Since relative humidity trend is related to the temperature, the stations chosen for this analysis have been selected between those of the temperature analysis. Therefore, we will compare the observed data coming from "Loiano" station for the hill area, "Mezzolara", "Castel San Pietro" and "Mirabello" stations for the rural area and finally "Bologna Urbana" and "Modena Urbana" for the urban

area.
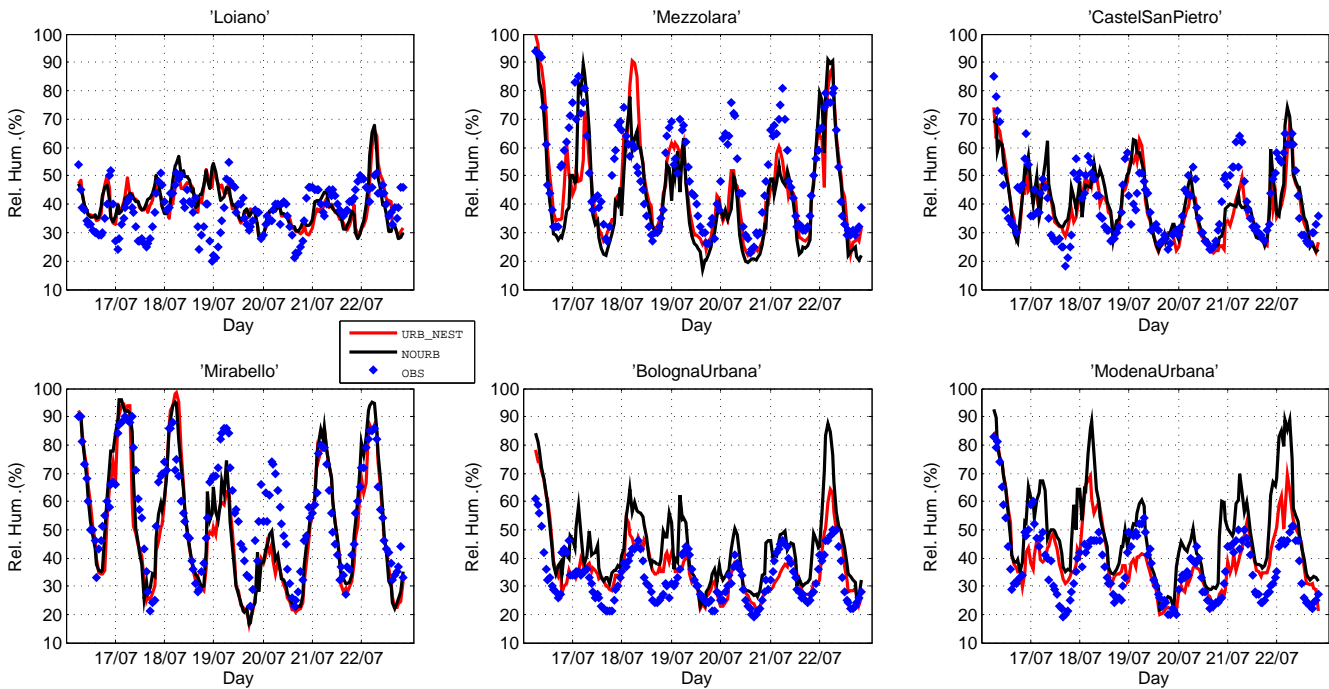
Figure 5.15: Relative Humidity time series of OBS (blue dot), URB_NEST (red line) and NOURB (black line) for six different weather stations. All the period of simulation have been taken into account (neglecting the spin-up period).The value in the x-axis refers to the 00:00 of each day.

Therefore we evaluate the behavior of RH for 1 hill station, 3 rural stations and 2 urban stations, comparing the same simulations of the previous section. In Fig. 5.15 the time series of relative humidity for the six stations cited above are shown. Clearly, the RH assumes higher values during the night than daytime, since the temperature is lower and air is closer to the saturation point. All the values for observed data lays in the range [20%, 92%] but trends strongly depends on the kind of area considered. In fact, the higher values are reached in rural areas ("Mezzolara", "Castel San Pietro" and "Mirabello"), with maximum values of 95%, since here the evapotranspiration takes place, forced by solar radiation. For "Loiano" station, the humidity never goes over the 55%, since at higher altitudes RH is lower than flatland areas.

On the other hand, the lowest values are assumed by urban stations. Since within urban structure evotranspiration takes place only in green urban areas, its contribute is very low, despite the anthropogenic latent heat release. In fact, the NOURB simulation in rural areas assumes always higher values than the observed data, since it is assumed that in this areas a croplands coverage is placed.

The pattern is different for all kinds of areas also for MB (Fig. 5.16).

For the hill station RH is slightly overestimated for all station (except for URB_BARR):
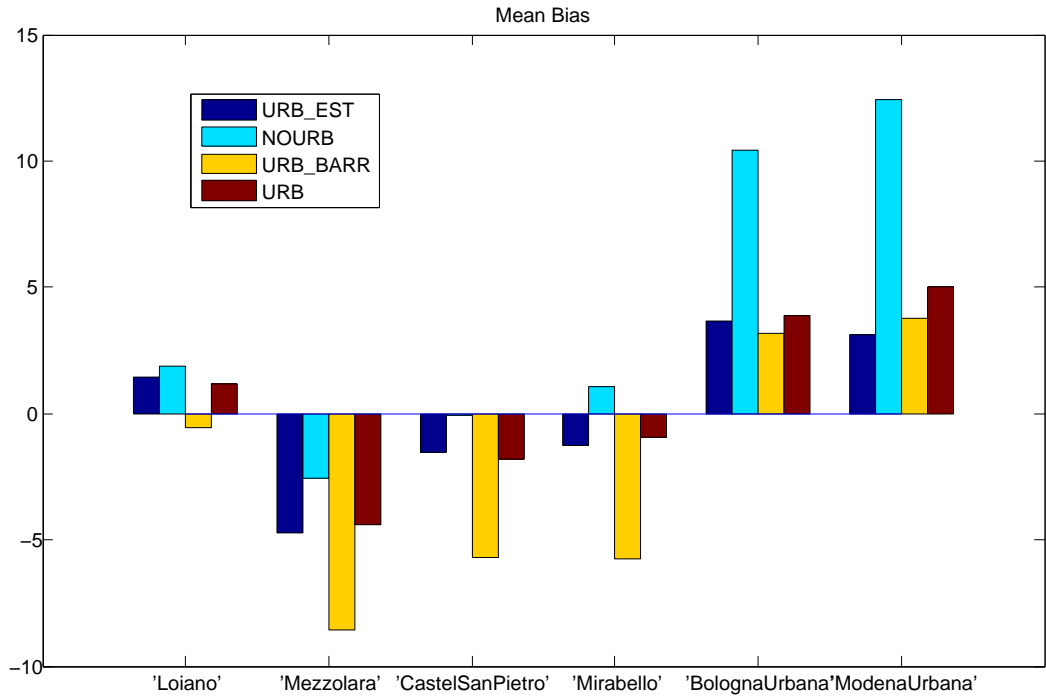
Figure 5.16: Relative Humidity Mean Bias between OBS and URB_NEST (blue bars), NOURB (cyan bars), URB_BARR (yellow bars) and URB (red bars) for the four rural weather stations considered.
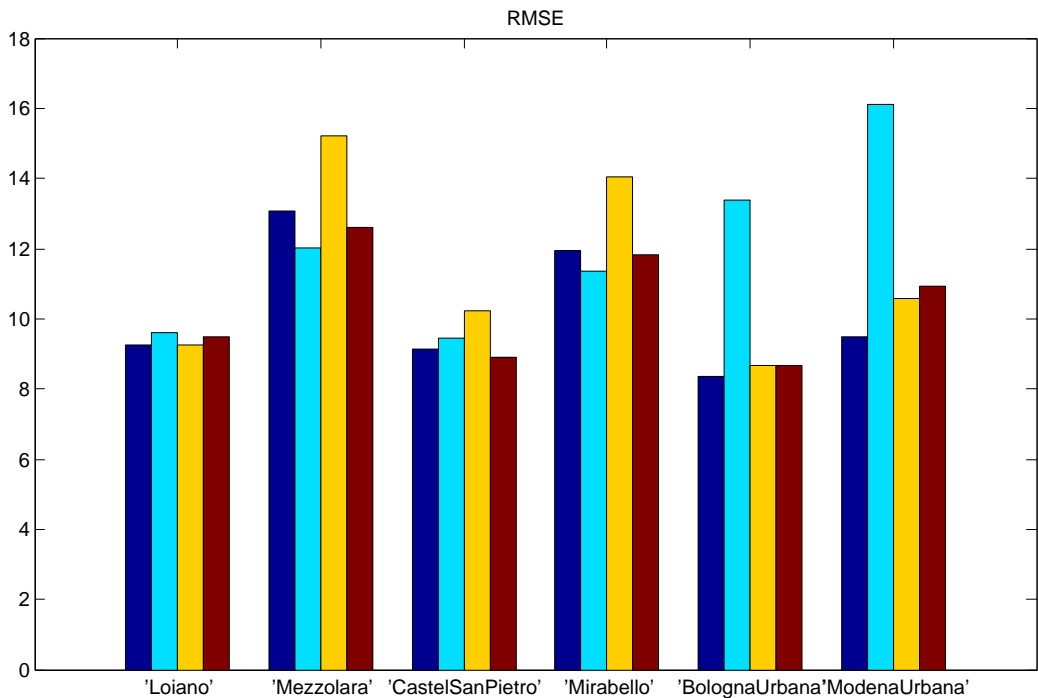
Figure 5.17: Relative Humidity Root Mean Squared Error between OBS and URB_NEST (blue bars), NOURB (cyan bars), URB_BARR (yellow bars) and URB (red bars) for the four rural weather stations considered.

URB and URB_NEST once again assume similar values, and the same for NOURB, since the cities does not affect this area.

For URB_BARR, RH is underestimated and close to zero, since (as said before) the rural land coverage is less vegetated. For the rural stations, on average RH is underestimated. URB and URB_NEST assume the same MB, while the best results are given by NOURB. At the same time, URB_BARR is the simulation which provides the worst output for RH because of the lesser fraction of vegetation. However, other rural stations (not shown in this work) show a better results for URB_BARR with respect to URB simulation for RELH. This demonstrates that the valley landuse is a mosaic of cultivated/not cultivated areas during the period considered. For urban areas, RH is always overestimated. In this case, the worst result is provided by NOURB, since the vegetation of this simulation is actually replaced by urban morphology. Once again, there are not evident difference between the 1WN and 2WN methods. The overestimation is probably due to the parametrization adopted for urban vegetation: while for rural zones it is possible to assign specific values for the kind of rural vegetation (such as the change from "Croplands" to "Barren and Sparsely Vegetated"), for urban areas the interaction between vegetation and atmosphere is computed in an unique way. We have demonstrated in the previous chapter that the "Barren and Sparsely Vegetated" category is that which better describe the temperature trend during the heat wave. On the other hand, within the city the parametrization of vegetation provides higher values of humidity with respect to the observational data, and would be necessary modify the code in order to reproduce the dryer conditions for urban vegetation.

The error cannot be linked to the anthropogenic latent heat release, because its contribute is too low to modify the relative humidity trend.

The best results for RMSE (Fig. 5.17), are provided by the "Bologna Urbana" station, followed by "Loiano" and "Castel San Pietro". In general, stations which overestimate RH assumes a lower error, both for RH and temperature.

5.4   The katabatic wind

In this section, we focus on the most relevant features of the katabatic wind for the city of Bologna, through a comparison between observational data and simulation outputs.

   The katabatic wind is a descending wind from higher altitude to the valley. It is caused by the temperature difference between the hills and the valley, and the consequent difference in air density: during night, air close to the slopes cools faster than
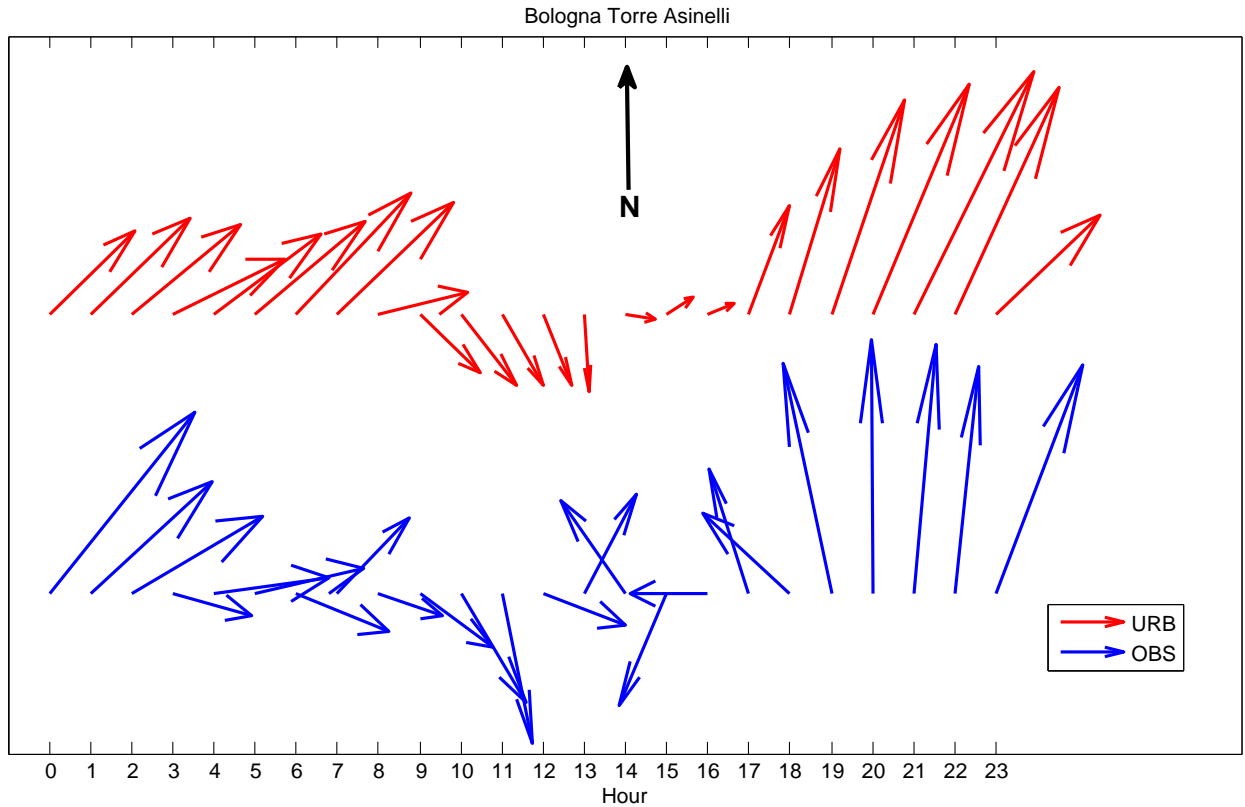
Figure 5.18: Diurnal cycle of wind for OBS and URB simulations. The black arrow on the top-right side of the picture refers to the North direction.

the air at the same height in the middle of the valley. The katabatic wind takes place along the hills, forced by gravity and temperature gradient. On the other hand, the anabatic wind behaves in the opposite way. When solar radiation heats mountain slopes, air masses become warmer than the air at the same altitude over the valley, and they are forced to rise along the mountain. Both katabatic and anabatic wind are mesoscale phenomenon, and they are clearly distinguishable in absence of synoptic forcing.

Focusing on our study area, the elevation gradient is present in the SW-NE direction, going from Apennines Mountains to the Po Valley.

Bologna is situated at the feet of Apennines, then we expect to capture the effect of katabatic/anabatic wind.

In Fig. 5.18 the diurnal cycle (from 0:00 to 23:00) of the wind vectors for the "Bologna Torre Asinelli" station is shown, both for URB simulation and observational data.

Since the hills are situated on the Southern side of the city, it is clear the presence of the katabatic wind from 0:00 to 07:00 in the SW-NE direction, due to cold air descending the hill's slopes. When the sun rises, we detect an inversion of the wind direction, with a simultaneous decrease of the speed: the heating both of mountain
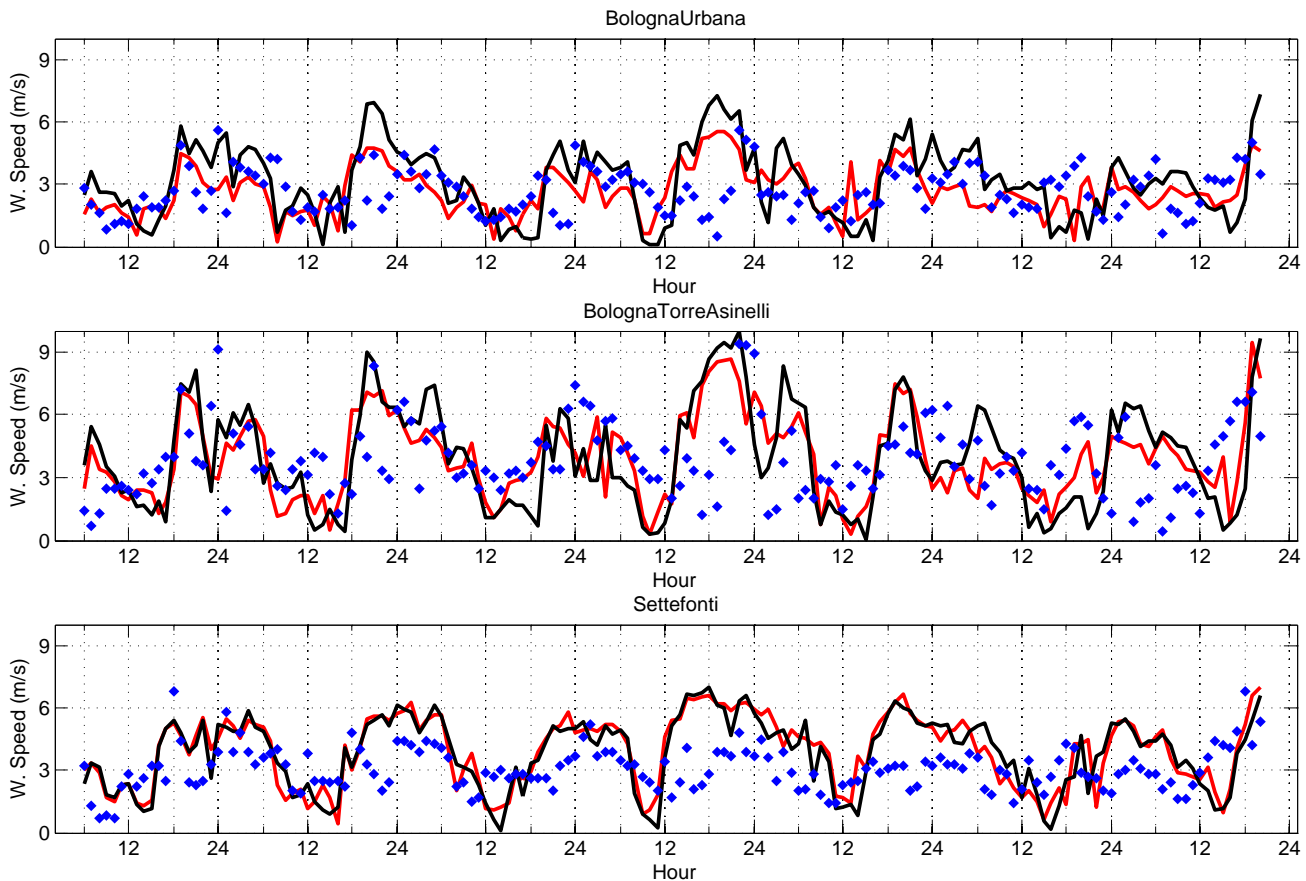
Figure 5.19: Time series of wind velocity for "Loiano", "Bologna Torre Asinelli" and "Sette-fonti" stations.

slopes and valley cancels the temperature gradient, and hot air masses slowly rise the slopes.

The simulation can capture the inversion, even though it is anticipated of one hour and on the central hours of the day the wind captured by the station presents random directions.

At the last hours of the afternoon, the cooling of hill's slopes due to the shadowing effect allows the katabatic wind to take place (from 17:00), both for simulations and observational data. However, the starting time of katabatic wind for simulation is delayed of one hour (it starts at 18:00).

Now, we focus on the evaluation of the model skills in reproducing the wind behavior. For this evaluation, we chose two urban stations ("Bologna Urbana" and "Bologna Torre Asinelli") and the hill station of "Settefonti". In Fig. 5.19 the wind velocity for the three stations considered for URB, NOURB and observational data are shown. In Fig. 5.20 the respective wind direction is presented. In Fig. 5.21 and 5.22 the RMSE and MB for wind velocity are shown, while Fig. 5.23 regards the RMSE of wind direction.

85
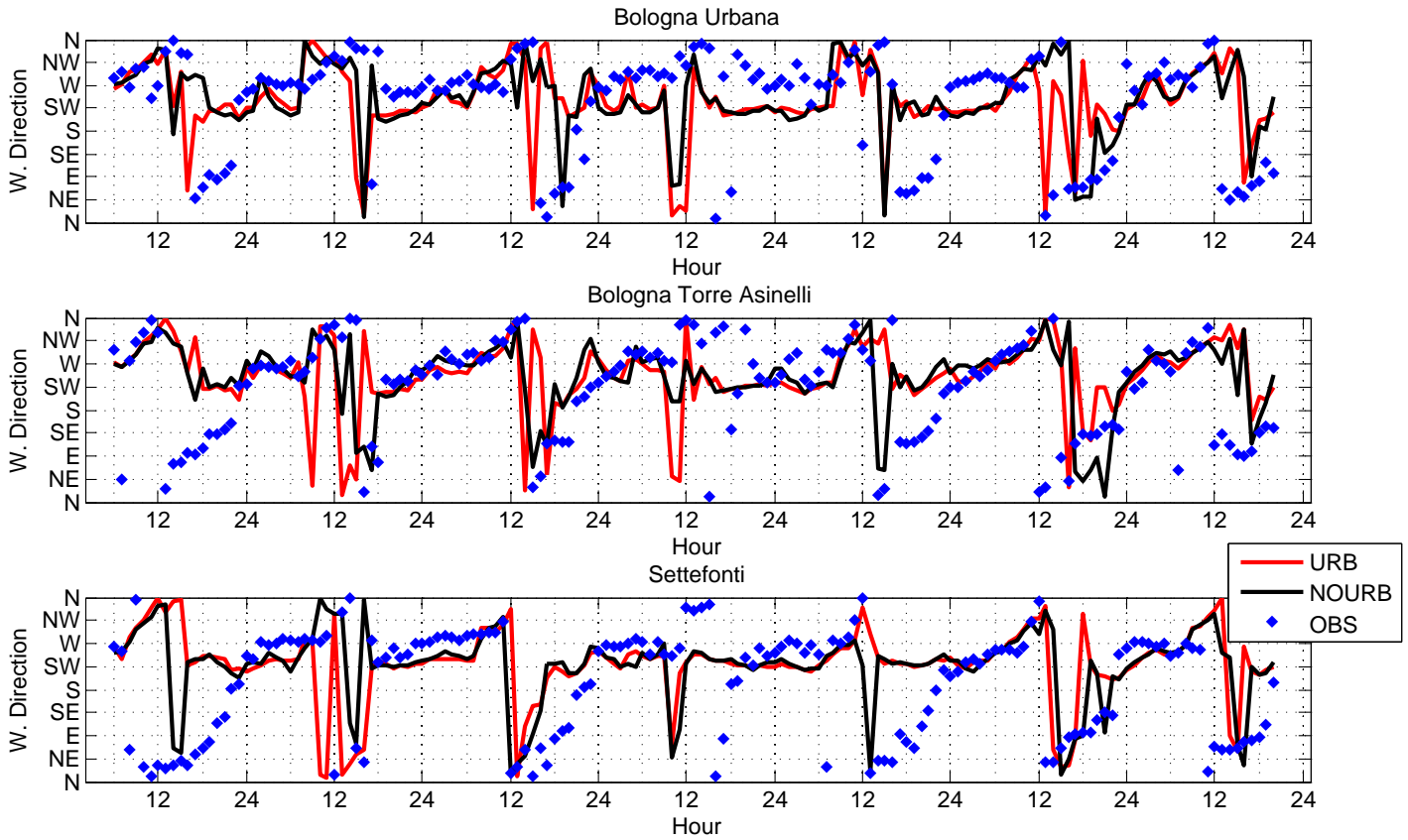
Figure 5.20: Time series of wind direction for "Bologna Urbana", "Bologna Torre Asinelli" and "Settefonti" stations. In ordinate the direction of the incoming wind.

The calculation of residuals (used to compute RMSE and MB) for wind direction have been conducted as follow [Jiménez and Dudhia, 2013]:

$$\Delta\theta = \begin{cases} \theta_{mod} - \theta_{obs} & \text{if } \theta_{mod} - \theta_{obs} \leq |180| \\ \theta_{mod} - \theta_{obs} - 360 & \text{if } \theta_{mod} - \theta_{obs} > 180 \\ \theta_{mod} - \theta_{obs} + 360 & \text{if } \theta_{mod} - \theta_{obs} < -180 \end{cases}$$

However, the MB has not been shown, since it has not been possible to observe substantial differences between stations and simulations. Terrain morphology is the principal cause of error,even though the different settings of simulations. It is always negative for all stations and simulations, in the range $[-2°, -10°]$.

Simulations always overestimate wind velocity for all simulations. The systematic error is linked to the morphology: the model cannot capture exactly the variation of elevation, leading to overestimations or underestimations of the wind velocity and direction, such as in this case.
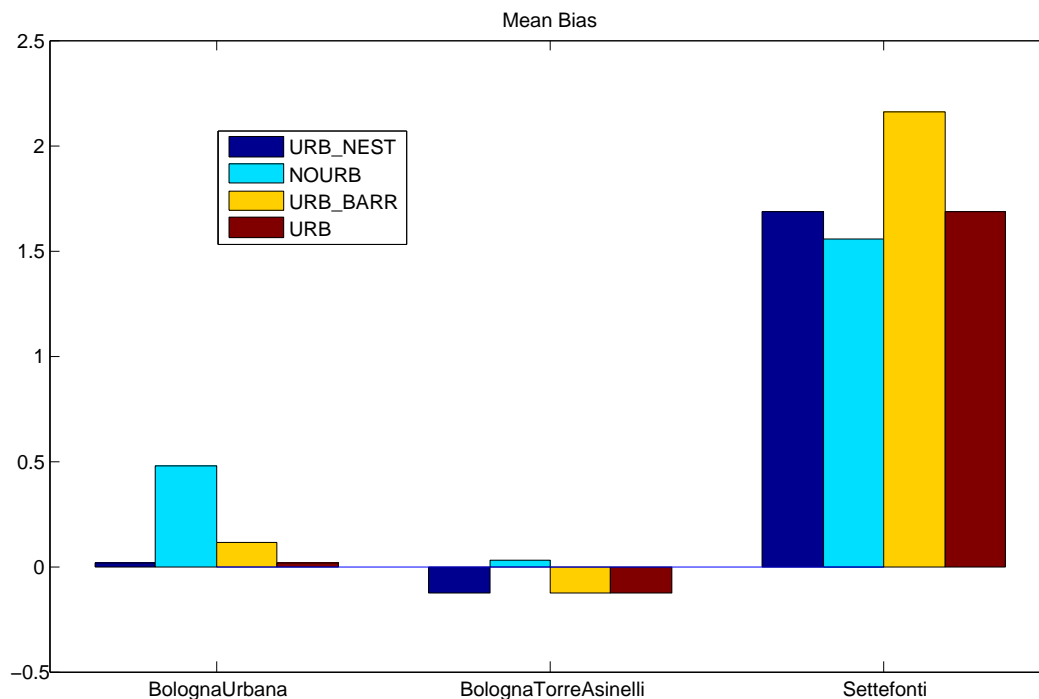
Figure 5.21: Wind velocity Mean Bias between Observational data and URB_NEST (blue bars), NOURB (cyan bars), URB_BARR (yellow bars) and URB (red bars) for the three weather stations considered.

On the contrary, for the urban stations wind velocity is in good agreement with observational data. Here the presence of buildings plays a key role: the building-induced drag converts mean velocity into its turbulent components, leading to the reduction of mean velocity.

The "Bologna Urbana" station is located at the height of buildings: the URB simulation is in good agreement with observational data (the MB for all simulations which takes into account the presence of the city is around 0). On the other hand, the NOURB simulation shows an overestimation (the MB is around 0.5 m/s): since the city has been replaced with croplands, buildings-induced drag is not present. Regarding the "Torre degli Asinelli" station (96 m) the drag is not present (more precisely, it slightly influences the wind velocity through the shear induced on the lower levels). Therefore, the difference of mean bias of wind velocity between URB and NOURB simulation is smaller than the "Bologna Urbana" case.
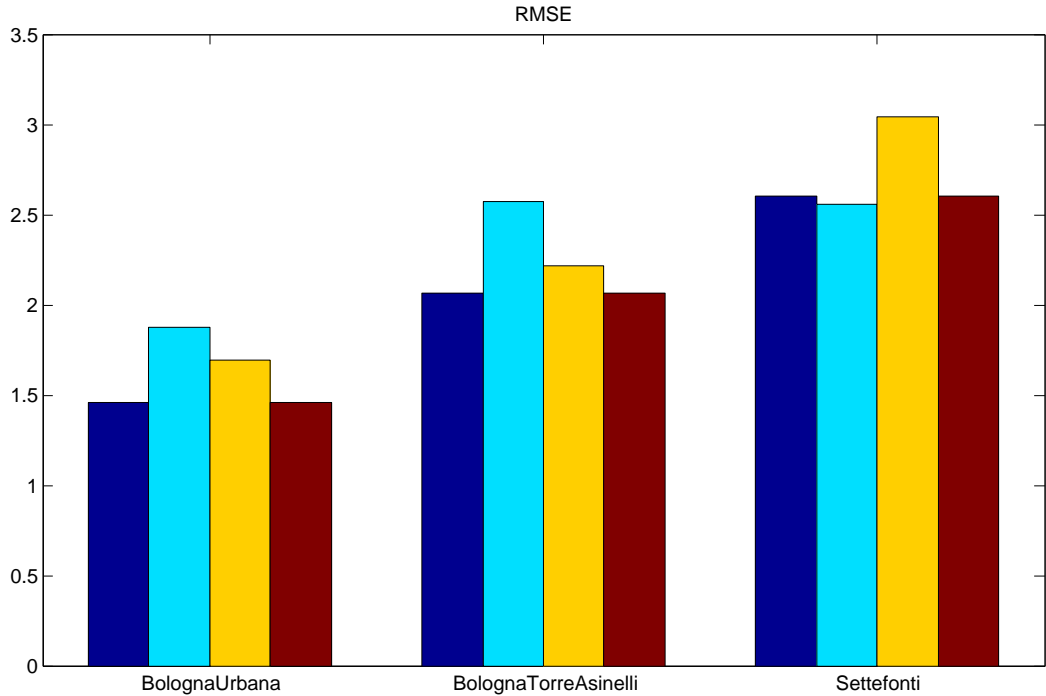
Figure 5.22: Wind velocity RMSE between OBS and URB_NEST (blue bars), NOURB (cyan bars), URB_BARR (yellow bars) and URB (red bars) for the three weather stations considered.

Looking at the wind directions, it is possible to identify for each station a typical diurnal trend.

The trend of "Bologna Torre Asinelli" and "Bologna Urbana" stations (since they are very close, the behavior of wind direction is very similar) is the same shown before: the simulations can capture the katabatic wind (present each day from the first hours of the night until the first hours of the day). However,simulations cannot always capture the transition from the absence to the presence of the katabatic wind for all the seven days, since the inversion is almost instantaneous. The inversion phase is captured only for the 6th day of simulation by both the urban stations.

The city does not seem to affect the katabatic wind: both URB and NOURB simulations capture the inversion of wind direction for all the days. Similar is the behavior for "Settefonti" station. It is located on the SE side of Bologna at 300 m over the sea level. The trend of direction is the same of Bologna, and the simulations once again cannot capture the transition phase from the N-E to S-W direction of the wind. Regarding the errors committed in the wind direction, for all stations the RMSE is around 70°, and it is not possible to identify differences between the different simulations. Then, the variation on setting these simulations does not affect the efficiency in capturing the wind direction.
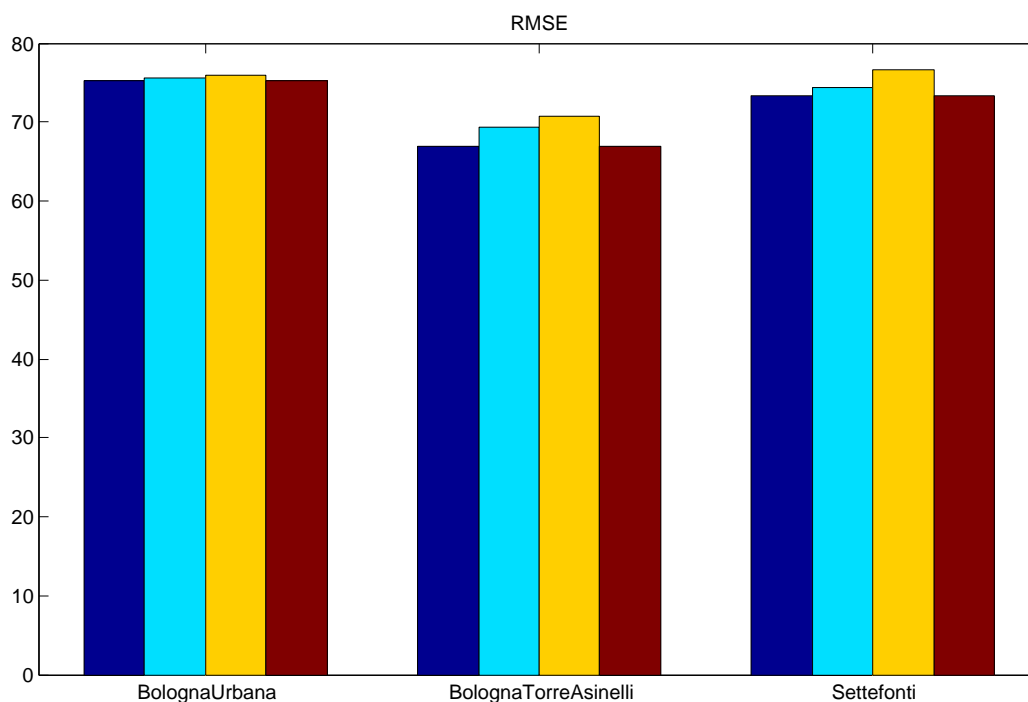
Figure 5.23: Wind DIRECTION RMSE between OBS and URB_NEST (blue bars), NOURB (cyan bars), URB_BARR (yellow bars) and URB (red bars) for the three weather stations considered.

5.5 Evaluation of the UHI for the cities of Bologna and Modena

In this section, the diurnal cycle of the UHI for the city of Bologna and Modena is discussed. Since the UHI effect is defined as the difference in temperature between urban and rural area, the temperature difference trend is evaluated comparing a station located within the city and another one situated in the surrounding rural area. The evaluation have been conducted comparing the observational data with URB and NOURB, with the aim to identify the effect of the city with respect to its absence.

In Fig. 5.24 the temperature difference between "Bologna Urbana" and "Mezzolara" stations, projected into a diurnal cycle is shown. "Mezzolara" is situated on the North-East side of the city in the open valley, 17 km far from the urban station. Comparing URB with observational data, the UHI is present during nighttime and absent during daytime. In particular, the temperature difference is greater from 23:00 until 6:00 for both simulation and observed data. However, for URB the UHI is of $\simeq 5\,°C$ while for OBS is of $\simeq 4\,°C$: URB overestimates the temperature difference of $\simeq 1\,°C$ during nighttime.
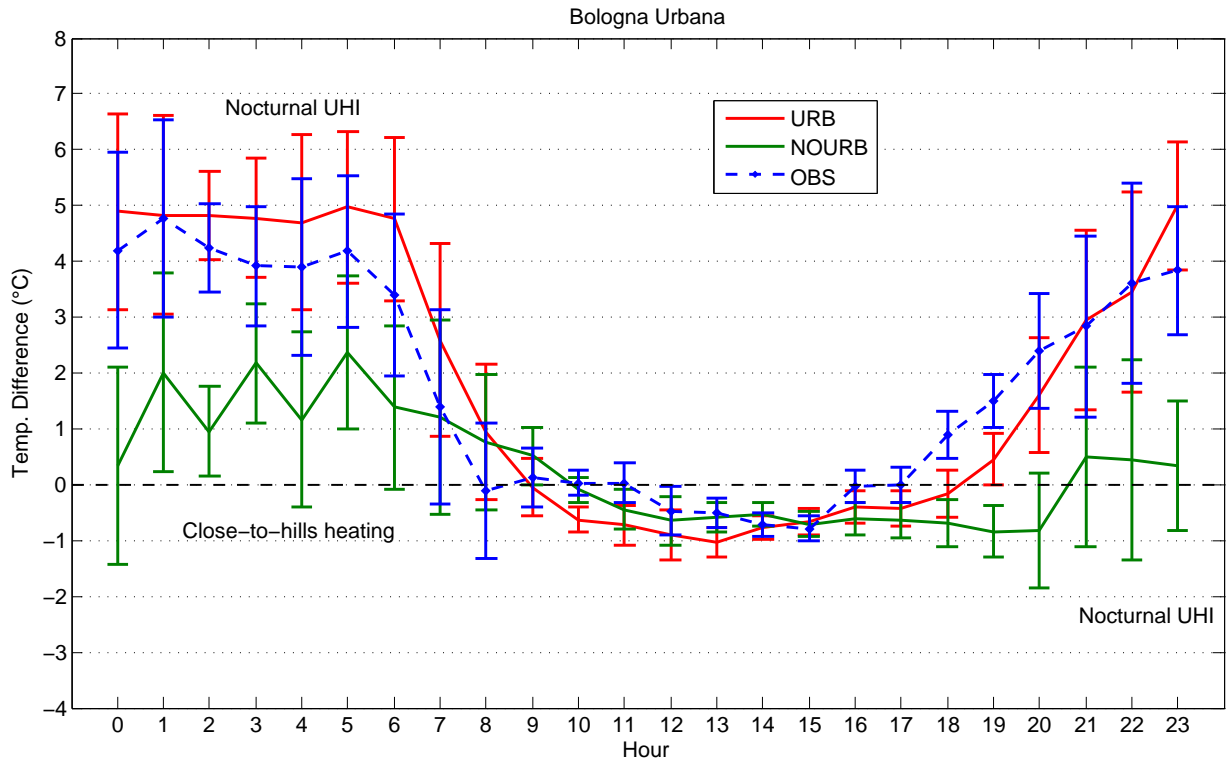
Figure 5.24: Diurnal cycle of temperature difference between the stations "Bologna Urbana" (urban) and "Mezzolara" (rural) for URB (red solid line), NOURB (green solid line) and OBS (blue dashed line). Errorbars represent the RMSE relative to the mean difference.

This overestimation, lies in the fact that temperature for the rural station of "Mezzolara" is underestimated, as discussed before in Sec. 5.2.1: since temperature is underestimated, the ΔT between the city and the close rural areas is overestimated. After the sunrise, the UHI rapidly fall down in both cases. The transition phase lasts three hours , but it is delayed of one hour for URB.

At the same time, the simulation can capture the lower value of temperature within the city with respect to the open valley during the second half of the daytime: this is due to the heat storage in building materials. In fact, the greater value of buidings materials capacity with respect to the rural one leads to the heat storage during daytime, and to its release during nighttime.

Both for URB and observed data, the UHI effect starts at 17:00, when the heat stored within the building materials starts to be released into the atmosphere. The ΔT keeps rising for all the transition period from daytime to nighttime, reaching its peak at 23:00 and lasting until 6:00 as said before. The observed ΔT rises more rapidly than that of the simulation, but it is in good agreement in timing. The error is probably linked to the definition of urban morphology (in particular in the definition of the thermal coefficients of building materials). For NOURB simulation, it is not possible to observe substantial differences during daytime: this demonstrates that the city

Figure 5.25: Diurnal cycle of temperature difference between the stations "Settefonti" (hill) and "Mezzolara" (rural) for URB (red solid line), NOURB (green solid line) and OBS (blue dashed line). Errorbars represent the RMSE relative to the mean difference.

does not influence the ΔT during daytime.

On the other hand we could expect a close to zero difference during nighttime: actually, the temperature in the area where the city would be placed is higher than the temperature in the open valley. This effect is due to the fact that Bologna is situated at the feet of mountains, while "Mezzolara" station on the open valley.

In order to better understand this phenomena, a comparison of temperature trend between the hill station "Settefonti" (where there are not urban structures) and the rural station "Mezzolara" have been performed (Fig. 5.25). "Settefonti" station is situated at 330 m above the sea level (198 m for the model) on the South-East side of Bologna. During daytime temperature is clearly lower in the hills rather than the valley (from 10:00 until 21:00), but during night the temperature is higher on hills (the difference oscillates between 2 °C and 3 °C). Both URB and NOURB can reproduce the variability of temperature showed by observational data. The same phenomenon has been observed by [Daly et al., 2010], and its causes have not been investigated in this work.

Dealing with the UHI effect for the city of Modena (Fig. 5.26), the comparison have been evaluated between the "Modena Urbana" urban station and the "Albareto"
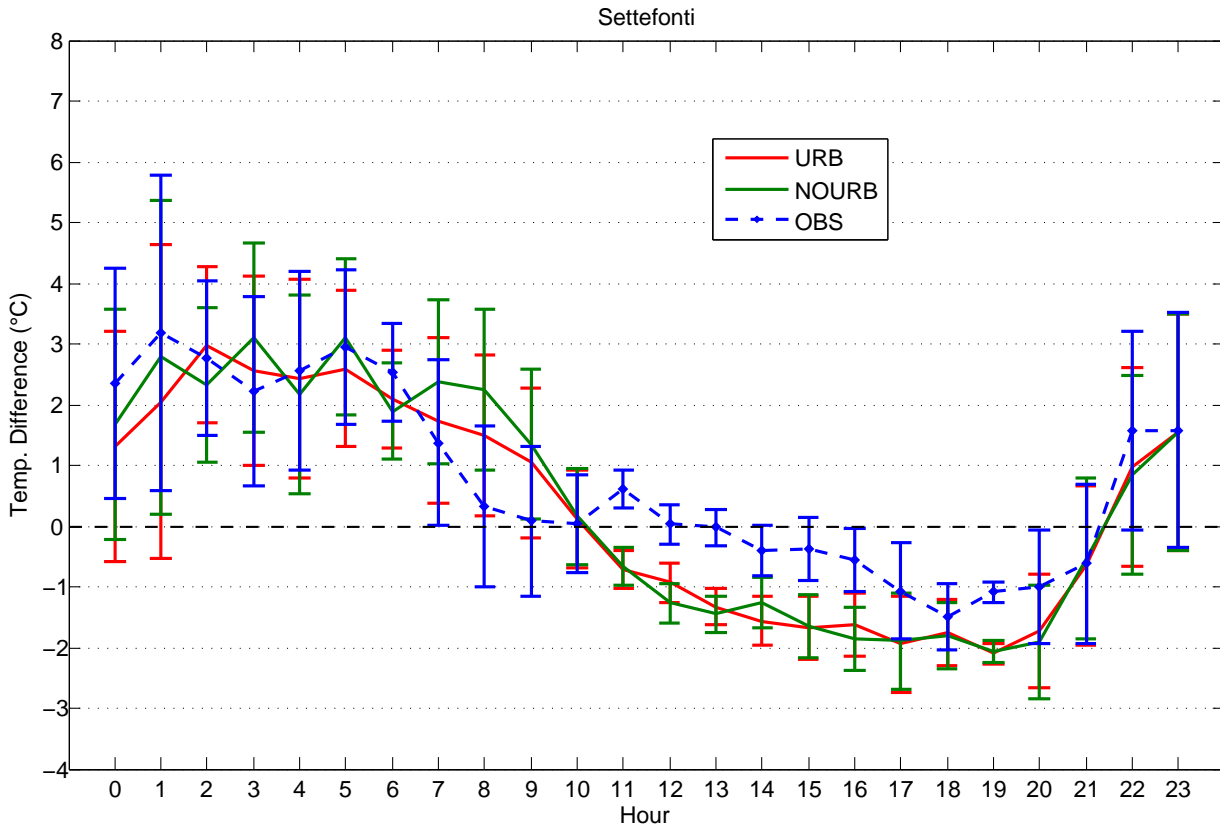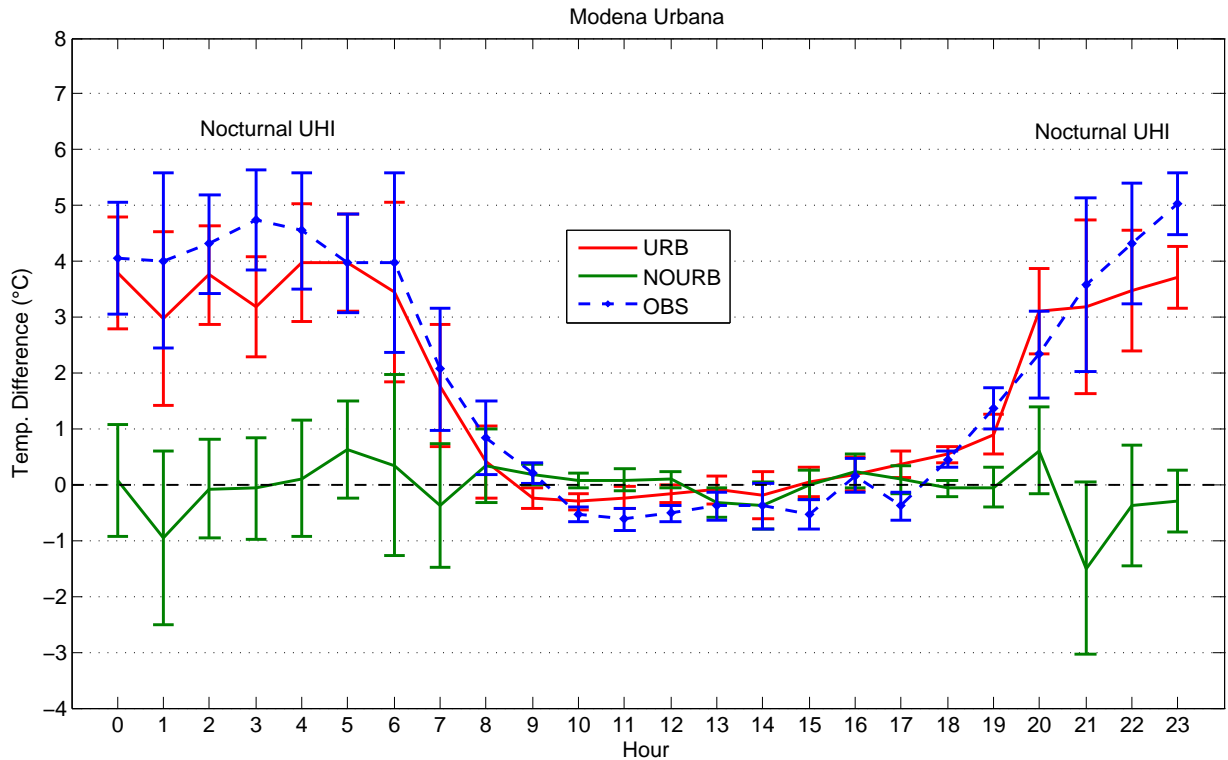
Figure 5.26: Diurnal cycle of temperature difference between the stations "Modena Urbana" (urban) and "Albareto" (rural) for URB (red solid line), NOURB (green solid line) and OBS (blue dashed line). Errorbars represent the RMSE relative to the mean difference.

rural station, 6 km far from the city in the North direction. First of all, since Modena is situated on the open valley (and not at hill's feet), it is not possible to detect for NOURB temperature differences during nighttime. Dealing with the evaluation of the UHI, it is present only during night, as in the case of Bologna. The simulation can better capture the morning transition to the vanishing of the UHI with respect to the case of Bologna. At the same time, the slope of the rising of UHI during the last hours of the afternoon is better reproduced. However, ΔT is overestimated during nighttime of around 1 °C, while during daytime, the temperature difference trend is in good agreement with observed data.

Summmary

In this chapter, the comparison between model outputs and observational data have been performed.

We focused on the trends of temperature, relative humidity and wind direction and velocity, evaluating the errors committed for each variable.

Several simulations have been compared with observational data provided by weather stations: the URB simulation, performed with the 1WN method; the URB_NEST simulation, performed with the 2WN method; the NOURB simulation, performed with the 1WN and replacing the urban landmask with croplands. Finally the URB_BARR simulation, performed with the 1WN method and replacing the "Croplands" rural class with the "Barren and Sparsely Vegetated" rural class.

Each variable have been evaluated for the three kinds of area considered in this work: rural areas, hill areas and urban areas. This distinction is helpful with the aim to evaluate the efficiency of the different simulations in reproducing the dynamics over a given zone.

For all areas, temperature is generally underestimated: it is not possible to notice substantial differences between URB and URB_NEST, while the best simulation representing the temperature trend is URB_BARR.

Relative humidity is underestimated for rural areas and overestimated for urban areas: the kind of vegetation coverage plays a key role.

Finally, we focused on the katabatic wind. All simulations can capture the katabatic wind which descends Appennine's slopes on average from 17:00 to 7:00 of each day, due to the temperature gradient between hills and valley in the SW-NE direction. However, the simulations cannot truly represent the transition between katabatic/anabatic wind. For the city of Bologna, it is possible to notice a relevant difference between URB and NOURB simulations: since the building-induced drag converts mean wind velocity into turbulent component, for the "Bologna Urbana" station the NOURB simulation overestimate wind velocity. In this case, the drag induced by buildings is not taken into account.

In the second part, the UHI effect for the cities of Bologna and Modena have been evaluated, validating the results through the comparison with observational data. In order to detect the UHI, the comparison has dealt the diurnal cycle trends of temperature for a urban station and a rural station close to the considered cities. For the city of Bologna, the UHI effect is present from 17:00 to 9:00 of the next day. The URB simulation slightly overestimate the ΔT during night: the temperature for the rural station is underestimated, and this underestimation is reflected into an higher tem-

perature difference. NOURB simulation shows an higher temperature for the area where the city would be located with respect to the open valley: this is due to the higher cooling rate of open valley zones with respect to areas at the feet of hills. This phenomena is well shown by the comparison between "Settefonti" and "Mezzolara" stations.

For Modena, the UHI effect is slightly underestimated for the URB simulation during nightime. At the same time, since Modena is situated in the open valley, NOURB simulation does not show temperature difference during nighttime.

Chapter 6

Results, Part II: analyzing the simulations results

In this chapter, we deal with the most relevant features shown by simulations. Comparison with observational data, shown in the previous chapter, is useful to evaluate the efficiency of the model used and to prove its skills in reproducing the boundary layer dynamics. However, observational data provides only punctual features. The analysis of simulations output allows to evaluate the horizontal and vertical variations of variables at different times.

In the first part of this chapter, the behavior of 2-meter air temperature and 10-meter wind within a diurnal cycle for the whole domain is shown. Later, we deal with the features of the vertical profiles of turbulent variable, focusing on the difference between urban and rural areas. Finally the effect of the implementation of rooftop photovoltaic panels (RPVP) is discussed, focusing on its effect on the UBL and energy consumption budget.

6.1   Temperature and wind maps

In this section, the features of 2-meter air temperature and 10-meter wind are presented, focusing on the variation during a diurnal cycle. In Fig. 6.1 the map of 2-meter temperature and wind vectors averaged over six days of simulation are shown. It is easy to detect the temperature difference between urban and rural areas: in the urban areas the temperature is around 31 °C, higher in the city centers (clearly distinguishable for the city of Modena) than its surrounding areas; in the rural areas of Po Valley far from cities, the mean temperature is between 28 °C and 29 °C.

At the same time, going in the SW direction, the temperature diminishes until 19 °C , since the altitude keeps increasing until 1536 m, which is the maximum height
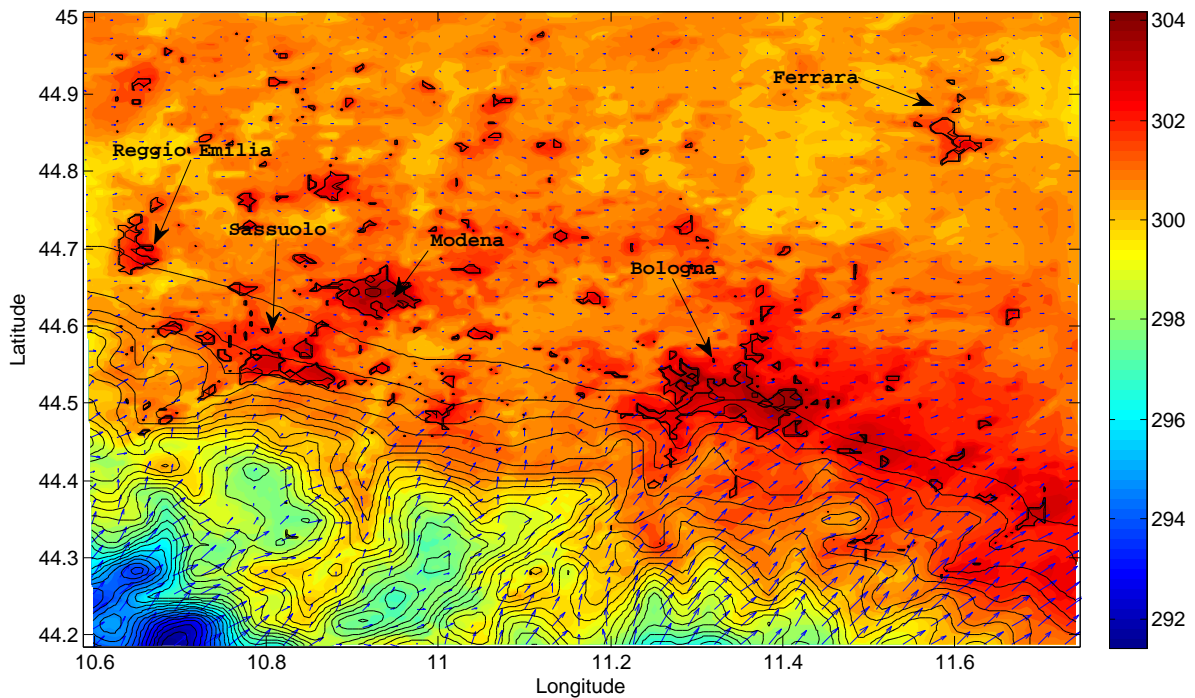
Figure 6.1: Map of 2-meter air temperature of URB averaged over six 24-hour period (fromt 6:00 of the first day to the 6:00 of the last day, i.e. from the 11th hour until the 155th hour). In the same way, 10-meter wind vectors averaged over the same period have been overlayed. The map also shows the contours of terrain height (plotted every 50 m) and urban morphology.

within this domain. Dealing with the wind vectors, it is clear that it is very stable in all the valley assuming the average over all the time period (i.e the averaged value of speed are close to 0, while it is not possible to identify a relevant direction). It is possible to detect a considerable non-zero value of wind speed in hills and mountain areas; the wind direction is from SW to NE: this is clearly a katabatic wind, due to the temperature gradient which generates in the same direction. The gradient is due to the terrain morphology; cold air descend from higher areas, and it reach the valley. Here the gradient is null, so the katabatic wind is not present anymore.

In Fig. 6.2 the difference between URB and NOURB 2-m air temperature averaged over six days of simulation, with the aim to evaluate the UHI between urban and rural areas during the heat wave considered. The temperature difference is higher in city centers ($\simeq 3\,^{\circ}$C), except for that of Bologna. In city centers (parametrized with LCZ 2), the vegetated fraction is 0 and building are highly clustered (road width = 10 m, building width= 10 m). The case of Bologna is slightly different: the Northern part of the city is warmer than the Southern part (especially industrial areas, LCZ 8). This effect is due to the katabatic wind which on average moves down colder and dense air and as consequence cools areas closer to hills.
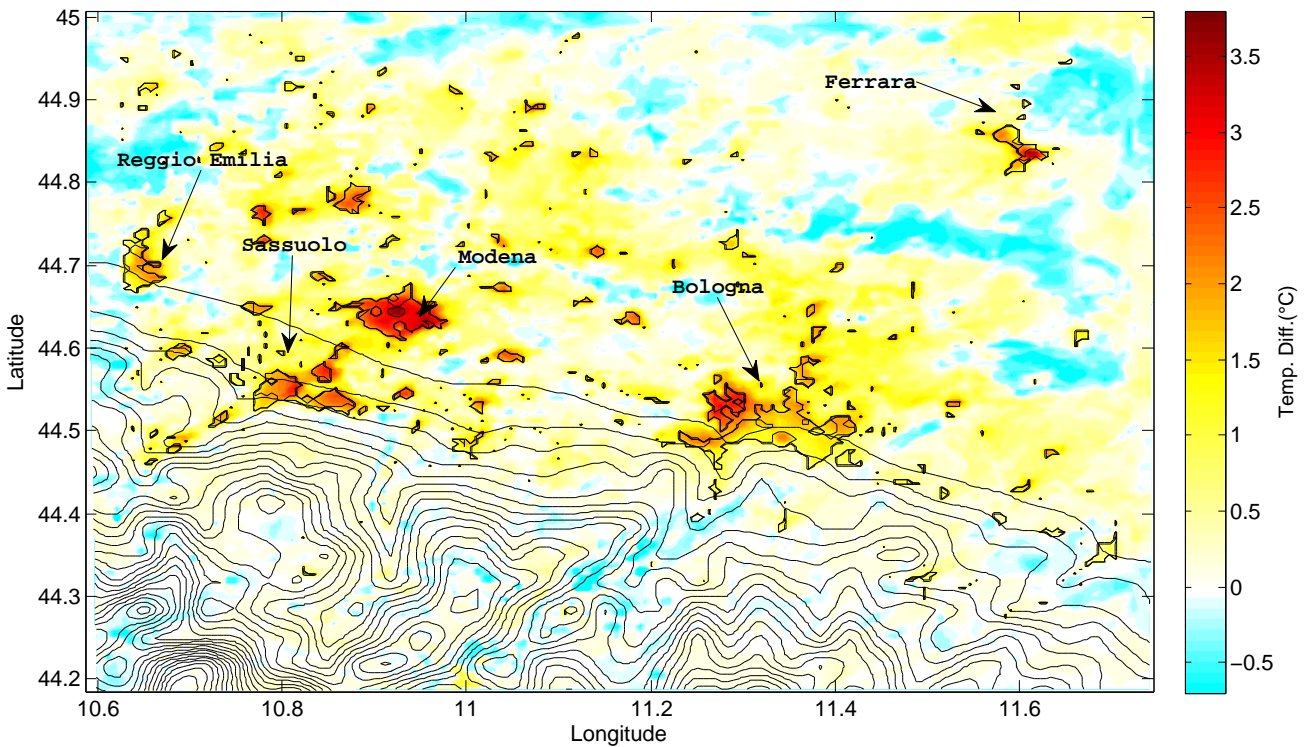
Figure 6.2: Map of 2-meter air temperature difference (URB-NOURB) averaged over six 24-hour period (fromt 6:00 of the first day to the 6:00 of the last day, i.e. from the 11th hour until the 155th hour).

After this explanation about the all-period averaged values of the simulation, we focus on the diurnal cycle and its most relevant characteristic: in Fig. 6.3, 6.4, 6.5, 6.6, 6.7 and 6.8 the 2-meter temperature averaged over all six days into a diurnal cycle is shown, respectively for the hours 10:00, 14:00, 18:00, 22:00, 2:00 and 6:00 local hour (i.e. the entire diurnal cycle with a time interval of 4 hours). At 10:00 (Fig. 6.3), the UHI is not present: temperature difference between rural and urban areas is null. At the same time, there is not katabic wind, since there is no horizontal temperature gradient between valley and hills. The situation at 14:00 (Fig. 6.4) is more or less the same: the only difference regards the higher temperature of city centers, warmer than the surrounding urban areas. The features of temperature and wind change radically at 18:00 (Fig. 6.5): hills slopes are become cooler than the close valley, and a horizontal temperature gradient is grown. This lead to the formation of the katabic wind in the north-east direction. At 22:00 (Fig. 6.6) and at 2:00 (Fig. 6.7) the UHI effect for the city is relevant: the temperature difference between rural and urban areas is around 4 °C for all cities.

In particular, the effect is stronger of the city of Bologna, since it is the bigger city within the domain. At 6:00 (Fig. 6.8) the sun is already risen, but this forcing is not
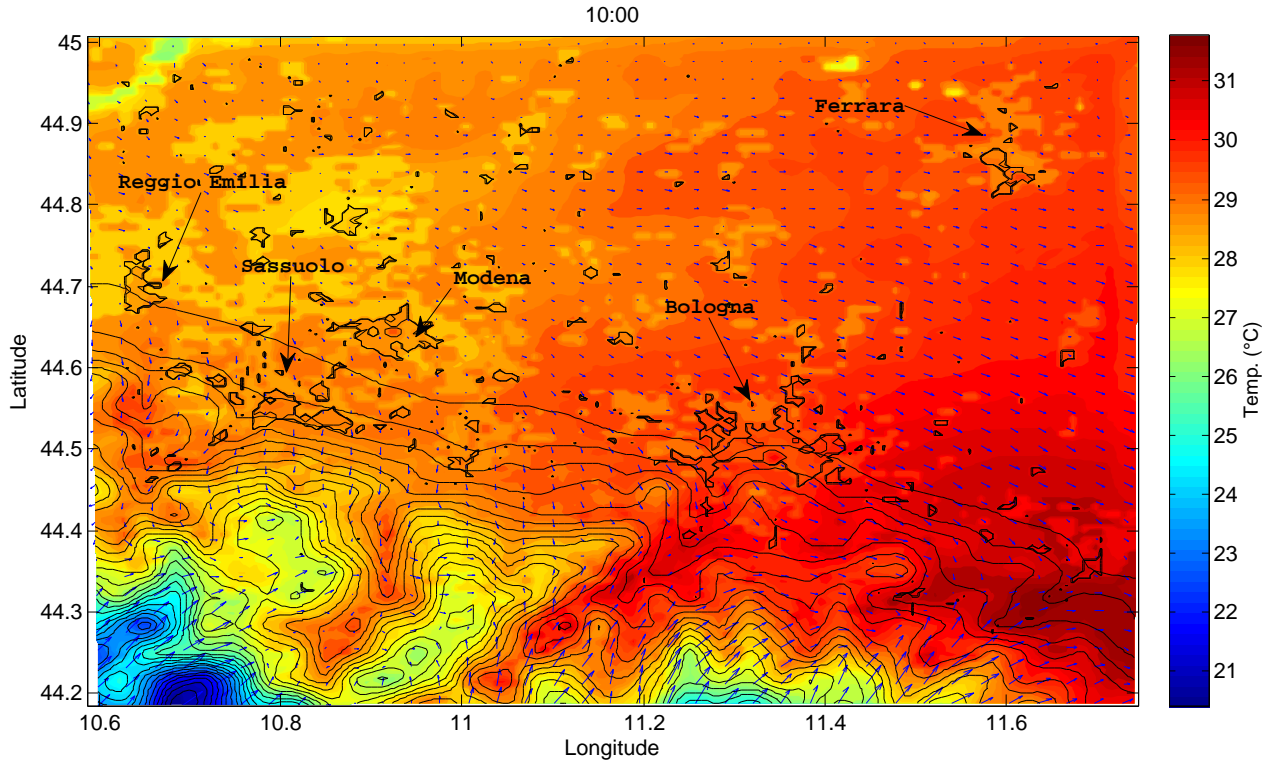
Figure 6.3: Map of 2-meter temperature and wind vectors (URB simulation) at 10:00 averaged over all the 6 days of simulation at the same hour.
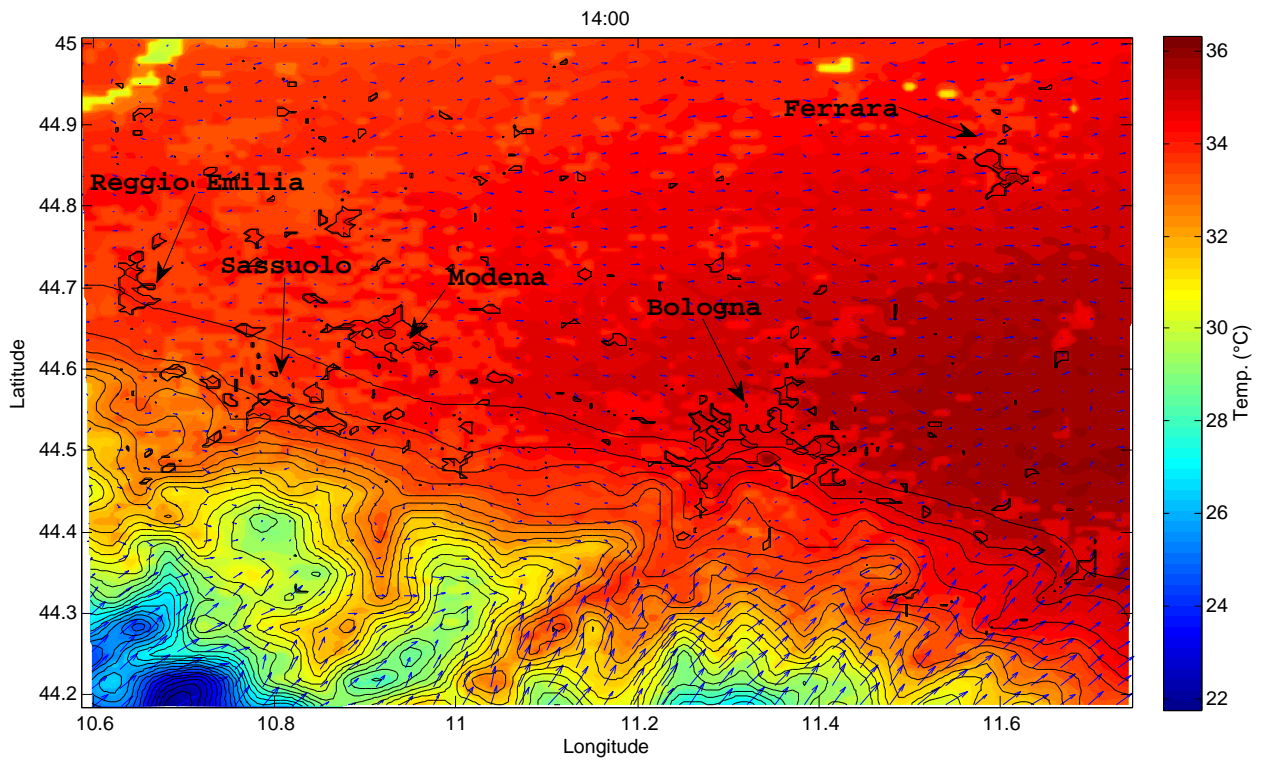
Figure 6.4: Map of 2-meter temperature and wind vectors (URB simulation) at 14:00 averaged over all the 6 days of simulation at the same hour.
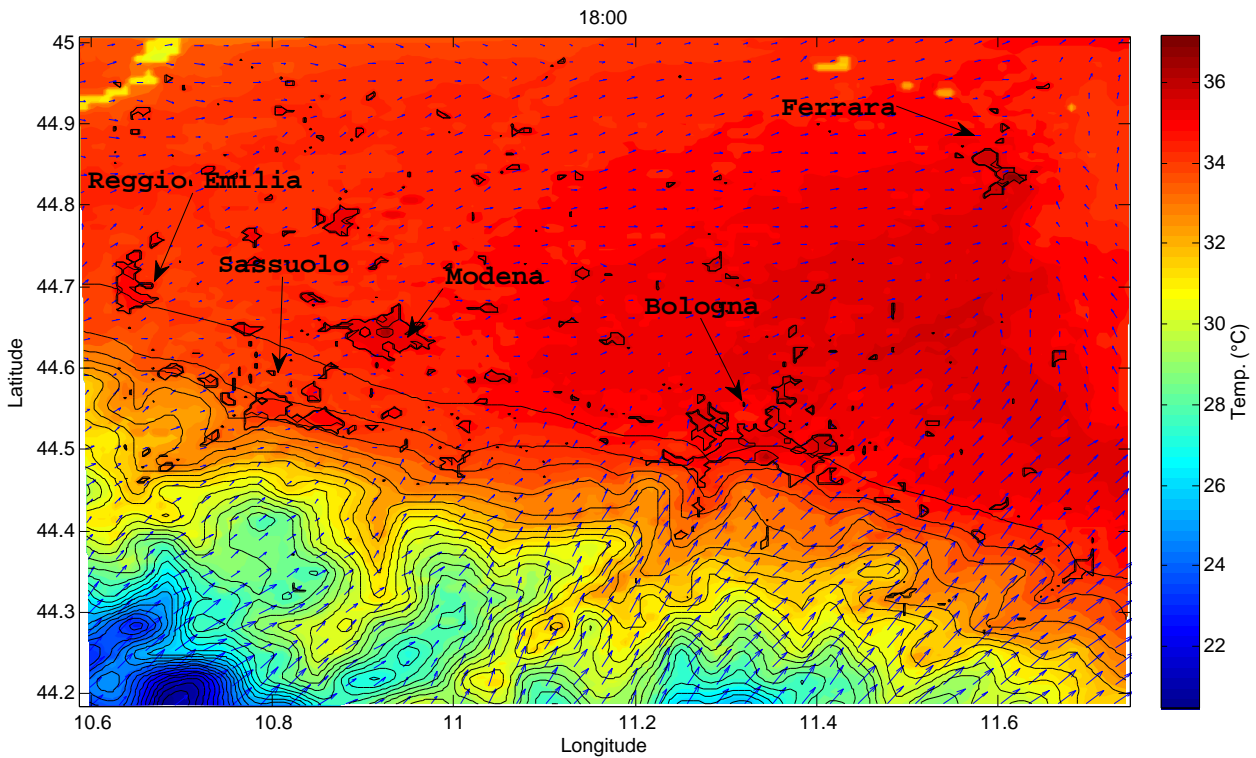
Figure 6.5: Map of 2-meter temperature and wind vectors (URB simulation) at 18:00 averaged over all the 6 days of simulation at the same hour.

yet strong enough to equalize the temperature between urban and rural areas, and the UHI effect is still present. On the other hand, the katabatic wind is still present, and the temperature of the hills close to the valley is greater than the temperature on the valley: this is the effect observed and discussed in the previous chapter for the "Settefonti" hill station.

The UHI effect, as said in the first chapter of this work, is mainly due to the heatstorage within the building materials.

As shown in Fig. 6.9 , during the day the sensible heat released to the atmosphere is greater for rural areas than urban areas. At 16:00, heat release in rural and urban areas assumes the same value. From 16:00 to 2:00, the heat stored within the urban morphology is released: in this time period it assumes always positive (i.e. the heat is released to the atmosphere). For rural areas, the heat release rapidly fall down zero (at 19:00) and keeps a negative value until the 8:00 of the next day.
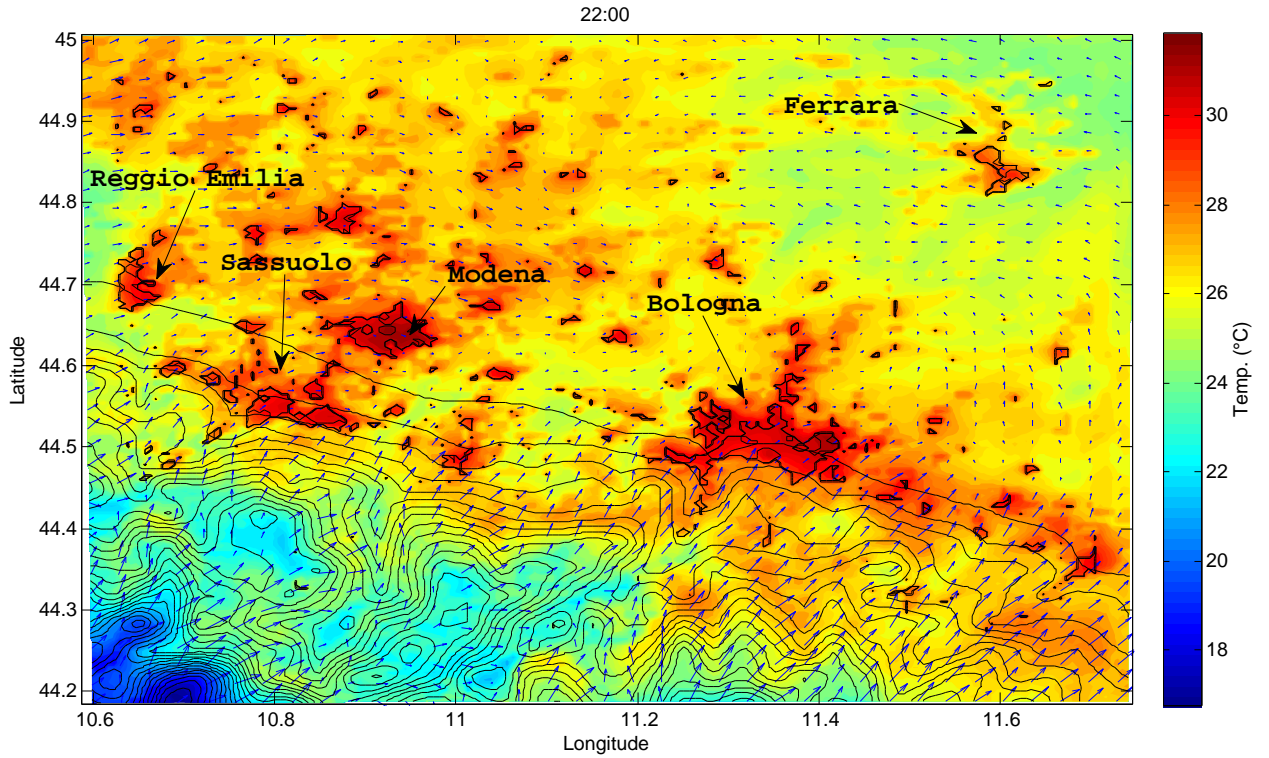
Figure 6.6: Map of 2-meter temperature and wind vectors (URB simulation) at 22:00 averaged over all the 6 days of simulation at the same hour.
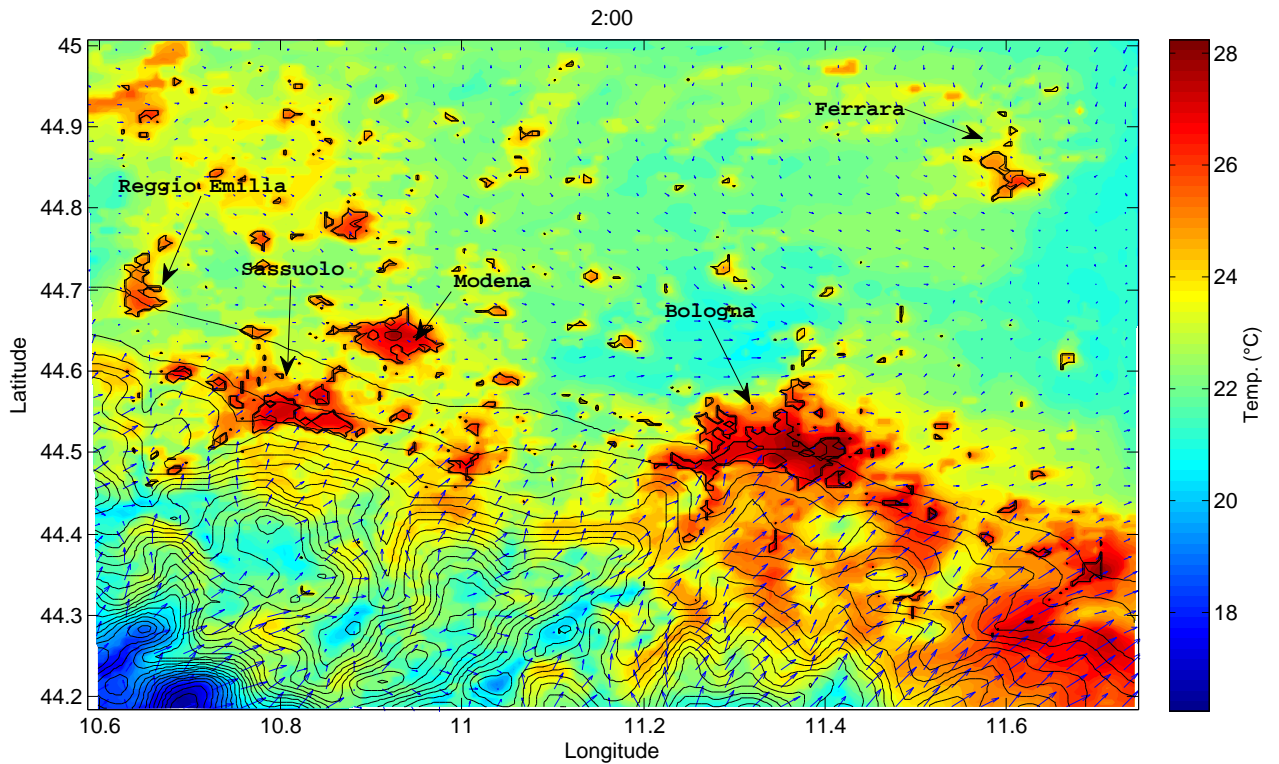
Figure 6.7: Map of 2-meter temperature and wind vectors (URB NEST simulation) at 2:00 averaged over all the 6 days of simulation at the same hour.
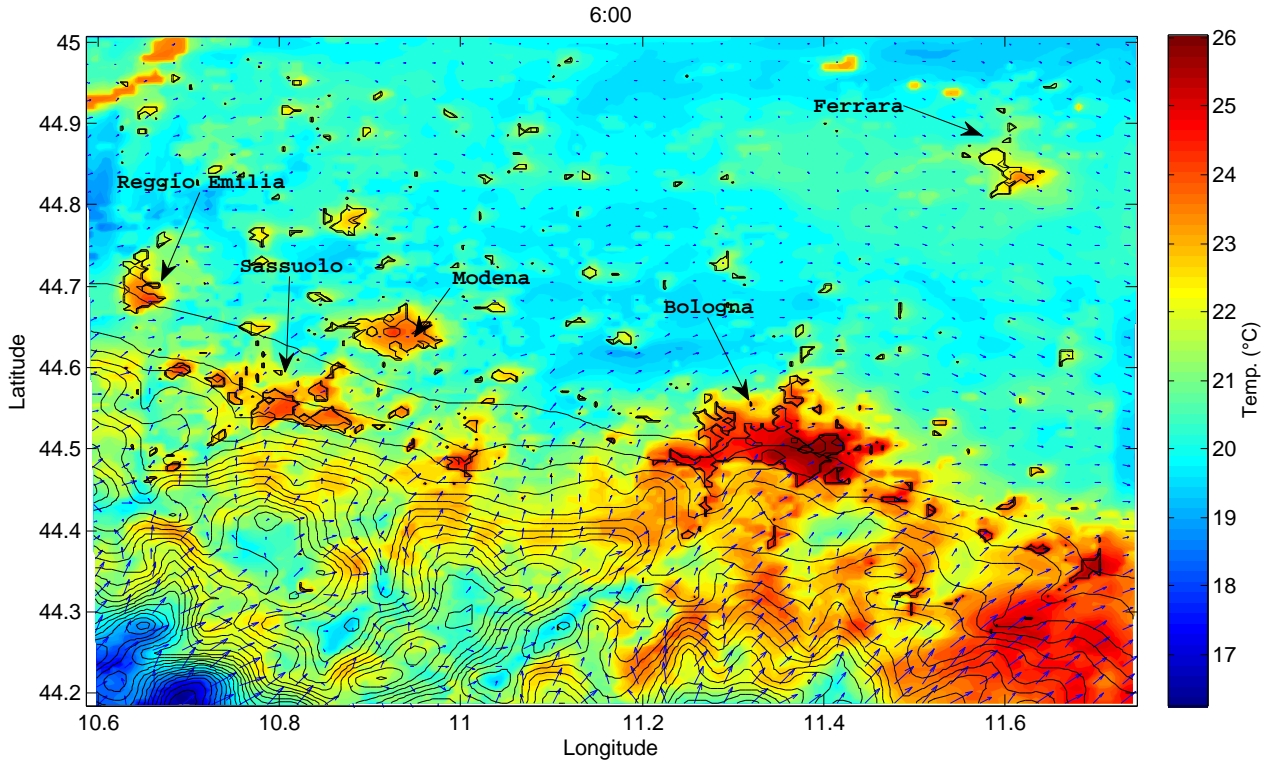
Figure 6.8: Map of 2-meter temperature and wind vectors (URB simulation) at 6:00 averaged over all the 6 days of simulation at the same hour.
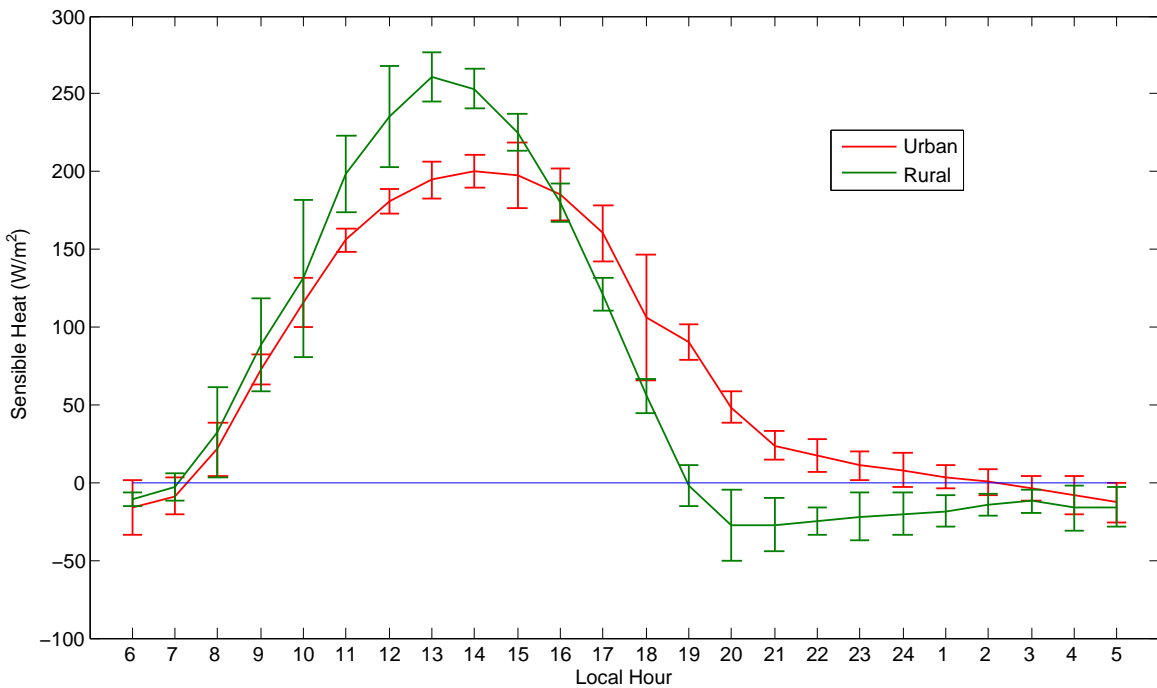
Figure 6.9: Diurnal cycle or sensible heat for the city of Bologna (Red Line) and a closer rural cell on the northern side of the city (Green Line) for URB simulation. Sensible heat assumes positive values when the heat is released from the surface to the atmosphere, and vice versa for negative values. Error bars are the MRSE calculated from the bias of each day.

6.2 Vertical profiles: potential temperature, turbulent kinetic energy and PBL height

In this section, we deal with the most relevant features of the vertical variability of potential temperature, TKE and PBL height.

In order to compare the characteristics of these variables in urban and rural areas, it is necessary to choose the right areas. Therefore, for the city of Bologna, the grid point (x=120,y=70) has been chosen, while for the rural areas the grid point (x=120,y=110), i.e a grid point in the northern direction 20 km far from Bologna.

At the same time, for the vertical sections, we chose to analyze the results from a line cutting Bologna in the South-North direction (x=120), starting 20 km in the southern part of the city and finishing 20 km on the northern part (30 < y < 110)(Fig. 6.10).
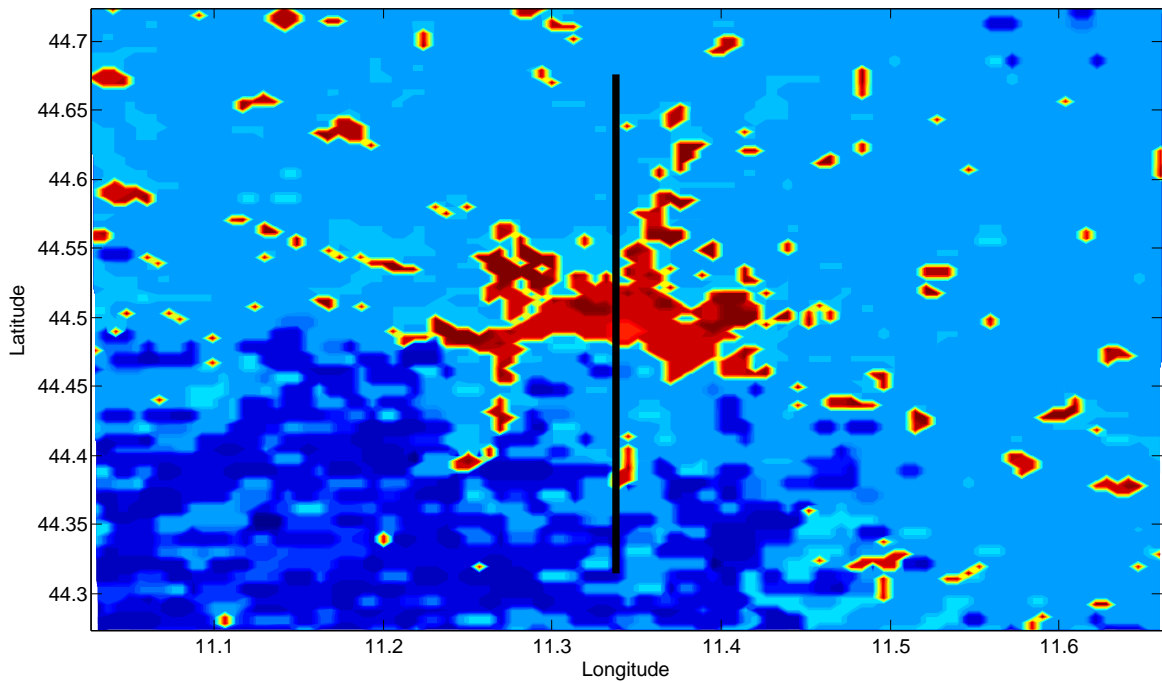
Figure 6.10: Representation of the vertical section used here projected on the map for the city of Bologna.

Since the variables considered vary substantially day by day, the projection on a single diurnal cycle leads to a loss on information. Then on the following analysis, for the time series all days of simulations are taken into account, while for single-hour plots the third day of simulation (18/07/2015) has been chosen.

In Fig. 6.11 the time variation of the PBL height is shown , both for urban and rural areas. The PBL height is defined as the height from the surface where TKE is lower than 0.0001 m^2/s^2. Since the TKE production depends mainly by the vertical shear
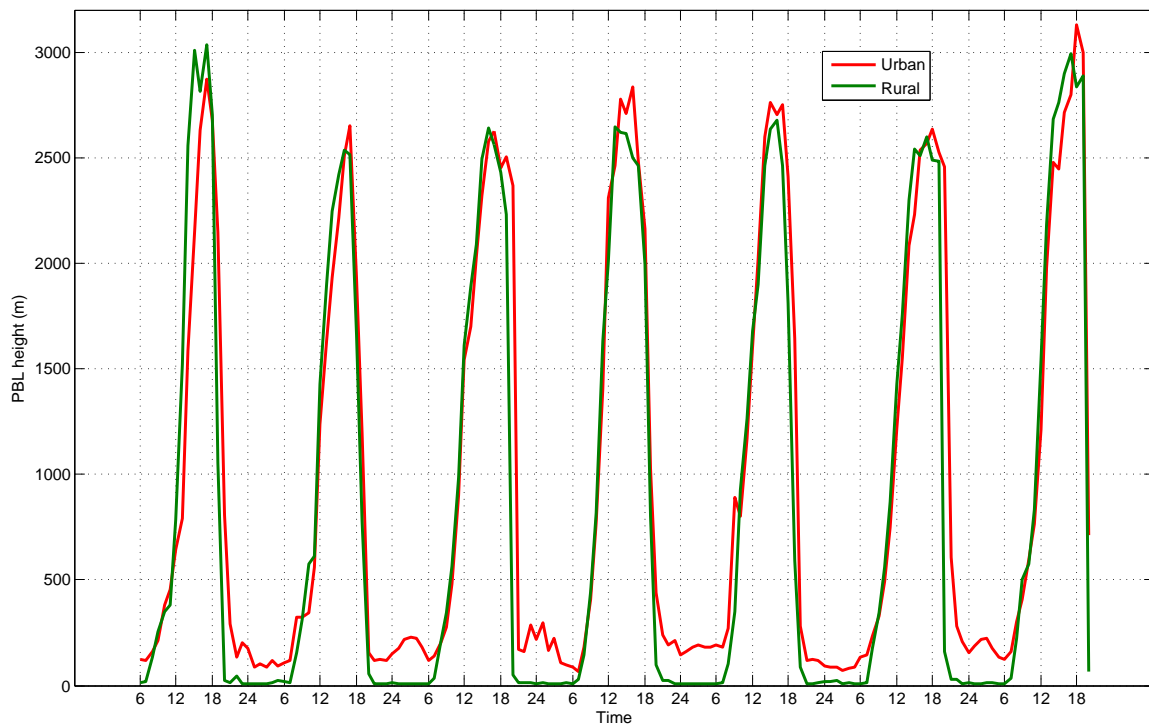
Figure 6.11: Time series of the PBL height for a urban grid (x=120,y=70) and for a rural one (x=120,y=110) for all the time of simulation. The simulation considered is URB_NEST.

and buoyancy, we expected a greater value during daytime (since the wind in very weak in these simulation, a strong dependence from buoyancy is expected). During daytime, both for rural and urban areas the PBL height assumes values around 2500 and 3000 meter, due to the solar radiation forcing and the atmospheric instability. After sunset, the solar forcing is no more present, then the height rapidly fall down. This happens both for urban and rural areas, but in the city it keep a greater value (between 100 and 250 meter greater than the rural PBL). This is due, as said before both to the wind shear (due to the building-induced drag) and the buoyancy (from the heat stored in the building materials) productions.

In fact, the building effect affects even the vertical profiles of potential temperature and TKE.

In Fig. 6.12 the vertical profiles of TKE for the third day of simulation, with a time interval of three hours are shown. Clearly, during daytime (4th 5th, 6th and 7th picture) the vertical profiles have the same shape, since the forcing governing the TKE production is solar radiation. They differ in intensity because of the dependence on the heat flux released to the atmosphere: while at 10:00 and 15:00 the heat flux is greater for rural areas, at 18:00 in greater within the city. This explain why during the central hours of the day the TKE is great for rural areas. Looking at 1st, 2nd, 3rd, 4th
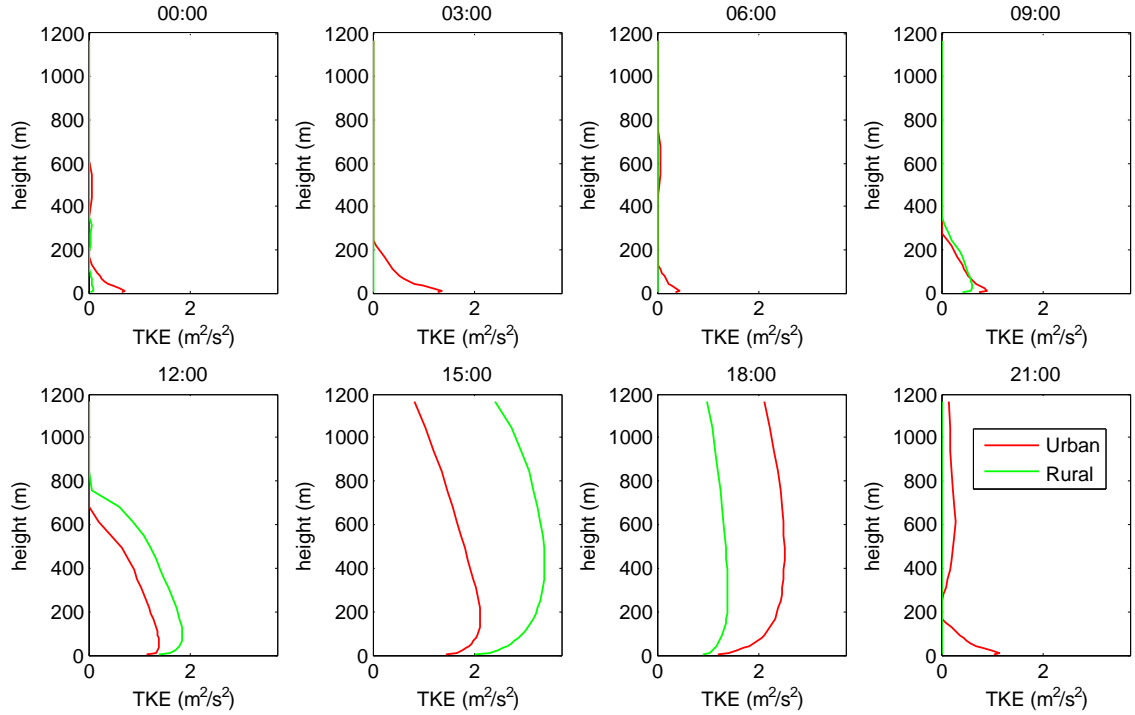
Figure 6.12: TKE vertical plots for a urban grid cell (x=120,y=70) and for a rural one (x=120,y=110). The TKE has been computed for the time period (00:00-21:00) of the 18th of July with a time interval of 3 hours.

and 8th pictures, it is possible to notice a different shape of the vertical profile of TKE with respect to the previous ones. In fact, during nighttime there is no forcing for rural areas, then the TKE is close to zero along all the vertical direction.

On the other hand, for Bologna TKE intensity reaches its maximum value around 10 m (as the length scale of building height), and rapidly decreases with height. Therefore, the forcing for TKE production is the buildings effect both for buoyancy and wind shear. The shape of urban TKE in the last picture (9:00) is very interesting: from the bottom to the top, the intensity rapidly decreases to zero (around 200 m), but at higher levels it increases and keeps non-zero values. Probably this is due to the formation of a warm air mass over the city (where turbulence is higher than the surrounding cold air), but the stability of the boundary layer does not allow this air mass to rise nor get off. Now, we focus on the vertical profiles of potential temperature (PT). Besides temperature trends, these profiles provide informations about the stability of boundary layer: if the PT does not grow with height, then an air parcel within this layer cannot rise nor get off, and this is the case of the neutral boundary layer.

On the other hand, if the PT grows with height, the vertical motion is suppressed and the PBL is called *stable*. By contrast, if the PT decreases with height, an air parcel can rise, and the PBL is *unstable*. In Fig. 6.13 the potential temperature profiles for

104
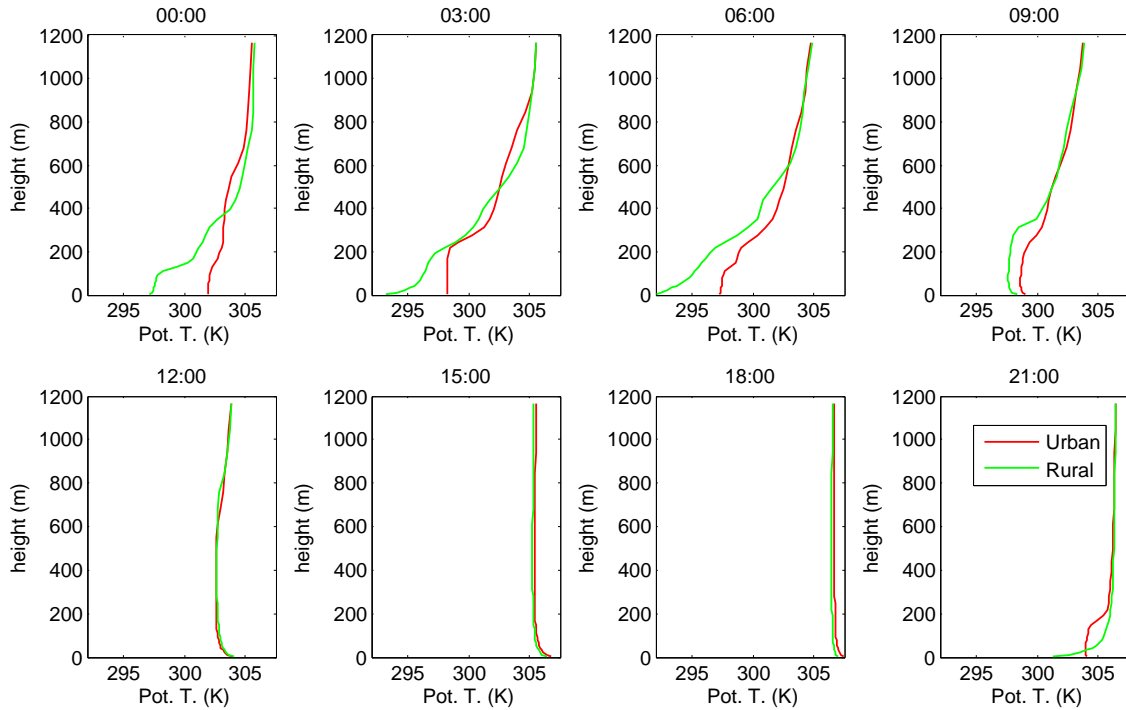
Figure 6.13: Potential Temperature vertical plots for a urban grid cell (x=120,y=70) and for a rural one (x=120,y=110). The TKE has been computed for the time period (00:00-21:00) of the 18th of July with a time interval of 3 hours.

the third day of simulation with a time interval of three hours are shown. During daytime (4th, 5th, 6th and 7th picture) the PBL is unstable both for urban and rural areas, since the vertical motion is forced by the positive heat flux. Above 100 m, both potential temperatures are constant: here the PBL is stable. However at 09:00 the stability is lower for urban areas, due to contribution of building presence.

During nighttime, potential temperature shows a different behavior: while rural PT profile is always stable (except at 21:00, where it is neutral at higher levels), urban potential temperature assumes always a neutral or quasi-neutral profile. This is once again the contribution of urban morphology, which does not allow the stratification of the PBL. The profile difference is evident once again at 21:00. After sunset, the rural PBL assumes a stratified shape, while the urban one is neutral up to 200 m, where stratification takes place.

Looking at the vertical sections of potential temperature (Fig. 6.14 and 6.15), it is clear the effect of the city on the stability of atmosphere. In these figures the behavior of PT is shown both for URB and NOURB simulations during daytime (14:00) and nighttime (02:00) . While during daytime the potential temperature trend assures a unstable boundary layer along all the longitude and both for URB and NOURB cases, during nighttime the situation is opposite. In fact, for the NOURB simulation the PT
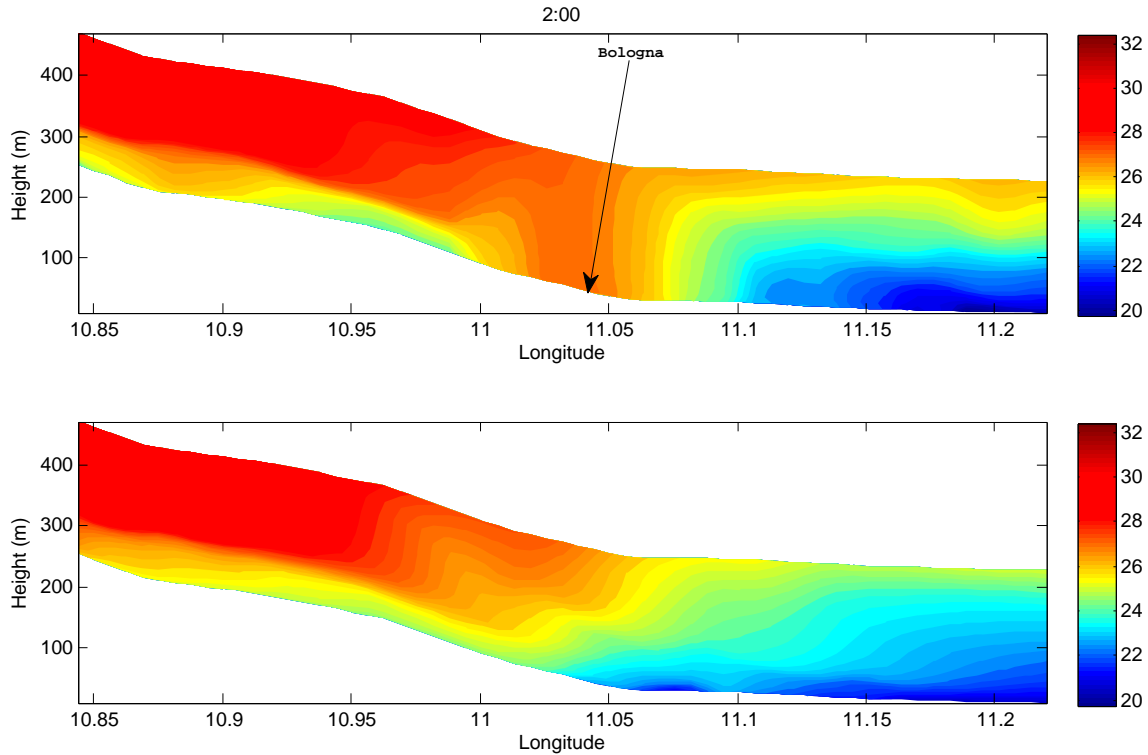
Figure 6.14: Vertical section of potential temperature,centered in Bologna, at 02:00 of the third day of simulation. The PBL is stable in rural zones, but unstable over the city. The sections refer to URB (top) and NOURB (bottom) simulations.

profile is stable along all the longitude, both for valley and hills (the white color on the bottom sides of figures identifies the terrain height). On the other hand, for URB simulation, the PBL is stable on the left and right sides of the city, but over the city it assumes a neutral shape. This is once again due to the presence of the city and a greater value of buoyancy generated from the heat released by building materials.

6.3   The rooftop photovoltaic panels effect

In the previous section, we hace discussed the horiziontal and vertical features of PBL dynamics, distinguishing between urban and rural areas, with the aim to evaluate the effect of urban structures on the near surface atmosphere. In this section, the effect of the deployment of photovoltaic panels (RPVP) over buildings roofs is discussed. Despite the production of electricity, RPVP act cooling the urban environment: therefore, the use of solar plants can be an efficient strategy to be employed for mitigation. In particular, we deal with the comparison of several different patterns (depending on the fraction of coverage for each roof) with the URB simulations. Four different simulations have been run, with 0.25, 0.50, 0.75 and 1.00 fraction of coverage for each
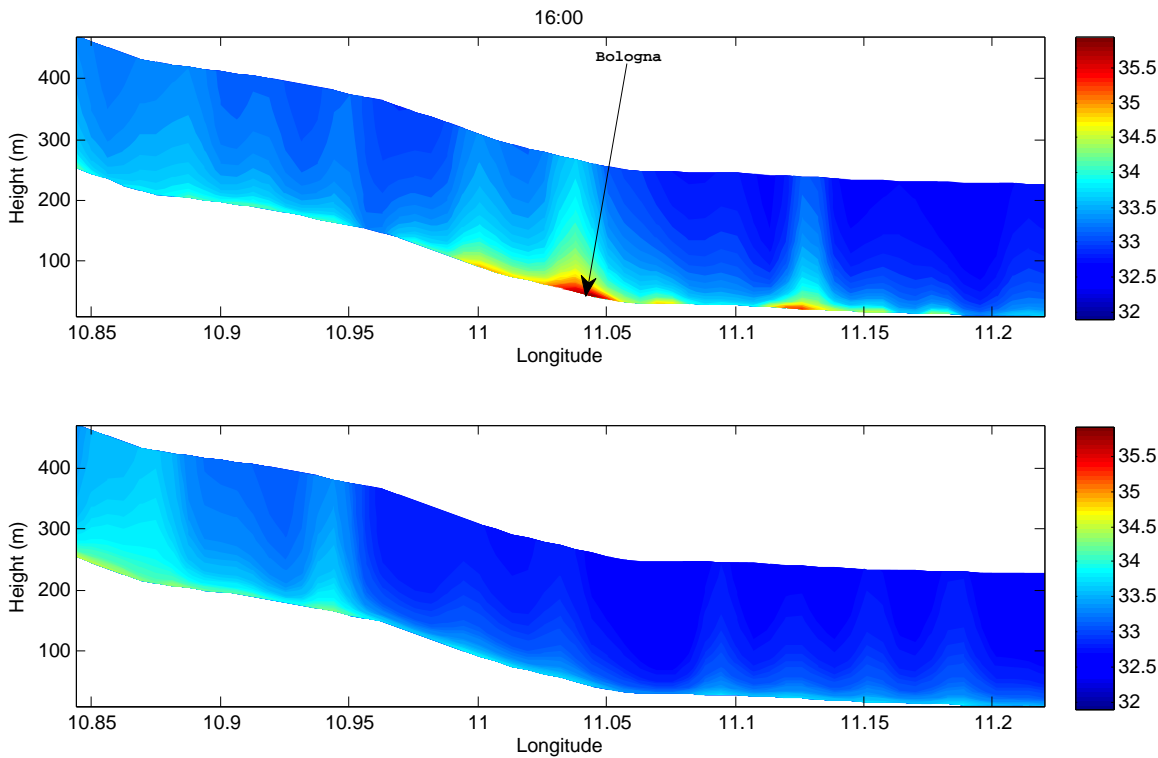
Figure 6.15: Vertical section of potential temperature,centered in Bologna, at 16:00 of the third day of simulation. The PBL is unstable along all the longitude. The sections refer to URB (top) and NOURB (bottom) simulations.

roof (simulation called PV_0.25, PV_0.50, PV_0.75, PV_1.00 respectively). All simulations with RPVP coverage have been run with the same boundary condition of the URB simulation (i.e, with the 1WN method all with the same boundary conditions). For this evaluation, we consider only the city of Bologna: this city is parametrized by 4 urban classes. Since UCZ for Bologna are very close each other, this configuration permit a comparison between classes. RPVP act absorbing incoming short-wave solar radiation, which is converted into electricity. This means that RPVP subtract solar radiation that would be transmitted to the underlying roof, than we expect a lower value of sensible heat released by buildings to the atmosphere.

Therefore, the deployment of RPVP indirectly affects the value of temperature and turbulent parameters within the urban context. The parametrization of RPVP has been treated in section 2.6: albedo has been set to 0.11 and emissivity is of 0.93, since the productivity of each RPVP is proportional to the absorbed solar radiation.

RPVP are supposed to be parallel to the roofs,then there is not further dependence on the inclination angle. The most important parameter from which depends the energy production of the RPVP is the efficiency. This parameter depends only on the assembly and material features of solar cells, and it goes from 0.10 for the monocrystalline silicon panels to 0.24 for the next-generation panels. It refers to the solar radiation
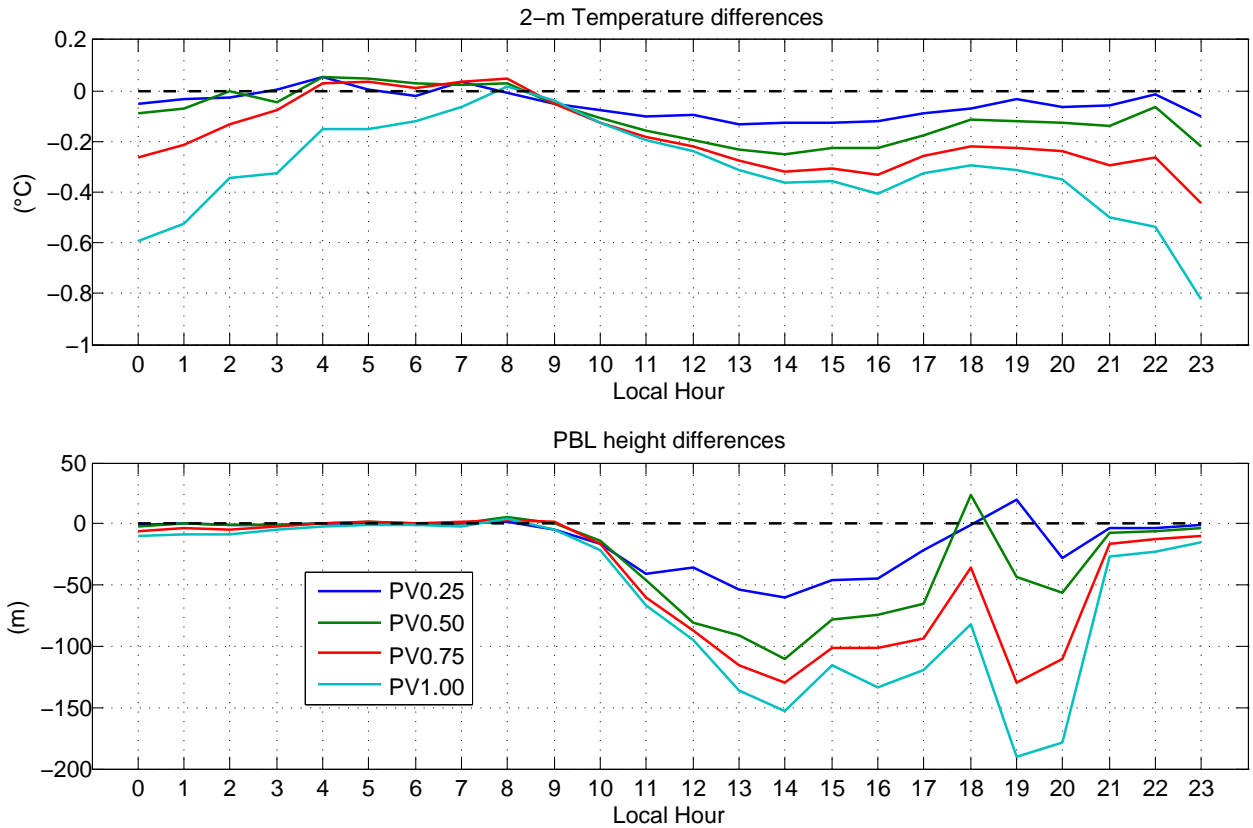
Figure 6.16: Diurnal cycle of 2-m temperature differences (top) and PBL height differences (bottom) averaged for the entire 6-day time period and across all urban cells of Bologna for all coverage rates of RPVP. Differences have been computed subtracting the URB simulation too all the PF_*fraction* simulations.

fraction entering inside the panel converted into electricity. In this thesis, the efficiency has been set to 0.15, a typical value for contemporary solar panels technology.

The presentation of the results for this topic will be conducted as follows: first of all we deal with the effect of RPVP on the urban boundary layer, in particular on their effects on the 2-m air temperature and PBL height (PBLH). Later, we will discuss the effect of RPVP on the energy production/consumption balance.

6.3.1 RPVP effect on the near surface atmosphere

In Fig. 6.16 the diurnal cycle of the difference of 2-m air temperature (top) and PBLH (bottom) between URB simulation and all RPVP simulations is shown. Both variables have been averaged over all the urban grid cells of Bologna metropolitan area. Error-bars have not been plotted in order to better distinguish the trend of the differences. The Root Mean Squared Difference (RMSD), calculated subtracting the difference of

each day to the mean difference is $RMSD = 0.15\,°C$ for PV_0.25, $RMSD = 0.18\,°C$ for PV_0.50, $RMSD = 0.20\,°C$ for PV_0.75, $RMSD = 0.24\,°C$ for PV_1.00 for 2-meter temperature. For PBL height, the error is $RMSD = 14\,m$ for PV_0.25, $RMSD = 15\,m$ for PV_0.50, $RMSD = 20\,m$ for PV_0.75, $RMSD = 24\,m$ for PV_1.00.

Clearly the effect of RPVP is more relevant as the fraction of coverage increases. The highest value of temperature difference is reached during nighttime for all fraction of coverage: the RPVP diminish the quantity of heat stored within the building materials. Since the heat stored is released after sunset and lasts for several hours, smaller storage of the RPVP simulations diminishes the value of 2-m air temperature up to $-0.8\,°C$ at 23:00.

From 4:00 to 8:00 the temperature is slightly higher when RPVP are present (except for the total coverage). During this period, the skin temperature [1] (ST) (Fig. 6.17) is greater in the case of RPVP [Dominguez et al., 2011], while during daytime is lower because of the solar radiation removal. The higher ST during night is due to the sensible heat flux: during daytime, buildings are colder, because of the solar radiation removal. The difference in ST leads to a higher temperature gradient between surfaces and air. This temperature gradient enhances the heat transfer to buildings surfaces during nighttime, when the sensible heat flux is negative (i.e. when air warms buildings surfaces). Therefore, higher STs lead to slightly higher air temperatures when the heat flux is negative, i.e from 4:00 to 8:00.

When the sun rises, RPVP start absorbing solar radiation, which is converted into electricity. The consequence is the temperature decrease with respect to the URB simulation. In fact, from 8:00 temperature differences are negative, with a secondary minimum at 16:00 (when 2-m air temperature reach its peak), and a primary minimum at 23:00, as said before.

Furthermore we cannot detect a reduction of PBL height due to the presence of RPVP during night: the effect in reducing the buoyancy turbulent term is too little to diminish the height of PBL. In fact, for all the fraction of coverage the difference rapidly fall down to zero from 20:00 to 21:00 and this value is maintained until 8:00. The PBL height starts to be lower than the URB case from 9:00, when the heat flux quantity subtracted by RPVP to the heat exchange budget start to be relevant (The RPVP energy production is proportional to the incoming solar radiation).

From 14:00, the difference rapidly decreases, since during this period the dominant phenomena is the heat release by building materials. The highest differences are

---

[1]Temperature of the face of the first ground layer.
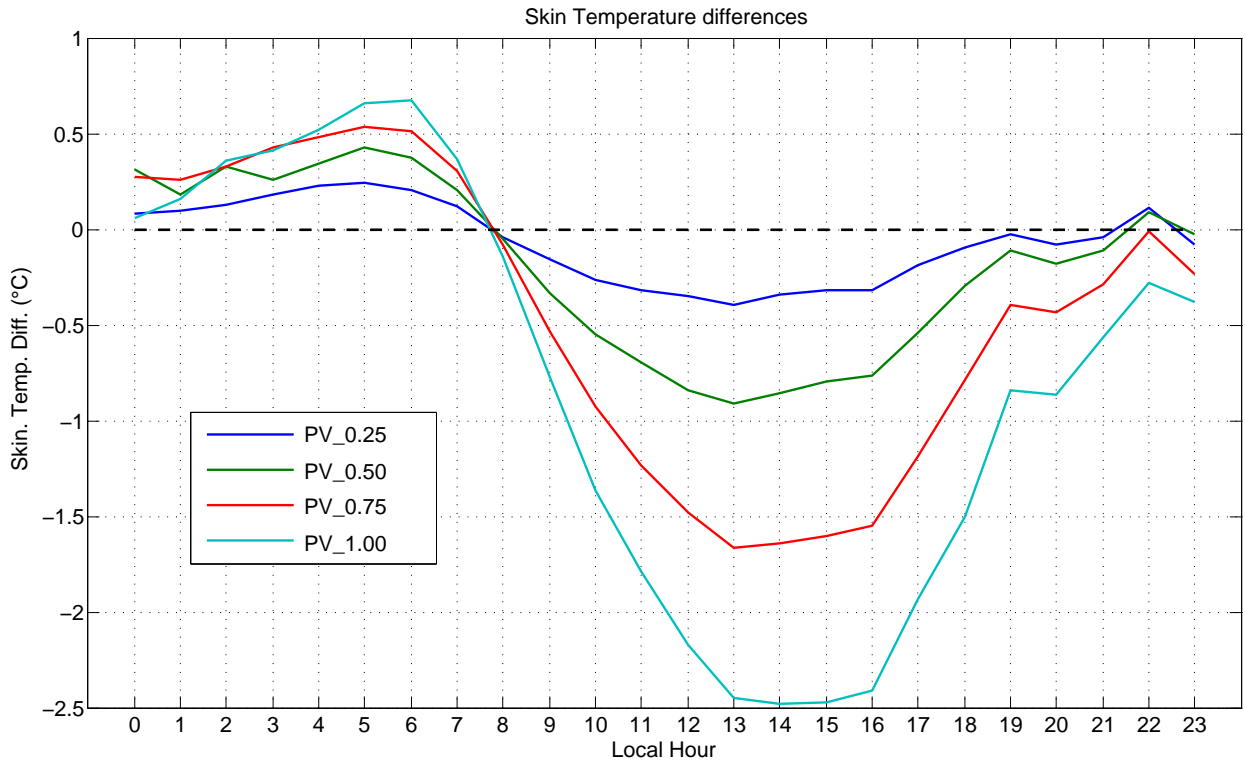
Figure 6.17: Diurnal cycle of skin temperature differences averaged for the entire 6-day time period and across all urban cells of Bologna for all coverage rates of RPVP. Differences have been computed subtracting the URB simulation too all the PF_*fraction* simulations.

reached between 19:00 and 20:00: in this period, the PBL height rapidly fall down (Fig. 6.11), and in the RPVP case, the sensible heat released by building material is smaller than the URB case, so the temporal derivative of PBLH is greater, leading to a more rapid decrease. The maximum value reached is $\simeq -200\,\mathrm{m}$ for the total fraction of coverage.

While the temperature cooling induced by RPVP is a positive effect for the urban context, the reduction of the PBL height is harmful for the dispersion of air pollution: since within the PBL air pollutant are diffused through turbulence, its reduction leads to a increase of the concentration of primary pollutants within the urban context.

Instead of the temporal variation of 2-m air temperature and PBL height differences, it is useful to investigate the horizontal variations, in order to understand how different urban classes are affected by the deployment of RPVP. We distinguish between the differences induced by RPVP during daytime and nighttime, and we investigate the variations of 2-m air temperature and PBL height, focusing once again on the city of Bologna.

   In Fig. 6.18 the 2-m air temperature air difference during nighttime (top) and

110
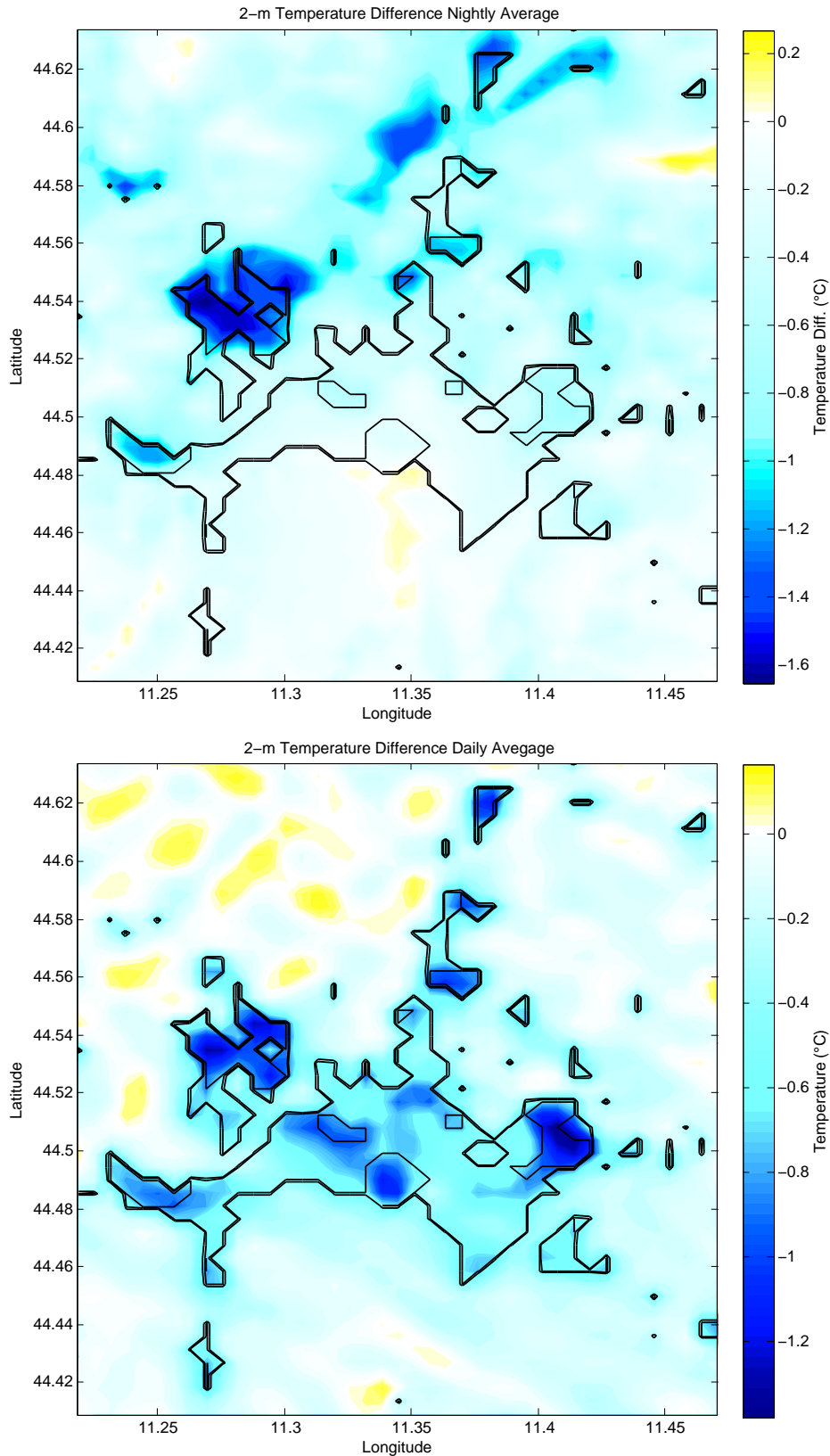
Figure 6.18: 2-m air temperature differences (URB-PV_1.00) during nighttime (top) and daytime (bottom) for the city of Bologna. Nightly average have been performed from 20:00 to 2:00, while daily average from 9:00 to 15:00 for each day of simulation.

daytime (bottom) for the city of Bologna are shown. The greater differences during nighttime are in the northern side of the city (identified by the black contours), while in the southern and central part the difference is almost null. This shift is due to the presence of the katabatic wind during the night: the temperature difference which is created over the city is moved northward by the wind. The katabatic wind is the dominant effect (stronger than the effect of RPVP), then the difference over the city is very slight. On the northern part on the city, the simulation with RPVP has temperature lower of $-1.2\,°C$, more relevant over industrial zones.

In order to understand the difference between different urban classes, we need to look at the 2-m air temperature differences during daytime, since the katabatic wind is not present (bottom figure), and the dominant phenomena is the solar radiation absorption by RPVP.

In this context it is possible to notice the different impact depending on the kind of urban classes: the most relevant effect is shown by the center of the city and by industrial zones on the surrounding areas of the city, while the lowest difference takes place in the residential zones around the city center. Obviously, more RPVP are present in a given urban area, greater is the effect induced on the atmosphere. The urban areas with the biggest fraction of building present within a grid cell are the LCZ 2 (which takes place on the city center) and the LCZ 8 (industrial zones, on the surrounding areas). For this areas, the fraction of coverage is 0.5 (for the city center) and 0.42 (for industrial areas). The effect is greater for industrial areas (despite the lower coverage) since the mean height of the buildings is lower, then the RPVP are more influent for the first level of atmosphere (where the 2-m air temperature is calculated).

Similar is the case of PBL height (Fig 6.19).

During nighttime (top figure) in the central and southern part of the city the katabatic wind "destroy" the effect of RPVP, and the PBL height difference between URB and PV_1.00 simulations is null. On the other hand, as for the 2-m air temperature, the effect is greater for industrial areas. The variation of PBL height is greater during daytime (bottom figure). While during nighttime the PBL is diminished at least 120 m, and it can reach 500 m. Once again the effect is stronger for industrial areas and city center.

6.3.2   RPVP effect on the energy consumption

In the previous section, we investigated the effect induced by the presence of RPVP on the temperature and PBL height within the urban context. At the same time, the deployment of RPVP not only allows the energy production, but even can diminish
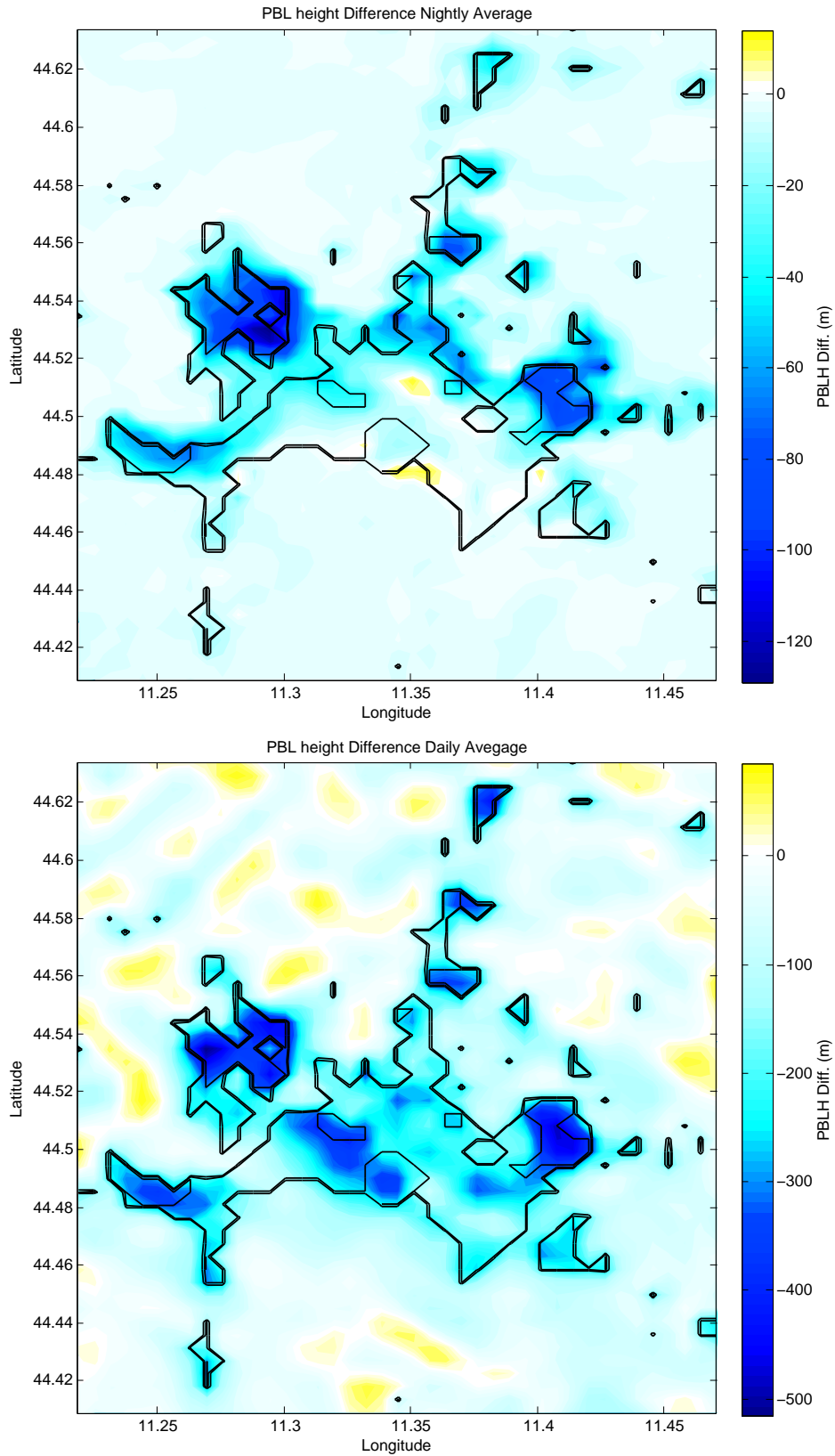
Figure 6.19: PBL height differences (URB-PV_1.00) during nighttime (top) and daytime (bottom) for the city of Bologna. Nightly average have been performed from 20:00 to 2:00, while daily average from 9:00 to 15:00 for each day of simulation.
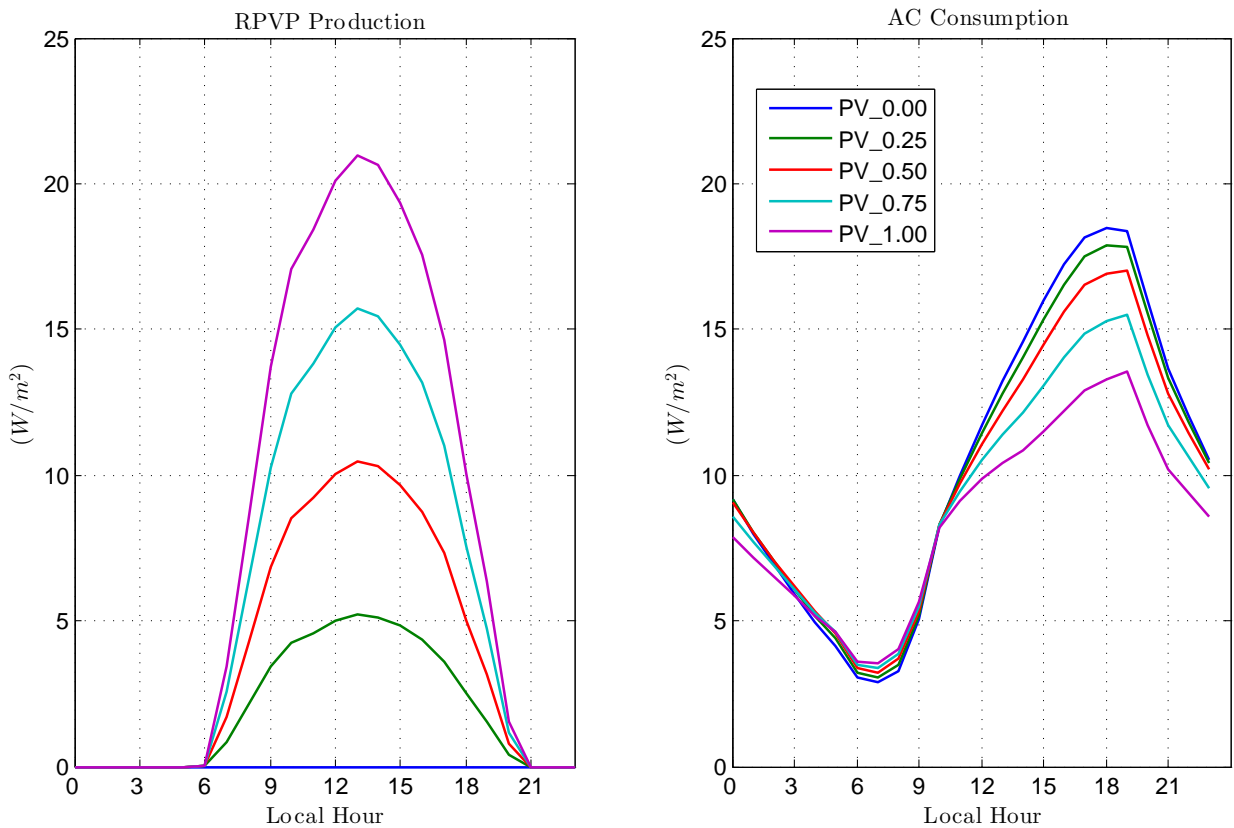
Figure 6.20: Diurnal cycle of energy production by RPVP (left) and energy consumption by ACS (right) for the URB simulation and all simulations with RPVP. Data have been averages over all days of simulation and over all urban grid cells of the city of Bologna. Unity of measurement refers to the power per unit of roof area.

the energy consumption of air conditioning systems (ACS). In fact, RPVP subtract solar radiation which would be stored within the buildings materials if RPVP would not be present. If the heat entering into the building is smaller, smaller is the energy consumption of ACS in order to maintain a given temperature within a building.

Fig. 6.20 shows the diurnal cycle of energy production by RPVP (left) and consumption by ACS (right) averaged over all urban grid cells of Bologna and over all days of simulation. The maximum energy production is given by PV_1.00, since the roofs are totally covered. The trend is the same for all simulations, and the rate of energy production is proportional to the fraction of coverage. The maximum of production takes place at 13:00 (with a maximum of $20.9\,W/m^2$ per unit of roof area for the total coverage of RPVP), when the maximum of solar radiation occurs. In fact, the production of energy by RPVP strongly depends on the incident solar radiation: we obtain non-zero values from 6:00 (when the sun rises) to 21:00 (when the sun sets). Different is the case of energy consumption: the trend does not depend on the solar

$AC_{CONS} - RPV\,P_{PROD}$
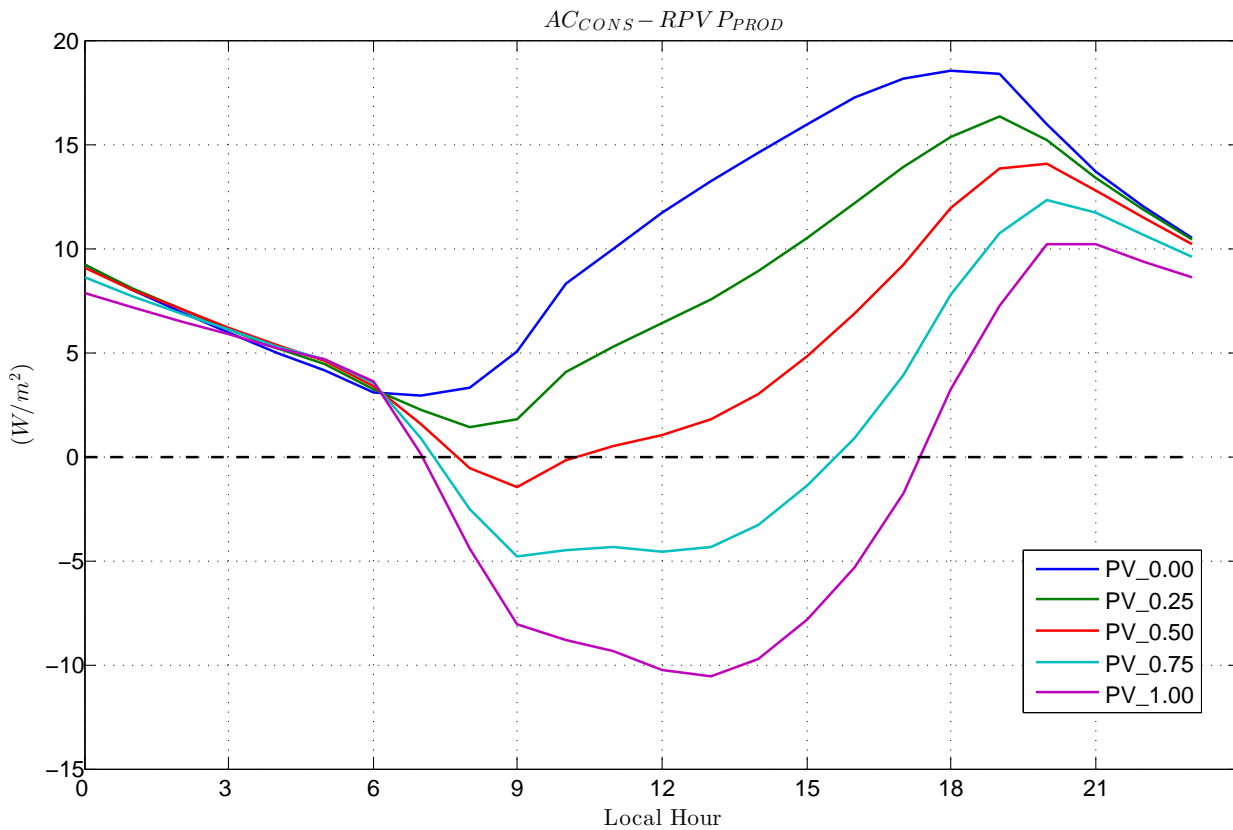
Figure 6.21: Diurnal cycle of difference between energy production by RPVP and energy consumption by ACS for the URB simulation and all simulations with RPVP. Data have been averaged over all days of simulation and over all urban grid cells of the city of Bologna. Unity of measurement refers to the power per unit of roof area.

radiation, rather on the air temperature. Assuming that the ACS work all day long, the minimum for all simulations is around (6:00) when the 2-m air temperature is minimum. When the sun rises, the energy consumption starts growing, with a maximum around 18:00. Successively, the sun sets and the consumption decreases all night long.

However, while the maximum of temperature is reached between 16:00 and 17:00, the maximum of energy consumption is reached at 19:00, then there is a shift between the maximum of outdoor air temperature and working rate of ACS. The difference lies in the fact that building materials store heat, and release it later. Then, the thermal inertia of walls and roofs plays a key role in shifting the energy consumption forward in time.

As said before, RPVP affect the ACS consumption: they do not permit to a fraction of solar radiation to penetrate into the roofs materials, diminishing the heat entering into the rooms closest to the top of buildings: for the PV_1.00 the energy consump-

tion is diminished on a diurnal cycle of 19% with respect to the absence of RPVP, with a maximum of 29% at 17:00.

In order to better understand the role of RPVP in diminishing the energy consumption of ACS, in Fig. 6.21 we subtracted the energy produced to the energy consumed (null in the case of no RPVP).

During nighttime, RPVP does not work, since there is no solar radiation: the energy consumption is more or less the same as in the case without RPVP, with a slightly distinguishable difference for PV_1.00, since the RPVP affect the heat stored in buildings materials.

The situation radically changes when the sun rises: RPVP start to work, and the peak of production is at 13:00. At the same time, RPVP act shifting forward the peak of consumption from 18:00 (in the case without RPVP) to 19:00 (in the total coverage case). Therefore, RPVP contributes to the energy budget for ACS. At 9:00 we can detect different trends: while for PV_0.25 the RPVP cannot never supply to the energy costs, for the other cases the production is greater than consumption. With a fraction of coverage of 0.25, there is never balance between consumption and production, while for a coverage of 0.50 RPVP can supply to the consumption just for three hours. On the other hand PV_0.75 and PV_1.00 shows a greater balance rate: PV_1.00 can supply to the energy consumption from 7:00 to 17:00 while PV_0.75 from 7:00 to 16:00 . Due to the shift in the maximum of consumption and production, it is never possible to balance the ACS costs when they work at maximum power, i.e at the last hours of the afternoon. However, PV_1.00 can cut of 47% the energy consumption when it reaches its peak. When the sun sets, the trend follows the energy consumption trend, since the RPVP are not working anymore.

Evaluating the total difference between consumption and production of energy during a diurnal cycle, it is never possible to supply to the ACS costs even for PV_1.00. In fact, the RPVP energy production can supply up to the 93% of energy consumption assuming the total coverage of roofs.

Summary

This chapter deals with the results provided by simulations.

After the validation of the model conducted in the previous chapter, simulations outputs have been analyzed in order to evaluate temporal and spatial variations of boundary layer dynamics, which are not possible to detect from the punctual infor-

Fraction of RPVP	% of ACS conspumption with respect to absence of RPVP	RPVP production/ ACS Consumption ratio
0.00	100%	0%
0.25	98%	19%
0.50	95%	40%
0.75	89%	64%
1.00	81%	93%

Table 6.1: Enrergy production/consumption budgets. In the second column the percentage of energy consumption with respect to the case without RPVP is shown. In the third column, the percentage of energy produced with respect to the energy consumed is reported. Values refers to an entire diurnal cycle.

mations provided by observational data.

In the first part, we have analyzed the temperature and wind variation over a diurnal cycle for the region of interest, focusing mainly on the UHI and katabatic wind trends.

UHI is not present during the central hours of the day, except for the city centers. At the same time, katabatic wind is not present, since there is no temperature gradient between hill slopes and valley. Radically different is the situation during nighttime: the katabatic wind is present along hill slopes, and the UHI is relevant for all cities. On the South-East side of the domain, it is possible to notice the higher temperature for hills with respect to the open valley, due to the lower cooling rate assumed by hill areas.

In the second part the vertical variation of PBL height, Turbulent Kinetic Energy (TKE) and Potential Temperature have been analyzed. This analysis have been conduced in order to distinguish between the feature of these variable over urban and rural areas, to better understand the effect of the city in modifying the boundary layer dynamics.

PBL is higher in urban areas with respect to rural areas during nighttime. In this case, the buoyancy term for urban areas is greater than that of rural areas, due to the heat released by urban structures. In fact, vertical profiles of TKE assumes the same shape in urban and rural areas during daytime, while during nighttime TKE is highly greater for urban areas, and reach its peak at the mean height of buildings.

On the other hand, the potential temperature (PT) provides informations about the PBL stability.

While during daytime for both urban and rural areas the PBL is unstable, during nighttime the vertical profile is different: for rural areas it is stable, since the sen-

sible heat flux is negative, while for urban areas it is neutral, due once again to the heat released by buildings.

In the last part, the effect of the rooftop photovoltaic panels (RPVP) have been analyzed, focusing on the modification induced on the temperature dynamics and anthropogenic energy consumption budget.

RPVP have a cooling effect on the urban environment: 2-m air temperature is lower with respect to the case without RPVP, and the lowest values are reached during nighttime (up to $0.8\,^{\circ}$C). At the same time, the RPVP diminish the PBL height, as a consequence of the reduction of sensible heat released by buildings.

Finally, the effect of RPVP on the energy consumption of air conditioning systems (ACS) have been evaluated. First of all, the solar plants convert into electricity part of the solar radiation which would be stored into urban structures.

Benefits are provided in two different ways: RPVP produces energy which can be used to make the ACS work, and at the same time they decrease the energy consumption by absorbing part of the solar radiation interacting with urban structures.

Chapter 7

Summary and Conclusions

The aim of is this thesis to improve the understanding of the Urban Heat Island effect for cities of the Emilia Romagna region, through numerical simulations. We have focused on a period of heat wave, in particular from the 16th of July 2015 to the 22nd of the same month. This period is characterized by high temperatures and weak synoptic conditions. An innovative method has been used to parametrize urban morphology. After the validation of the model, a mitigation strategy has been tested for the study area: the effect of rooftop photovoltaic panels deployment on the urban environment has been evaluated. The thesis is divided in 5 parts. The first one is used to present the state of the art of urban boundary layer and UHI modeling; the second one deals with the definition of the urban morphology. The third one contains the description of the case study and simulations setup. Finally, the last two are dedicated to the results of simulations and their comparison with observational data.

The presence of the city affects the near surface atmosphere at several spatial scales, from microscale (single buildings and streets) to city scales (differences between city and its surrounding area). The progressive replacement of natural surfaces by built surfaces, through urbanization, constitutes the main cause of the UHI formation. The UHI, especially during heat waves, causes thermal discomfort on urban population and great amounts of energy consumption due to ACS. Several mitigation strategies can be adopted in order to contrast this harmful phenomenon. These strategies mainly deal with the improvement of urban vegetation and the modification of buildings materials parameters.

A coherent urban landuse is fundamental for a robust modeling; in this study it has been created with the WUDAPT software. The combination of satellite data with manually digitized areas permits to built the urban morphology with a spatial res-

olution of 100 m. Four different urban classes have been detected within the region of interest. They differ one from another in terms of building height and width, fraction of vegetation and thermal coefficients of buildings materials. The urban landuse has been interpolated into the mesoscale model (with a spatial resolution of the 500 m), with a consequent loss of information. In fact, the model grid has not been able to detect the smaller buildings clusters. At the same time, large urban clusters have been coherently reproduced.

Five nested grids have been created for simulations with the finest domain with 500 m of resolution. The boundary conditions have been updated every 6 hours with a resolution of 1°, while morphological parameters derive from the MODIS satellite with a resolution of 30". Several simulations have been performed: they differs on the nesting method, on the kind of vegetation for cultivated area and on the fraction of photovoltaic panels on the building roofs. One control simulation has been set replacing urban coverage with croplands. Simulations outputs have been compared with observational data provided by several weather stations located within the finest domain.

Temperature trends show a good agreement with observational data. Root mean square errors are never greater than $2\,°C$ for all stations and all simulations considered. Temperature is slightly underestimated for all simulations and for all areas. An exception is the URB_BARR simulation, which has been performed replacing the vegetation category "Croplands" with "Barren and Sparsely Vegetated". This category better describes the temperature trend for rural areas. Regarding the difference between *one-way/two-way nesting* (1WN,2WN) methods, a great difference has never been observed: therefore, it is possible to affirm that the 1WN is a strong way to perform simulations with a lower computational time. Moreover, this method allows the comparison of simulations with the same boundary conditions. Relative humidity is underestimated for rural areas and overestimated for urban areas. Clearly, the error is strongly affected by the type of vegetation involved. For rural areas, despite URB_BARR is the simulation that better describes the temperature trend, it shows the highest error for humidity. The negative mean bias between simulation and observed data can be linked to the lack of irrigation for cultivated area in the model parametrizations, or to the behavior of vegetation during a heat wave. The katabatic wind is observed on average from 17:00 to 7:00 of the next day. It is caused by the horizontal temperature gradient in the SW-NE direction, due to hills morphology.The building-induced drag for the city of Bologna converts mean kinetic energy into tur-

bulent kinetic energy. In fact, the wind velocity inside the city is better reproduced by the simulations which consider the presence of buildings.

The UHI effect has been evaluated for a diurnal cycle for the city of Bologna and Modena, comparing observed temperature with URB and NOURB simulations. UHI takes place from 17:00 to 8:00 of next day for both cities, reaching a maximum value of $\simeq 4\,^{\circ}$C. While for Bologna the UHI is slightly overestimated, for Modena it is slightly underestimated.

The RPVP, beside the conversion of solar radiation into electricity, have a cooling effect on the urban environment. For the city of Bologna, the maximum cooling rate is reached during nighttime . At the same time, RPVP deployment decreases the thickness of PBL during daytime since they diminish the building-induced turbulence. For ACS, RPVP indirectly diminish energy consumption by subtracting a fraction of heat which would be absorbed by buildings. The reduction of energy consumption caused by RPVP (assuming the total coverage) is of 19% on a diurnal cycle. The deployment of RPVP can be a powerful mitigation strategy, both for cooling and reduction of anthropogenic heat release.

This thesis has revealed the powerful skills of the coupling of a mesoscale NWP model with multilayer urban canopy parametrizations and the WUDAPT software. WUDAPT has resulted a very efficient and universal method to consider the effect of the urban morphology in a given context. In particular, it has permitted to take into account of several clustered urban buildings (from larger cities to smaller and scattered structures) in absence of building coverage datasets. The use of WUDAPT shows that it coherently describes urban heterogeneities. This means that urban centers, residential zones and industrial areas can be resolved even with a 500 m grid resolution. At the same time, areas described by the same Urban Climate Zone (UCZ), are sensitive to their location. In other words, UCZs react depending on their neighborhood and on the meteorological circulation (for example, urban structures of Bologna interact with the katabatic wind, which reduces the UHI in areas closer to hills).

An other skill of WUDAPT is its versatility. It may be used to evaluate the microclimate of any city in the world, through the use of free available data. Moreover, this is the first numerical mesoscale study of urbanization effect conducted for Emilia-Romagna: this permitted to evaluate general features of PBL dynamics in this region.

In particular, the absence of synoptic forcing during the heat wave period considered allowed to identify the mesoscale phenomena, such as the UHI and the katabatic wind variations.

Furthermore, the robustness of the model revealed by the comparison with observational data has allowed the evaluation of effect of RPVP. Although the original role of solar photovoltaic panels is the energy production, in this thesis we have proven that in addition to diminish the dependence on fossil fuels, they also contribute to reduce near surface temperature. As a consequence of this, they can be used as a mitigation strategy. Further benefits can be provided by the enhancement of RPVP efficiencies.

As an outlook of the work considered in this thesis, it could be worth extending the research to compare the WUDAPT landmask with a building coverage dataset to evaluate its efficiency in representing mean features of urban morphology. Moreover, the introduction of finer mesoscale grids can be used to better resolve urban heterogeneities and its internal circulation, especially for small cities like those considered. Actually, a 166 m spatial resolution simulation has been performed. However, the enhancement of the grid resolution did not lead to the enhancement of the results, since the PBL schemes need to be adjusted for these resolutions.

Moreover, the cooling effect of RPVP could be compared with other methods in order to find the most efficient mitigation strategy which also has the lower impact on the urban environment.

Bibliography

[Arnfield, 2003] Arnfield, A. J. (2003). Two decades of urban climate research: A review of turbulence, exchanges of energy and water, and the urban heat island. *International Journal of Climatology*, 23(1):1–26.

[Barlow, 2014] Barlow, J. F. (2014). Progress in observing and modelling the urban boundary layer. *Urban Climate*, 10(P2):216–240.

[Bechtel et al., 2015] Bechtel, B., Alexander, P., Böhner, J., Ching, J., Conrad, O., Feddema, J., Mills, G., See, L., and Stewart, I. (2015). Mapping Local Climate Zones for a Worldwide Database of the Form and Function of Cities. *ISPRS International Journal of Geo-Information*, 4(1):199–219.

[Bechtel and Daneke, 2012] Bechtel, B. and Daneke, C. (2012). Classification of local climate zones based on multiple earth observation data. *IEEE Journal of Selected Topics in Applied Earth Observations and Remote Sensing*, 5(4):1191–1202.

[Bougeault and Lacarrere, 1989] Bougeault, P. and Lacarrere, P. (1989). Parameterization of Orography-Induced Turbulence in a Mesobeta–Scale Model.

[Bowler et al., 2010] Bowler, D. E., Buyung-Ali, L., Knight, T. M., and Pullin, A. S. (2010). Urban greening to cool towns and cities: A systematic review of the empirical evidence. *Landscape and Urban Planning*, 97(3):147–155.

[Brousse et al., 2016] Brousse, O., Martilli, A., Foley, M., Mills, G., and Bechtel, B. (2016). WUDAPT, an efficient land use producing data tool for mesoscale models? Integration of urban LCZ in WRF over Madrid.

[Centro Operativo per la Meteorologia, 2015] Centro Operativo per la Meteorologia (2015). Monthly bulletin.

[Charabi and Bakhit, 2011] Charabi, Y. and Bakhit, A. (2011). Assessment of the canopy urban heat island of a coastal arid tropical city: The case of Muscat, Oman. *Atmospheric Research*, 101(1-2):215–227.

[Chen and Dudhia, 2001] Chen, F. and Dudhia, J. (2001). Coupling an Advanced Land Surface Hydrology Model with the Penn State NCAR MM5 Modeling System. Part I: Model Implementation and Sensitivity. *Monthly Weather Review*, 129(4):569–585.

[Chen et al., 2011] Chen, F., Kusaka, H., Bornstein, R., Ching, J., Grimmond, C. S. B., Grossman-Clarke, S., Loridan, T., Manning, K. W., Martilli, A., Miao, S., Sailor, D., Salamanca, F. P., Taha, H., Tewari, M., Wang, X., Wyszogrodzki, A. A., and Zhang, C. (2011). The integrated WRF/urban modelling system: Development, evaluation, and applications to urban environmental problems. *International Journal of Climatology*, 31(2):273–288.

[Christidis et al., 2011] Christidis, N., Stott, P. A., and Brown, S. J. (2011). The role of human activity in the recent warming of extremely warm daytime temperatures. *Journal of Climate*, 24(7):1922–1930.

[Conrad et al., 2015] Conrad, O., Bechtel, B., Bock, M., Dietrich, H., Fischer, E., Gerlitz, L., Wehberg, J., Wichmann, V., and Bohner, J. (2015). System for Automated Geoscientific Analyses (SAGA) v. 2.1.4. *Geoscientific Model Development*, 8(7):1991–2007.

[Daly et al., 2010] Daly, C., Conklin, D. R., and Unsworth, M. H. (2010). Local atmospheric decoupling in complex topography alters climate change impacts. *International Journal of Climatology*, 30(12):1857–1864.

[De Munck et al., 2013] De Munck, C., Pigeon, G., Masson, V., Meunier, F., Bousquet, P., Tréméac, B., Merchat, M., Poeuf, P., and Marchadier, C. (2013). How much can air conditioning increase air temperatures for a city like Paris, France? *International Journal of Climatology*, 33(1):210–227.

[D'Ippoliti et al., 2010] D'Ippoliti, D., Michelozzi, P., Marino, C., De'Donato, F., Menne, B., Katsouyanni, K., Kirchmayer, U., Analitis, A., Medina-Ramón, M., Paldy, A., Atkinson, R., Kovats, S., Bisanti, L., Schneider, A., Lefranc, A., Iñiguez, C., and Perucci, C. A. (2010). The impact of heat waves on mortality in 9 European cities: results from the EuroHEAT project. *Environmental health : a global access science source*, 9(1):37.

[Dominguez et al., 2011] Dominguez, A., Kleissl, J., and Luvall, J. C. (2011). Effects of solar photovoltaic panels on roof heat transfer. *Solar Energy*, 85(9):2244–2255.

[Gago et al., 2013] Gago, E. J., Roldan, J., Pacheco-Torres, R., and Ordóñez, J. (2013). The city and urban heat islands: A review of strategies to mitigate adverse effects. *Renewable and Sustainable Energy Reviews*, 25:749–758.

[Heaviside et al., 2015] Heaviside, C., Cai, X.-M., and Vardoulakis, S. (2015). Attribution of mortality to the Urban Heat Island during heatwaves in the West Midlands, UK. *Environmental Health*, 15(Suppl 1).

[Jiménez and Dudhia, 2013] Jiménez, P. A. and Dudhia, J. (2013). On the ability of the WRF model to reproduce the surface wind direction over complex terrain. *Journal of Applied Meteorology and Climatology*, 52(7):1610–1617.

[Knievel et al., 2007] Knievel, J. C., Bryan, G. H., and Hacker, J. P. (2007). Explicit Numerical Diffusion in the WRF Model. *Monthly Weather Review*, 135(11):3808–3824.

[Lazzeri, 2006] Lazzeri, M. (2006). Introduzione a Dexter. *http://www.arpae.it/*.

[Martilli et al., 2016] Martilli, A., Brousse, O., and Ching, J. (2016). Urbanized WRF modeling using WUDAPT(1). Technical Report March, Cientro de Investigaciones Energeticas MedioAmbientales y Tecnologicas (CIEMAT), Madrid.

[Martilli et al., 2002] Martilli, A., Clappier, A., and Rotach, M. W. (2002). An Urban Surface Exchange Parametrization for Mesoscale Models. *Boundary-Layer Meteorology*, pages 261–304.

[Masson, 2006] Masson, V. (2006). Urban surface modeling and the meso-scale impact of cities. *Theoretical and Applied Climatology*, 84(1-3):35–45.

[Masson et al., 2014] Masson, V., Bonhomme, M., Salagnac, J.-L., Briottet, X., and Lemonsu, A. (2014). Solar panels reduce both global warming and urban heat island. *Frontiers in Environmental Science*, 2(June):1–10.

[Mirzaei, 2015] Mirzaei, P. A. (2015). Recent challenges in modeling of urban heat island. *Sustainable Cities and Society*, 19:200–206.

[National Centers for Environmental Prediction, 2016] National Centers for Environmental Prediction (2016). http://dx.doi.org/10.5065/D6M043C6, Research Data Archive at the National Center for Atmospheric Research, Computational and Information Systems Laboratory, Boulder, Colo.

[Nations, 2014] Nations, U. (2014). *World Urbanization Prospects: The 2014 Revision, Highlights (ST/ESA/SER.A/352)*. United Nations.

[Oke, 1987] Oke, T. R. (1987). *Boundary layer climates. 2ª edition.* Routledge.

[Rizwan et al., 2008] Rizwan, A. M., Dennis, L. Y. C., and Liu, C. (2008). A review on the generation, determination and mitigation of Urban Heat Island. *Journal of Environmental Sciences*, 20(1):120–128.

[Robitu et al., 2006] Robitu, M., Musy, M., Inard, C., and Groleau, D. (2006). Modeling the influence of vegetation and water pond on urban microclimate. *Solar Energy*, 80(4):435–447.

[Salamanca et al., 2016] Salamanca, F., Georgescu, M., Mahalov, A., Moustaoui, M., and Martilli, A. (2016). Citywide Impacts of Cool Roof and Rooftop Solar Photovoltaic Deployment on Near-Surface Air Temperature and Cooling Energy Demand. *Boundary-Layer Meteorology*.

[Salamanca et al., 2010] Salamanca, F., Krpo, A., Martilli, A., and Clappier, A. (2010). A new building energy model coupled with an urban canopy parameterization for urban climate simulations-part I. formulation, verification, and sensitivity analysis of the model. *Theoretical and Applied Climatology*, 99(3-4):331–344.

[Skamarock et al., 2008] Skamarock, W., Klemp, J., Dudhi, J., Gill, D., Barker, D., Duda, M., Huang, X.-Y., Wang, W., and Powers, J. (2008). A Description of the Advanced Research WRF Version 3. *National Center for Atmospheric Research (NCAR)*.

[Stewart, 2011] Stewart, I. D. (2011). *Redefining the Urban Heat Island.* PhD thesis, University of British Columbia.

[Stewart and Oke, 2012] Stewart, I. D. and Oke, T. R. (2012). Local climate zones for urban temperature studies. *Bulletin of the American Meteorological Society*, 93(12):1879–1900.

[Stewart et al., 2014] Stewart, I. D., Oke, T. R., and Krayenhoff, E. S. (2014). Evaluation of the 'local climate zone' scheme using temperature observations and model simulations. *International Journal of Climatology*, 34(4):1062–1080.

[Tran et al., 2006] Tran, H., Uchihama, D., Ochi, S., and Yasuoka, Y. (2006). Assessment with satellite data of the urban heat island effects in Asian mega cities. *International Journal of Applied Earth Observation and Geoinformation*, 8(1):34–48.

[Trenberth et al., 2012] Trenberth, Jerry, Masters, and Somerville (2012). Heat Waves and Climate Change. Technical report, National Center for Atmospheric Research.

[Wong et al., 2011] Wong, N. H., Jusuf, S. K., Syafii, N. I., Chen, Y., Hajadi, N., Sathya-
    narayanan, H., and Manickavasagam, Y. V. (2011). Evaluation of the impact of the
    surrounding urban morphology on building energy consumption. *Solar Energy*,
    85(1):57–71.

Ringraziamenti

Desidero ringraziare tutti coloro che mi sono stati vicini in questi ultimi anni; coloro
che con consigli tecnici, incitazioni o semplici sorrisi hanno contribuito al raggiung-
imento di questo risulato.

Innanzitutto volevo ringraziare la Prof.ssa Silvana Di Sabatino, che con grande pro-
fessionalità e dedizione mi ha permesso di affrontare questo argomento e di portare
a compimento la stesura della tesi, .

Un ringraziamento speciale va ad Alberto Martilli. Durante il periodo a Madrid, con
estrema umanità e disponibilità mi ha permesso di crescere sotto ogni punto di vista,
trasmettendomi la passione per il proprio lavoro oltre a moltissimi insegnamenti
riguardanti l'argomento di questa tesi.
Aprovecho de la ocasiòn por dar las gràcias a todo el increìble equipo del CIEMAT:
Fernando, por haberme acogìdo en el grupo de investigaciòn , Beatriz e Ester para
haberme aiudado con el idiòma espanol y sobre de todo por sus gentileza, Oscar por
haber compartido conmigo joyas y dolores, Jose Luis e Juan Luis por sus disponibili-
dad. Nunca me olvidarè de la esperiencia en CIEMAT!

Ringrazio sentitamente colleghi e amici, Matteo Matteo Alfonso Thomas e Giovanni,
per aver condiviso con me bellissimi momenti durante questi tre anni. In particolare,
Francesco Arianna Aldo e Giacomo per avermi consigliato, supportato e soprattutto
sopportato negli ultimi mesi.

Un grazie di cuore va a Alessandro Elena Elisabetta e Sam, la mia famiglia bolognese:
oltre ad avermi riaccolto e sopportato per molto tempo, innumerevoli sono stati i
bei momenti trascorsi insieme, le cene, ed i discorsi che hanno reso estremamente
sereno ed indimenticabile il periodo trascorso in quel di Via Orfeo 25.

Ringrazio tutti gli amici di Montagnana, Padova e Madrid, che nel corso di questi
anni hanno condiviso con me gioie, risate, serate, viaggi e passioni, nella speranza

che le amicizie durino negli anni a venire.

In particolare, un grazie gigante va a Zii e Steno: li ringrazio per la loro profonda amicizia, per aver condiviso con me passioni, sensazioni, dolori, complicità e soprattutto momenti felici, per aver sempre tirato fuori il massimo da me e per la fiducia reciproca.

Infine, il grazie piu' grande va alla mia famiglia. A mamma e papà per il sostegno incondizionato, assoluto e totale che mi hanno assicurato in ogni singolo momento della mia vita, prentendendo sempre il massimo da me e allo stesso tempo chiudendo un occhio anche quando non avrebbero dovuto. Alle mie donne Elisa, Michela, Valeria, Sofia, Anita e Clara, che sempre mi hanno dovuto (e ho dovuto) sopportare, ma che non smetterò mai di essere grato per la vivacità, l'entusiasmo e il senso di famiglia che mi hanno trasmesso e continuano a trasmettermi.

Andrea